

- I. THE PHASE-CURRENT RELATION AT ZERO VOLTAGE
IN PROXIMITY EFFECT BRIDGES
- II. THE INTERACTION OF PROXIMITY EFFECT BRIDGES
WITH SUPERCONDUCTING MICROSTRIP RESONATORS

Thesis by
Tomas Ganz

In partial fulfillment of the requirements
for the degree of
Doctor of Philosophy

California Institute of Technology
Pasadena, California
1975

(Submitted March 5, 1976)

To Patti and our parents.

ACKNOWLEDGEMENTS

This work could not have been undertaken without the intellectual, technical and financial assistance from many sources. Their contribution is gratefully acknowledged. By necessity, only a partial listing is given.

Dr. James Mercereau who provided the leadership and direction which made the Low Temperature Physics group at Caltech an exciting place to learn physics,

Dr. Harris Notarys who tried to teach me his own perfectionist brand of experimental physics and who was involved in the development of all the technology used in my experiments (I cannot thank him enough),

Dr. G. John Dick who exposed me to resonators and computer programming and whose insights into experimental problems saved me from many a blind alley,

Bob MacNamara who cooperated closely on some of the experiments with bridge-resonator circuits and who will carry on when I leave,

The fellow graduate students in weak superconductivity Dave Palmer, Steve Decker, Ming Lun Yu and Run Han Wong whose hard work and inventiveness broke the ground for my own efforts and whose friendship and good humor was much appreciated,

Sandy Santantonio and Ed Boud who helped design and make much of the equipment needed in our work and whose meticulous craftsmanship set a high standard for all of us,

Gail Kusudo who made me look forward to lunch even when the experiments were going well and assisted with many organizational matters, orders, manuscripts and travel,

Karen Cheetham whose intelligent and resourceful typing from my messy manuscript is an admirable accomplishment,

IBM Corporation who awarded me a predoctoral fellowship (1973-4),

The California Institute of Technology which generously contributed much financial and logistical support and a highly creative environment which I will sorely miss.

ABSTRACT

Experimental investigations on the proximity effect bridge (a Josephson device) at zero voltage and at finite voltages in the μV range are reported.

The phase-supercurrent relation at zero voltage was measured using an asymmetric superconducting quantum interferometer circuit. The data are in agreement with the Josephson supercurrent-phase relation $I_S = I_C \sin \delta$ with deviation less than 5% of the critical current I_C . The supercurrent density in the measured bridges reached as high as $50\text{-}100 \mu\text{A}/\mu\text{m}^2$.

Using microcircuitry techniques, proximity effect bridges were strongly coupled to superconducting microstrip resonators. Self-induced steps in the I-V characteristics of bridges coupled to resonators were observed in the GHz region at voltages (frequencies) corresponding to the expected modes of the resonators. Two types of steps were seen depending on whether the resonator impedance on resonance was much higher or much smaller than the bridge resistance. A simple two fluid model of the bridge-resonator circuit was developed and the size and shape of self-induced steps were calculated for a generalized Josephson oscillator relation $I_S = I_C (1 - q + q \sin \int \frac{2e}{\hbar} V dt)$ where $q = 1$ corresponds to the original Josephson relation and $q = 1/2$ represents the phase slip regime. At low critical currents ($I_C < 10 \mu\text{A}$) and low voltages ($\bar{V} < 3 \mu\text{V}$) the size and shape of experimentally observed self-induced steps agree with the $q = 1$ model. At higher voltages and/or critical currents the step size increasingly deviates from the

$q = 1$ model towards $q = 1/2$. These observations are interpreted to indicate a progressive reduction of the amplitude of the oscillating Josephson supercurrent in proximity effect bridges from I_c towards $I_c/2$ as the critical current and/or voltage are increased.

TABLE OF CONTENTS

	Page
Acknowledgements	iii
Abstract	iv
Introduction	1
I. Macroscopic Quantum Effects - Theory	2
1.1 The Macroscopic Wavefunction	2
1.2 The Boundary of a Superconductor	5
1.3 Junctions in the Weak Coupling Limit	8
1.4 The Phase Slip Model	11
1.5 The Current-Voltage Characteristic of Josephson Devices	20
1.6 Quantum Interference Effects in Magnetic Fields	24
References	36
II. The Phase-Current Relation at Zero Voltage in Proximity Effect Bridges	38
2.1 Historical Background	38
2.2 The Small Asymmetric Interferometer	39
2.3 Sample Preparation	43
2.4 The Measurement of the Interferometer Critical Current as a Function of Applied Magnetic Field	47
2.5 Data Analysis, Results and Discussion	54
2.6 Conclusion	66
References	67

TABLE OF CONTENTS (Cont'd)

	Page
III. The Interaction of Proximity Effect Bridges with Superconducting Microstrip Resonators	68
3.1 Introduction	68
3.2 Self-induced Steps -- General Considerations	69
3.3 Experimental Technique	76
3.4 Observations	88
3.5 Self-induced Steps for a Simple Harmonic Phase-Supercurrent Relation -- Theory	101
3.6 Results and Discussion	110
3.7 Conclusion	114
References	124

INTRODUCTION

The study of Josephson phenomena in weakly coupled superconductors has advanced greatly since its beginning in 1962. Chapter 1 of this thesis catalogs the ideas which in the author's opinion form the foundation of current effort in this area. Chapter 2 and Chapter 3 report on research conducted by the author in an attempt to describe in more detail the dynamics of the proximity effect bridge, a Josephson device showing major promise in applications ranging from magnetometry to far-infrared radiation detectors.

Chapter 2 deals with the zero voltage regime in which equilibrium thermodynamics applies. The superconducting quantum interferometer was used as a tool to establish that the proximity effect bridge obeys the same equations at zero voltage as were proposed by Josephson for the tunneling junction.

Chapter 3 covers situations in which nonequilibrium processes are expected to cause major deviations from the Josephson tunneling equations. The interaction of proximity effect bridges with superconducting microstrip resonators was explored both as an end in itself and as a means to estimate the amplitude of the supercurrent oscillation in these bridges. It was found that as the voltage increases the amplitude undergoes a transition from that expected from classical Josephson equations towards the smaller relative amplitude expected from the nonequilibrium phase-slip theories. Similar but less marked trend towards a relative reduction of the oscillation amplitude was seen with increasing critical current in these devices.

I. MACROSCOPIC QUANTUM EFFECTS - THEORY

1.1 The Macroscopic Wavefunction

The macroscopic wavefunction concept was introduced by London (Ref. 1) who proposed that superconductivity is a phase in which electrons are condensed into a single state described by a single wavefunction $\psi = \psi(\vec{r}, t)$. This description was taken further by Ginzburg and Landau (GL) (Ref. 2) with particular attention to the temperature regime in the vicinity of the superconducting transition. In 1957, Bardeen, Cooper and Schrieffer (BCS) (Ref. 3) developed a microscopic theory of superconductivity based on the phonon mediated electron-electron interaction. Since both the London and GL theories are derivable from the BCS theory, the latter will be used as a starting point in this discussion.

In the BCS picture pairwise attraction between electrons near the Fermi level occurs via the distortion of the lattice induced by each member of a pair. Below a certain transition temperature this attraction results in the formation of bound electron pairs with antiparallel spins. These pairs have many characteristics of bosons and are condensed into a single state as predicted by London. According to BCS a certain minimum energy is required to break up an existing pair. The energy is designated $E_g = 2\Delta(T)$ and is referred to as the energy gap at temperature T . The excitations resulting from pair breaking are called quasiparticles, and it can be shown (Ref. 4) that they behave like electrons in a normal (non-superconducting) metal.

At finite temperatures, pairs are broken by thermal agitation which leads to a dynamic equilibrium between quasiparticles and pairs. The two fluids, the pair fluid and the quasiparticle fluid can be approximately considered as mutually noninteracting.

The condensate of electron pairs can be represented by a London wavefunction

$$\psi(\vec{r}, t) = \sqrt{\rho(\vec{r}, t)} e^{i\varphi(\vec{r}, t)} \quad (1.1)$$

where $\rho(\vec{r}, t)$ is the electron pair density and $\varphi(\vec{r}, t)$ is the phase of the wavefunction. In general the pair density depends on temperature and pair velocity and should be calculated using the full BCS or GL theory. Nevertheless, at a given temperature and velocity well below critical velocity the condensate obeys simple quantum mechanics (Ref. 5). Applying the quantum mechanical expression for electrical current density to the form (1.1) leads to

$$\vec{J} = -\frac{2e\hbar}{m} (\vec{\nabla}\varphi + \frac{2e}{\hbar} \vec{A}) \rho \quad (1.2)$$

where \vec{A} is the magnetic vector potential and $-2e$ is the charge of an electron pair. For bulk simply connected superconductors, one can work in the London gauge (Ref. 6) where $\vec{\nabla} \cdot \vec{A} = 0$ in the superconductor. Assuming $\rho(\vec{r}, t) = \text{const.}$ and $\vec{\nabla} \cdot \vec{J} = 0$ (steady state) it can be seen that in the superconductor

$$\nabla^2 \varphi = 0 \quad (1.3)$$

This implies $\vec{\nabla}\varphi = 0$ everywhere since on the surface of the superconductor $(\vec{\nabla}\varphi)_n = 0$. Therefore equation (1.2) yields

$$\vec{J} = -\frac{4e^2}{m} \rho \vec{A} \quad (1.4)$$

Equation (1.4) is the London equation. The magnetic vector potential is related to its source current by

$$\nabla^2 \vec{A} = - \frac{1}{\epsilon_0 c^2} \vec{J} \quad (1.5)$$

Combining (1.4) and (1.5)

$$\nabla^2 \vec{A} = \frac{4e^2 \rho}{\epsilon_0 c^2 m} \vec{A} \equiv \frac{1}{\lambda^2} \vec{A} \quad (1.6)$$

where λ is the London penetration depth (typ. $10^2 - 10^3 \text{ \AA}$). The physical solution of equation (1.6) is a potential \vec{A} which decays exponentially from the surface of the superconductor inward with decay length λ . Thus the magnetic field many penetration depths λ inside the superconductor is zero (Ref. 7). From equation (1.4) it follows that the supercurrent density \vec{J} is distributed similarly to the magnetic vector potential.

Next a piece of superconductor which is not simply connected (e.g., a ring) shall be considered. Rewriting equation (1.2) one obtains

$$\vec{\nabla} \varphi = - \frac{m}{2e\hbar\rho} \vec{J} - \frac{2e}{\hbar} \vec{A} \quad (1.7)$$

Integrating once around the ring

$$\Delta\varphi_\sigma = - \frac{m}{2e\hbar} \oint \frac{\vec{J}}{\rho} \cdot d\vec{\ell} - \frac{2e}{\hbar} \oint \vec{A} \cdot d\vec{\ell} \quad (1.8)$$

But the wavefunction (1.1) must have only one value at a given point which implies that

$$\Delta\varphi_\sigma = 2\pi n$$

and

$$\oint \vec{A} \cdot d\vec{\ell} + \frac{m}{4e} \oint \frac{\vec{J}}{\rho} \cdot d\vec{\ell} = \frac{\hbar n}{2e} = n \Phi_0 \quad (1.9)$$

i. e.,

$$\oint \vec{A} \cdot d\vec{l} + \mu_0 \oint \lambda^2 \vec{J} \cdot d\vec{l} = n \Phi_0 \quad (1.10)$$

where Φ_0 is called the flux quantum. The first left hand side term of equation (1.10) is just the magnetic flux through the path of integration. If the path is taken deep inside the superconducting material of the ring, $J_s = 0$ and the magnetic flux through the ring is

$$\Phi = \oint \vec{A} \cdot d\vec{l} = n \Phi_0 \quad (1.11)$$

which is referred to as "quantization of flux". This phenomenon has been observed experimentally (Ref. 8).

1.2 The Boundary of a Superconductor

At the boundary between a superconductor and vacuum two processes take place. Some electrons which are bound in pairs in the superconductor penetrate the boundary (with roughly the velocity v_F , the Fermi velocity) and "depair" (lose their pair binding energy 2Δ). Also, the penetrating electrons find themselves in the negative energy region outside the superconductor formed by the work function of the metal W and the image potential, and are reflected back into the superconductor. The characteristic lengths for the two processes are the depairing length ξ and the tunneling length d . These can be estimated using the uncertainty principle with $\Delta \sim 1$ meV, $W = 5$ eV,

$$v_F = 2 \times 10^6 \text{ m/sec}$$

$$\begin{aligned} \xi &\sim v_F \cdot \frac{\hbar}{2\Delta} \sim 2000 \text{ \AA} \\ d &\sim \frac{\hbar}{\sqrt{2m_e W}} \sim 2 \text{ \AA} \end{aligned} \quad (1.12)$$

Therefore at a superconductor-vacuum interface the distance for pair penetration is dominated by the tunneling length d . Similarly, at a boundary of a superconductor and an insulating dielectric, the electrons leaving a superconductor encounter an energy barrier in the form of the band gap (typically a few eV). The resulting tunneling length d is of the same order as at the superconductor-vacuum interface.

At a superconductor-normal metal interface (S-N) the situation is different. The Fermi levels in the two metals have equalized and single electrons are energetically free to move between the two metals. The decay length of the pair wavefunction will therefore be determined by the depairing distance for Cooper pairs. It can be shown that this distance is (in the long mean free path limit)

$$\xi_{SN} = v_F \frac{\hbar}{3k_B(T-T_{c2})} \quad (1.13)$$

where T_{c2} is the superconducting transition temperature of the normal metal (i.e., $T > T_{c2}$). The pair wavefunction therefore has a finite amplitude in the normal metal due to pair diffusion and similarly normal electrons diffuse in the opposite direction into the superconductor. Such normal electron diffusion diminishes the equilibrium pair density in the vicinity of the boundary, thereby decreasing the gap energy $2\Delta(T)$ as if the temperature of the superconductor at the boundary were raised. This is referred to as the "proximity effect".

If the S-N interface carries a current through the interface

in either direction the equilibrium between the condensed pairs and quasiparticles is upset, i.e., the injected particles exceed their equilibrium concentration. The disequilibrium is described in terms of electrochemical potentials for pairs μ_P (per electron) and quasiparticles μ_Q with definitions

$$2\mu_P \equiv \frac{\partial\varphi}{\partial t} \quad (1.14)$$

$$\mu_Q = \frac{\partial G_Q(T, \rho_Q, \bar{\Phi})}{\partial \rho_Q} \quad (1.15)$$

where φ is the phase of the macroscopic wavefunction and $G_Q(T, \rho_Q, \bar{\Phi})$ is the Gibbs free energy of quasiparticles as a function of temperature, quasiparticle density and electrostatic potential. The position dependence of electrochemical potentials μ_P and μ_Q near an S-N interface has been studied by Yu and Mercereau (Ref. 9) who showed that while μ_Q has a gradient across the boundary, μ_P stays constant. This is reasonable since for quasiparticles

$$\vec{J}_N = \sigma \frac{\nabla\mu_Q}{e} \quad (1.16)$$

where σ is the normal conductivity of the metal, whereas for pairs (see equation 1.2) ($\partial\vec{A}/\partial t = 0$ assumed).

$$\frac{\partial\vec{J}_S}{\partial t} = \frac{\partial}{\partial t} \left(\frac{-2e\rho\hbar}{m} \vec{\nabla}\varphi \right) = \frac{4e^2\rho}{m} \cdot \frac{\vec{\nabla}\mu_P}{e} \quad (1.17)$$

If the pair electrochemical potential developed a gradient, the supercurrent would accelerate and a steady state could not be achieved. Since the total current density $\vec{J} = \vec{J}_S + \vec{J}_N$ is constant across the S-N boundary, the decay of the supercurrent \vec{J}_S in

space must correspond to an appropriate increase in the normal current \vec{J}_N so that

$$\nabla \cdot (\vec{J}_S + \vec{J}_N) = 0 \quad (1.18)$$

The other assumption used in S-N interface studies is the relaxation approximation according to which the deviation from equilibrium $\mu_Q - \mu_P$ is proportional to the rate of "minority carrier" accumulation

$$\mu_Q - \mu_P \propto \nabla \cdot \vec{J}_N = -\nabla \cdot \vec{J}_S \quad (1.19)$$

Combining this expression with equation (1.16) and the constancy of μ_P one obtains

$$\nabla^2 (\mu_Q - \mu_P) = \frac{\mu_Q - \mu_P}{\lambda_{QP}^2} \quad (1.20)$$

where λ_{QP} is the relaxation length describing the spatial extent of the nonequilibrium region for mutual pair-quasiparticle conversion (Ref. 10). The constant λ_{QP} presumably depends both on the material and the nature of the dominant relaxation process for pair-quasiparticle conversion. Since deep inside the superconductor both pair and quasiparticle densities are nonzero (at finite temperatures) $\mu_Q - \mu_P = 0$ must hold there. Deep inside the normal metal the tail of the pair wavefunction is broken by thermal agitation and μ_P is not defined.

1.3 Junctions in the Weak Coupling Limit

When two pieces of superconductor are brought into proximity such that the behavior of the pair wavefunction in one superconductor perturbs the pair wavefunction in the other

superconductor, a device with many interesting properties is produced--a Josephson device. The situation first considered by Josephson (Ref. 11) involved two pieces of superconductor separated by a small (= a few tunneling lengths d) insulating oxide space (typically 30 \AA thick); but as expected from the discussion in section 1.2, this distance may be made longer ($\sim 400 \text{ \AA}$) if the space separating the superconductors is filled with a semiconductor (Ref. 12). A Schroedinger equation for the two coupled superconductors (Ref. 13) may be written as

$$i \hbar \frac{\partial}{\partial t} \begin{pmatrix} \psi_1 \\ \psi_2 \end{pmatrix} = \begin{pmatrix} \mu_1 & K \\ K^* & \mu_2 \end{pmatrix} \begin{pmatrix} \psi_1 \\ \psi_2 \end{pmatrix} \quad (1.21)$$

where ψ_1 , and ψ_2 are the macroscopic wavefunctions in superconductors 1 and 2 and K is the coupling between them, while μ_1 and μ_2 are the electrochemical potentials (per electron) for pairs in the two superconductors. Writing the wavefunctions in the form (1.1) and the coupling $K = ke^{i\kappa}$ one obtains that

$$\dot{\varphi} \equiv \frac{\partial}{\partial t} (\varphi_2 - \varphi_1) = \frac{2(\mu_2 - \mu_1)}{\hbar} \quad (1.22)$$

and

$$\dot{\rho}_1 = -\dot{\rho}_2 = -k\sqrt{\rho_1\rho_2} \sin(\varphi + \kappa) \quad (1.23)$$

where $\dot{\rho}_1$ is the initial rate of pair density loss that would occur if an external battery did not supply more electrons. Let ξ be the characteristic length over which the pair wavefunction responds to perturbation--the coherence length (Ref. 14) of the superconductor. Then the supercurrent flowing through a current biased junction is

$$J_S = -2e \dot{\rho}_1 \xi = k \xi \sqrt{\rho_1 \rho_2} \sin(\varphi + \kappa) \quad (1.24)$$

It is customary to define $J_0 \equiv k \xi \sqrt{\rho_1 \rho_2}$ and $\delta = \varphi + \kappa$ so that the Josephson equations can be written in simple form

$$J_S = J_0 \sin \delta \quad \text{and} \quad \dot{\delta} = \frac{2(\tilde{\mu}_1 - \tilde{\mu}_2)}{\hbar} = \frac{2eV}{\hbar} \quad (1.25)$$

where the chemical potential $\tilde{\mu} \equiv \mu - \hbar\kappa/2$.

It should be observed that for zero voltage $V = 0$ current still can flow, i.e., the Josephson device superconducts. The maximum supercurrent density that can be thus conducted is J_0 , called the critical current density of the junction. In the absence of a directional influence in the junction (such as magnetic field or voltage) we may set $\kappa = 0$. In the presence of magnetic field gauge invariance requires that

$$\kappa = -\frac{2e}{\hbar} \int_1^2 \vec{A} \cdot d\vec{\ell}$$

where the integral is taken between the reference points for the phase difference $\varphi = \varphi_2 - \varphi_1$.

If by some means a voltage $V = \frac{\tilde{\mu}_2 - \tilde{\mu}_1}{e}$ is maintained across the junction, the Josephson equations indicate that the supercurrent will oscillate at the frequency

$$f = \frac{2e}{h} V \quad (1.26)$$

The factor $\frac{2e}{h}$ has the magnitude 484 MHz/ μ V. In addition the voltage across the junction will also produce a flow of quasiparticles across the barrier,

$$J_N = V/R \quad (1.27)$$

where \mathcal{R} is the resistance per square of the junction. The total current density through a Josephson device is then

$$J = J_S + J_N = J_0 \sin \delta + V/\mathcal{R} \quad (1.28)$$

where

$$\delta = \frac{2e}{\hbar} \int V dt \quad (1.29)$$

In the original paper by Josephson (Ref. 11) an additional so-called pair-quasiparticle interference term was included. Its size is currently under active scrutiny in many laboratories (Ref. 15).

1.4 The Phase Slip Model

Whereas the weak coupling model deals with a situation where two pieces of superconductor are separated by an insulating barrier, Josephson phenomena have also been observed in geometries where the barrier is not insulating. In such situations the so-called phase slip process is believed to be responsible. It is convenient to consider the case where a section of a superconducting strip is locally "weakened" by one of several techniques (Ref. 16). The "weakening" leads to a local decrease in the transition temperature compared to the surrounding superconductor. Often the proximity effect (see section 1.2) is used to depress the transition temperature in a section of the superconducting strip and such structures are called proximity effect bridges (Ref. 17). If the weak link is not much longer than the pair decay length ξ_{SN} and the bridge is operated just above the transition temperature of the weak section the decaying tails of the pair wavefunction produce a small but finite pair density within the

weak link (Fig. 1). To consider the behavior of the proximity effect bridge it will be assumed for simplicity that the bridge is sufficiently narrow to be treated as one-dimensional (Ref. 18). In the absence of voltage the phase-slip model predicts that the bridge behaves like an ordinary superconductor. When voltage is applied the model predicts that a relaxation oscillation of the supercurrent will occur. The gradient of the pair potential maintained by the battery voltage and concentrated in the weak link region accelerates the pairs until the depairing velocity (Ref. 19) is exceeded. At that point the further existence of pairs is energetically unfavorable and the pairs will depair. (Such depairing is a non-equilibrium dissipative process and its occurrence invalidates the assumptions (Ref. 20) of the weak coupling model.) However, if depairing becomes complete in the junction region, only normal current is conducted by the bridge--a situation which is also energetically unfavorable. The pair wavefunction therefore reforms but the reformed pairs have a subcritical velocity. They are again accelerated and the process repeats itself. A rigorous treatment of this phenomenon would involve the dynamics of pairing and depairing in space and time (cf. the weak coupling model). A complete theory of the phase-slip process is not currently available but attempts have been made to extract the significant features. These use the time-dependent Ginzburg-Landau theory (Ref. 21) or various forms of weak coupling theory with the inclusion of some non-equilibrium effects (Ref. 22). The gist of the phase-slip theory

and some results will be presented.

The weak link is treated as a superposition of an S-N and N-S boundary separated by the length of the link (Fig. 1). For zero current the pair wavefunction decays with decay length ξ_{SN} (see section 1.2) from both sides towards the center of the bridge. Since the supercurrent density is (assuming the vector potential $\vec{A} = 0$)

$$J_S = - \frac{2e\rho_S \hbar}{m} \nabla\varphi \quad (1.30)$$

there is no phase difference across the bridge for zero supercurrent. In order to change the supercurrent a voltage must be applied across the bridge since, by definition

$$\hbar \frac{\partial\varphi}{\partial t} = 2\mu_P \quad (1.31)$$

the total phase difference across the bridge will be

$$\varphi_2 - \varphi_1 = \int_0^t \frac{2(\mu_{P2} - \mu_{P1})}{\hbar} dt \quad (1.32)$$

The phase difference is not distributed evenly along the weak link. At the center where the pair density is the smallest the flow of supercurrent must be accompanied by a large phase gradient. During the acceleration part of the cycle the phase gradient increases until the critical value $|\nabla\varphi| \sim \frac{1}{\xi_{SN}}$ is reached at the center. In the GL theory the pair density is given by

$$\rho_S \propto 1 - \xi_{SN}^2 |\nabla\varphi|^2 \quad (1.33)$$

so that when $|\nabla\varphi| = 1/\xi_{SN}$ the pair density is zero and superconductivity breaks down at the center. This allows the phase to slip by 2π and decrease the phase gradient so that a finite pair

Figure 1. (not to scale) The distribution of pair density ρ along a proximity effect bridge of length L .

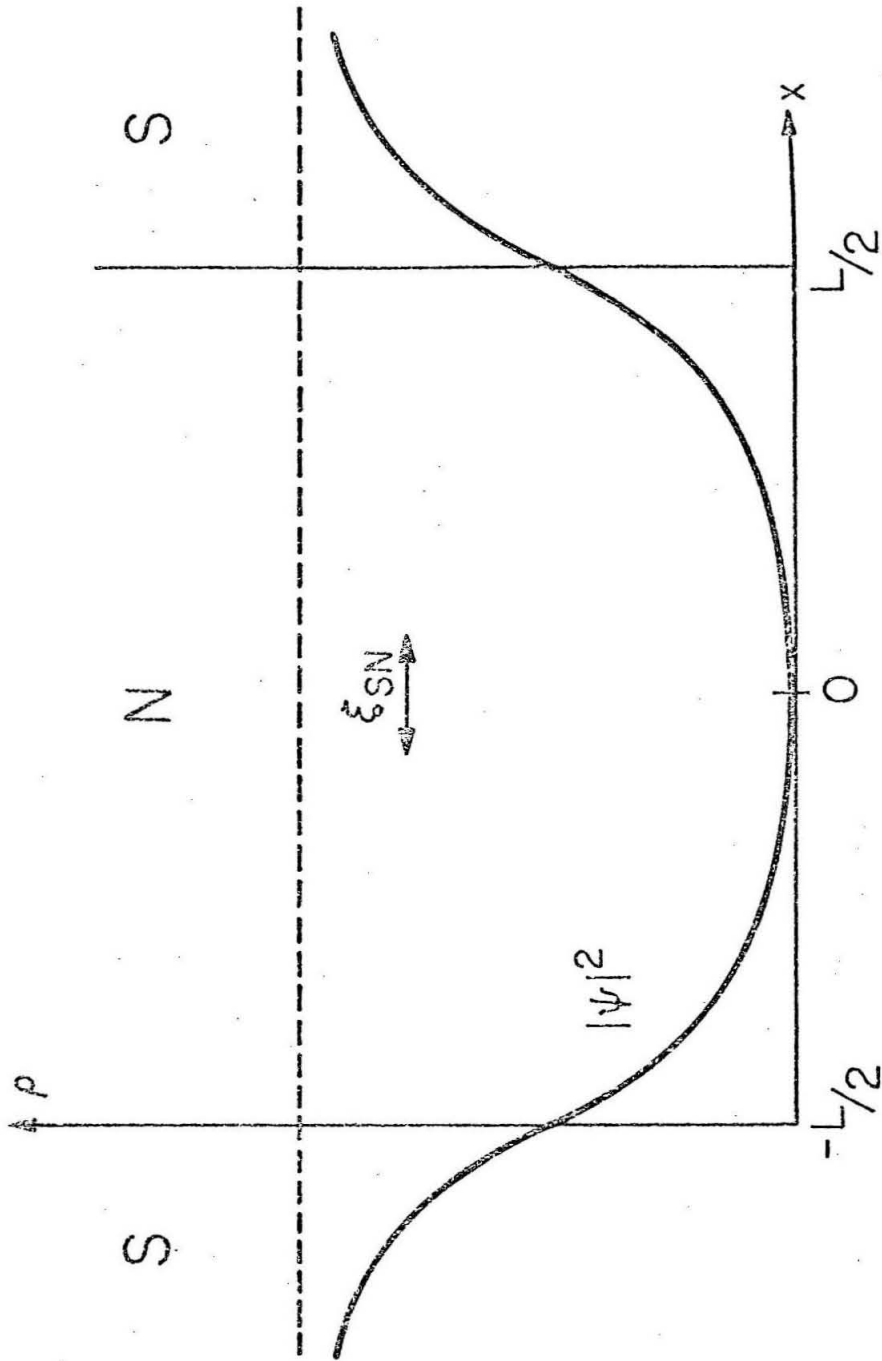


Figure 1

density can be reestablished. Detailed models have been constructed to describe the time-dependence of the supercurrent under the phase-slip conditions (Ref. 21). According to these models the supercurrent through the phase-slip center undergoes a relaxation oscillation at the Josephson frequency $\omega = \frac{2eV}{\hbar}$.

The time average supercurrent density is

$$\bar{J}_S \approx 0.5 - 0.6 J_C \quad (1.34)$$

where J_C is the peak supercurrent density (= the critical current density).

Experimentally it is found that in a sufficiently short weak link (proximity effect bridge) the oscillating current extends over the entire length of the bridge $L \gg \xi_{SN}$, even though the size of the region over which superconductivity breaks down periodically is expected to be only ξ_{SN} . This is not understood in detail at present. A semiquantitative theory was worked out for the situation where a phase-slip center (a small weak spot?) is located in a homogeneous superconducting whisker or thin film strip (Ref. 23). In such cases experiments show that oscillating currents extend over distances $\sim 10\mu$ around the phase-slip centers in tin whiskers and strips. This distance ($\sim 10\mu\text{m}$ in tin) is thought to be the characteristic distance (eq. 1.20) for the relaxation of the quasiparticle chemical potential μ_Q and the pair potential μ_P to each other, i. e.,

$$\nabla^2(\mu_P - \mu_Q) = \frac{\mu_P - \mu_Q}{\lambda_{QP}^2} \quad (1.35)$$

where $\lambda_{QP} \sim 10 \mu\text{m}$ in tin. Consistently with this equation, the normal current distribution can be written as

$$J_N \equiv \frac{\sigma}{e} \nabla \mu_Q = \frac{V\sigma}{2\lambda_{QP}} e^{-|x|/\lambda_{QP}} \quad (1.36)$$

where $|x|$ is the distance from the phase-slip center and V is the voltage across the phase-slip center between points many λ_{QP} distant from it (Fig. 2). For short weak links ($\xi_{SN} \ll L \ll \lambda_{QP}$) the normal and supercurrents probably have little spatial variation along the link since the S-N boundaries at the ends of the link function as quasiparticle mirrors (Ref. 24) cutting off the exponential decay (eq. 1.36) before a significant drop occurs.

The spatial constancy of the supercurrent and the normal current along a short weak link justifies the use of the two-fluid model of the weak link in which the voltage across the link is assumed to be

$$V = \mathcal{R}(J_T - J_S) \quad (1.37)$$

where \mathcal{R} is the normal resistance per unit width of the link, J_T is the total (bias) current density and J_S , the supercurrent density, is calculated at the phase-slip center. For weak links whose length $L \sim \lambda_{QP}$, substantial deviations from the simple two-fluid model are likely to occur.

In summary, the phase-slip model of a weak link describes the periodic breakdown of superconductivity at the center of the weak link in a region of size $\sim \xi_{SN}$ which causes the supercurrent at the center to undergo relaxation oscillation at the Josephson

Figure 2. The distribution of normal current J_N and the pair (μ_P) and quasiparticle (μ_Q) chemical potentials as a function of the distance \bar{x} from the phase-slip center in a homogeneous superconductor (above), and in a short ($L < \lambda_{QP}$) proximity effect bridge (below).

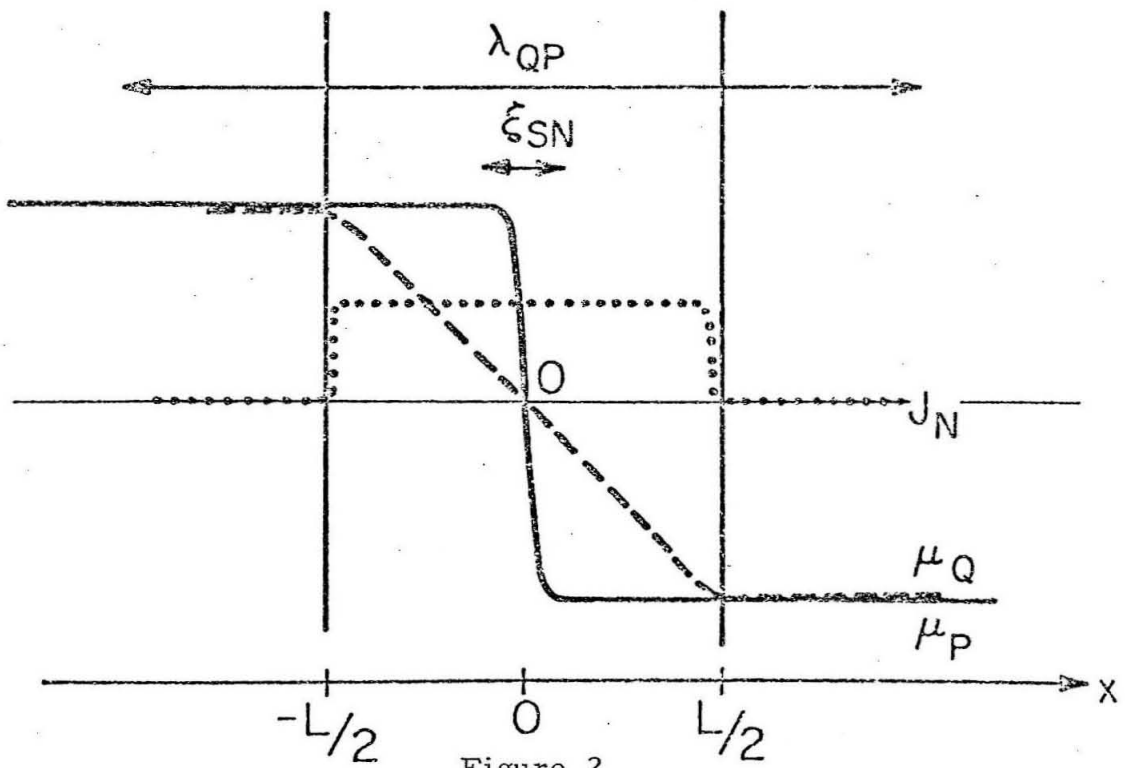
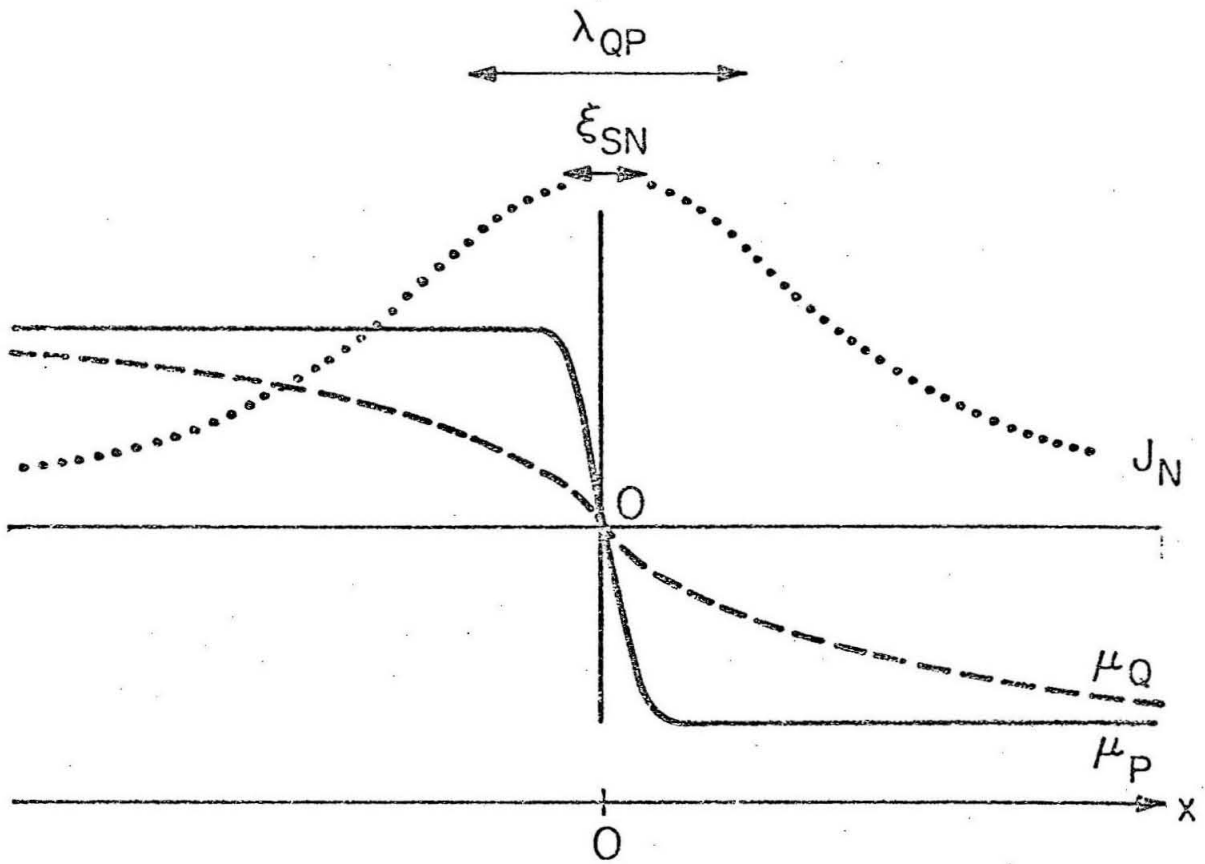


Figure 2

frequency $\omega = \frac{2e\bar{V}}{\hbar}$. In a current biased weak link the oscillation of the supercurrent is accompanied by the counter-oscillation of the quasiparticle current. If the weak link is shorter than the relaxation length λ_{QP} both the quasiparticle and the pair currents are spatially uniform along the weak link and follow the dynamics at the phase slip center. Accordingly the time-average supercurrent density through the entire weak link is given by equation (1.34).

Kirschman, Notarys and Mercereau (Ref. 25) proposed that experimental measurements on proximity effect bridges are consistent with

$$J_S = \frac{J_c}{2} \left[1 + \cos\left(\frac{2e}{\hbar} \int V dt\right) \right] \quad (1.38)$$

This waveform differs little from detailed theoretical phase-slip waveforms (Ref. 21).

1.5 The Current-Voltage Characteristic of Josephson Devices

In the previous sections the weak coupling and the phase-slip models were presented. The voltage in both cases was given by the equation

$$V = R(J_T - J_S) \quad (1.39)$$

where J_T , J_S are the total and super current densities and R is the resistance per square of the current carrying area of the device. If the current is distributed uniformly across a uniform junction area (cf. section 1.6) then

$$V = R(I_T - I_S) \quad (1.40)$$

where R is the total resistance of the device and I_T , I_S are the

total and super currents respectively. In the preceding equations the capacitance of the device has been neglected. Typically, for proximity effect bridges $R = 0.1 \Omega$ and $C < 1 \text{ pF}$ so that the shunt capacitive impedance becomes important at $f \sim 10^{12} \text{ Hz} = 10^3 \text{ GHz}$.

In DC measurements the time average voltage \bar{V} is measured. It can be shown (see Chapter 3) that for the weak coupling model (Fig. 3) the time average voltage is

$$\bar{V} = R \sqrt{I_T^2 - I_c^2} \quad (1.41)$$

whereas for the phase slip model (Fig. 3)

$$\bar{V} = R \sqrt{I_T(I_T - I_c)} \quad (1.42)$$

In both cases I_c is the critical current, i.e., the maximum supercurrent of the device at the given temperature. Asymptotically, for $I_T/I_c \gg 1$ we obtain in the weak coupling model that

$$\bar{V} \rightarrow RI_T$$

but in the phase-slip model

$$\bar{V} \rightarrow R(I_T - I_c/2)$$

The term $I_c/2$ in the phase-slip characteristic is referred to as "Excess supercurrent" and is a direct consequence of the non-equilibrium nature of the model. Experimentally, R is roughly the resistance of the bridge at a temperature above the onset of any measurable supercurrent. Excess supercurrent $\sim 0.5 I_c$ is seen in proximity effect bridges (Ref. 26), tin bridges and whiskers and S-N-S junctions. It is not seen in insulating or semiconductor barrier bridges.

Figure 3. The I-V characteristics (normalized) of a Josephson device of resistance R and critical current I_C in the weak coupling model (solid curve) and in the phase-slip model (dashed curve). The respective asymptotes are also shown (thin lines).

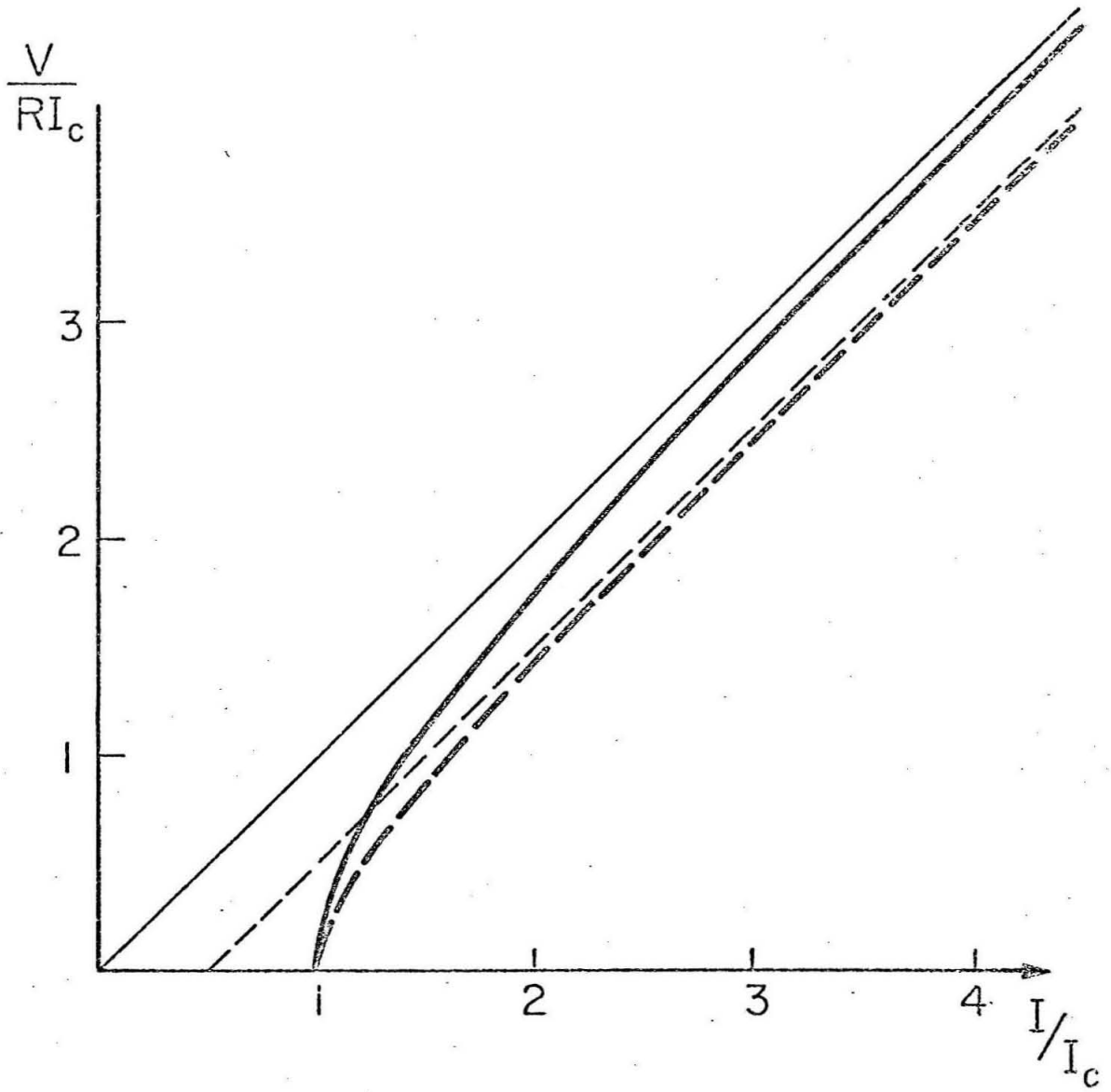


Figure 3

The addition of an RF current to the biasing current of a Josephson device causes constant voltage "steps" to appear in the I-V characteristic of the device (Fig. 4). The mathematical details of this behavior are complicated but have been subject to much investigation (Ref. 27). Physically the steps are a result of phase locking between the external RF current and the oscillating supercurrent of the bridge, accompanied by frequency pulling, so that the voltage (and also the frequency of the supercurrent oscillation) stays constant over a range of DC bias currents. The phenomenon has been used in microwave and far infrared detectors.

1.6 Quantum Interference Effects in Magnetic Fields

The phenomenon of quantum interference in magnetic fields has been of much importance both in the understanding of superconductivity as a macroscopic quantum state (Ref. 28) and in applications (Ref. 29). Experimentally it is manifested by periodic changes of the supercurrent as a function of magnetic field. Fundamentally, the effects stem from the requirement of gauge invariance of the supercurrent density.

The behavior of a thin film Josephson device (\equiv bridge) will be considered next. Suppose that a bridge is formed in a thin superconducting film by local weakening of the superconductor (Fig. 5). The structure will be described by a general phase-supercurrent density relation (gauge invariant)

$$J_S = J_c f\left(\varphi + \frac{2e}{\hbar} \int_0^L A_x dx\right) \quad (1.43)$$

Figure 4. External RF (2 GHz) induced steps in the I-V and $\overline{dV/dI}$ vs. I characteristics of an experimental proximity effect bridge. The dashed curve is the characteristic in the absence of external RF radiation.

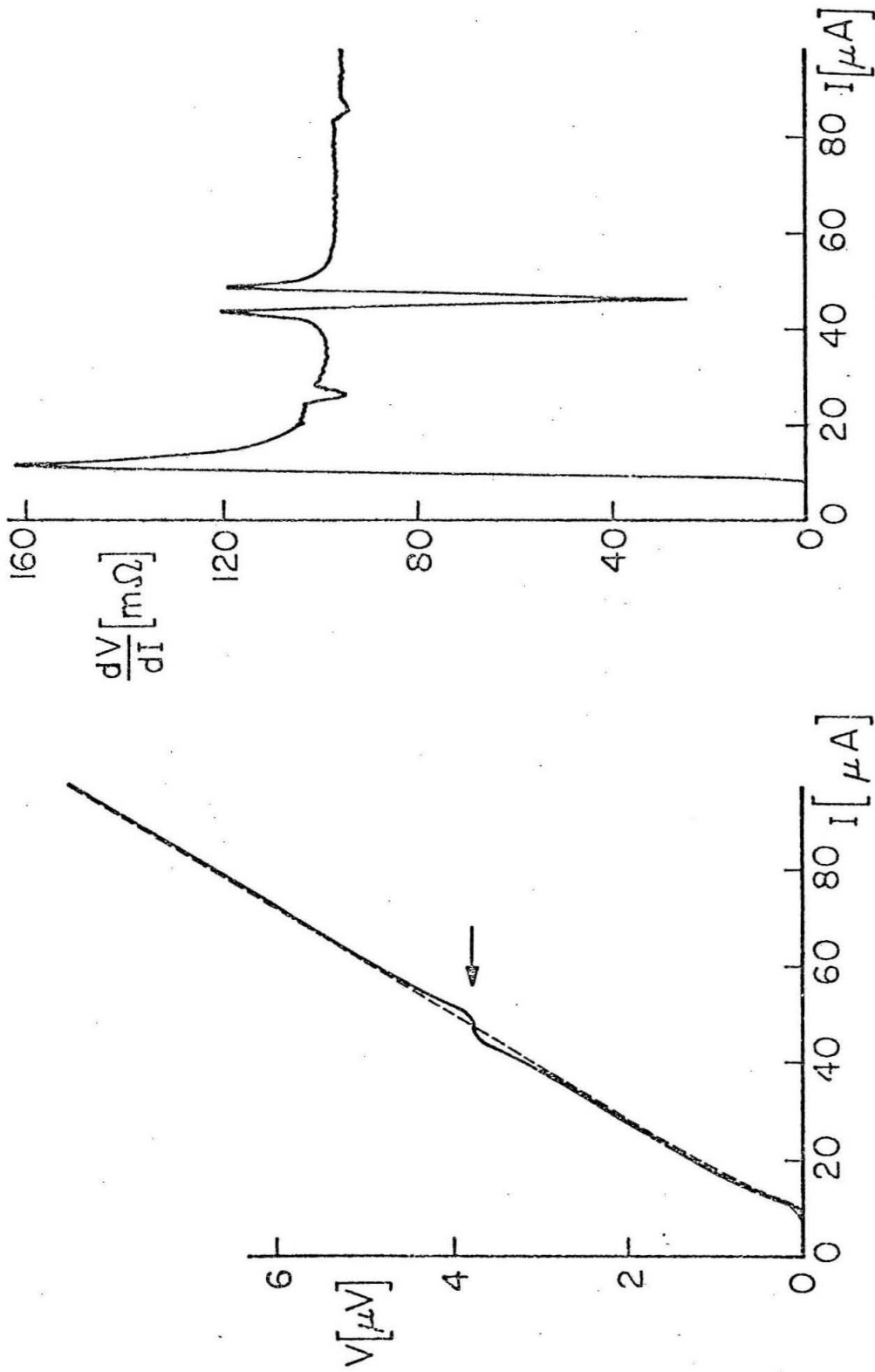


Figure 4

Figure 5. The geometry of a bridge of length L , width w , and thickness d .

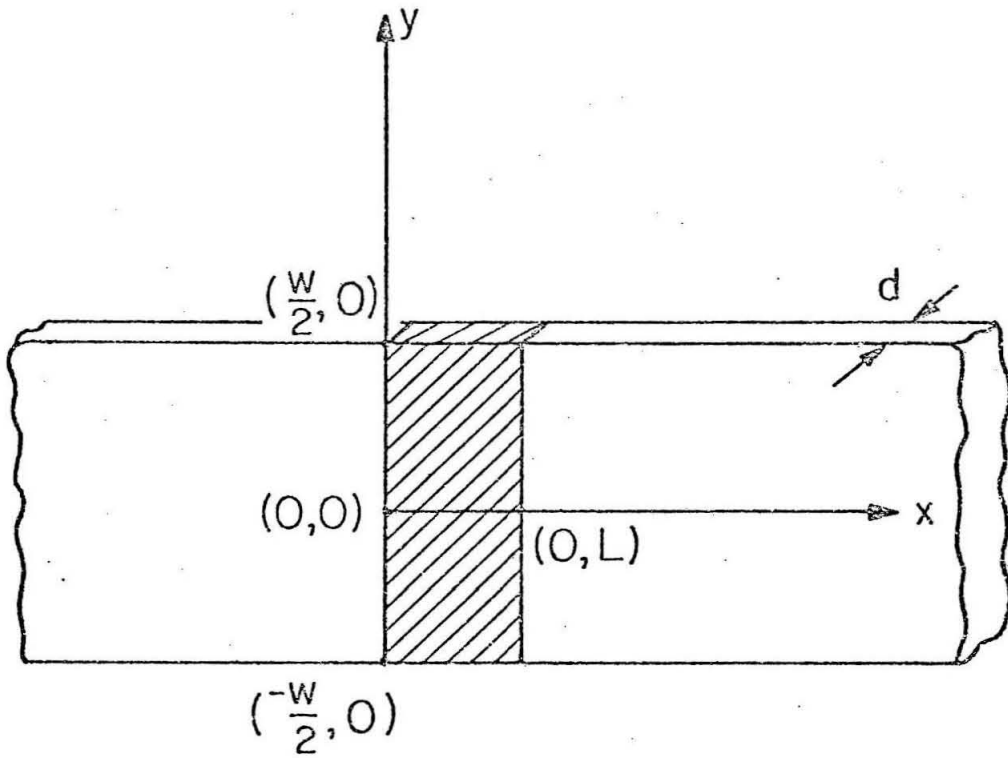


Figure 5

where f attains a maximum value of 1 and $\varphi(y)$ is the phase difference across the bridge between the points $(0, y)$ and (L, y) .

It is assumed that both the phase φ and the vector potential $\vec{A} = (A_x, A_y, A_z)$ do not vary over the film thickness d . (In Nb-Ta proximity effect bridges $d \sim 100 \text{ \AA}$, width $w = 5-50 \text{ \mu m}$, $L = 0.3-1.0 \text{ \mu m}$). The supercurrent variation across the thickness of the film is therefore neglected and the supercurrent I_S is given by

$$I_S = J_c \cdot d \cdot \int_{-w/2}^{w/2} f \left[\varphi(y) + \frac{2e}{\hbar} \int_0^L A_x(y) dx \right] dy \quad (1.44)$$

Expressing the transverse dependence of the phase as

$$\varphi(y) = \int_0^y \frac{\partial \varphi}{\partial y} dy + \varphi(0) \quad (1.45)$$

and using equation (1.7)

$$\partial \varphi(y) / \partial y = \partial \varphi_1(L, y) / \partial y - \partial \varphi_2(0, y) / \partial y \quad (1.46)$$

$$\partial \varphi(y) / \partial y = -\frac{m}{2e\hbar\rho} [J_y(L, y) - J_y(0, y)] - \frac{2e}{\hbar} [A_y(L, y) - A_y(0, y)]$$

the equation for the bridge supercurrent can be rewritten to obtain

$$I_S = J_c \cdot d \cdot \int_{-w/2}^{w/2} f \left[\varphi(0) - \frac{2e}{\hbar} \int_0^L A_x(0) dx - \frac{\pi \Phi_B(y)}{\Phi_0} \right] dy$$

where

$$\Phi_B(y) = \frac{2e}{\hbar} \left[\oint_{\Gamma(y)} \vec{A} \cdot d\vec{\ell} - \frac{m}{2e\hbar\rho} \int_0^y [J_y(L, y) - J_y(0, y)] dy \right] \quad (1.47)$$

The quantity $\Phi_B(y)$ has contributions from two sources: it includes the magnetic flux through the part of the bridge between 0 and y but in addition it contains terms due to transverse currents screening the film at the two ends of the bridge from the bridge

magnetic flux. In the absence of magnetic field, $\Phi(y) = 0$ and

$$I_S = J_c \cdot d \cdot w f(\varphi(0)) \equiv I_c f(\varphi(0)) \quad (1.48)$$

For small magnetic fields such that $\bar{\Phi}_B (w/2) \ll \Phi_0$ the supercurrent is

$$I_S = I_c(0) \left\{ f \left[\varphi(0) + \frac{2e}{\hbar} \int_0^L \vec{A} \cdot d\vec{\ell} + \frac{\pi \bar{\Phi}_B^2}{\Phi_0^2} f'(\varphi(0)) \right] \right\} \quad (1.49)$$

where

$$\bar{\Phi}_B^2 = \frac{1}{w} \int_{-w/2}^{w/2} \Phi_B^2(z) dz$$

The dependence of the supercurrent on the magnetic field B can be solved in a closed form if a sinusoidal current-phase relation is assumed (Ref. 30). In general magnetic fields decrease the maximum supercurrent I_S in a periodic fashion so that a diffraction-like pattern (Ref. 31) is seen as a function of applied magnetic field B.

The behavior of two bridges joined in a ring (Fig. 6) is simpler. It will be considered in the limit that the magnetic field is small enough so equation (1.49) holds. The total phase change along a circle going through the center of the bridges is

$$\Delta\varphi_\sigma = (\Delta\varphi)_{AB} + (\Delta\varphi)_{BC} + (\Delta\varphi)_{CD} + (\Delta\varphi)_{DA} \quad (1.50)$$

For path segments outside the bridges equation (1.7) holds, i.e.,

$$\vec{\nabla}\varphi = -\frac{m}{2e\hbar\rho} \vec{J} - \frac{2e}{\hbar} \vec{A} \quad (1.51)$$

so that

$$\Delta\varphi_\sigma = (\Delta\varphi)_{AB} - (\Delta\varphi)_{DC} - \frac{2e}{\hbar} \oint' \vec{A} \cdot d\vec{\ell} - \frac{m}{2e\hbar\rho} \oint' \vec{J} \cdot d\vec{\ell} \quad (1.52)$$

where the prime indicates that the bridge regions are left out of

Figure 6. The superconducting quantum interferometer.

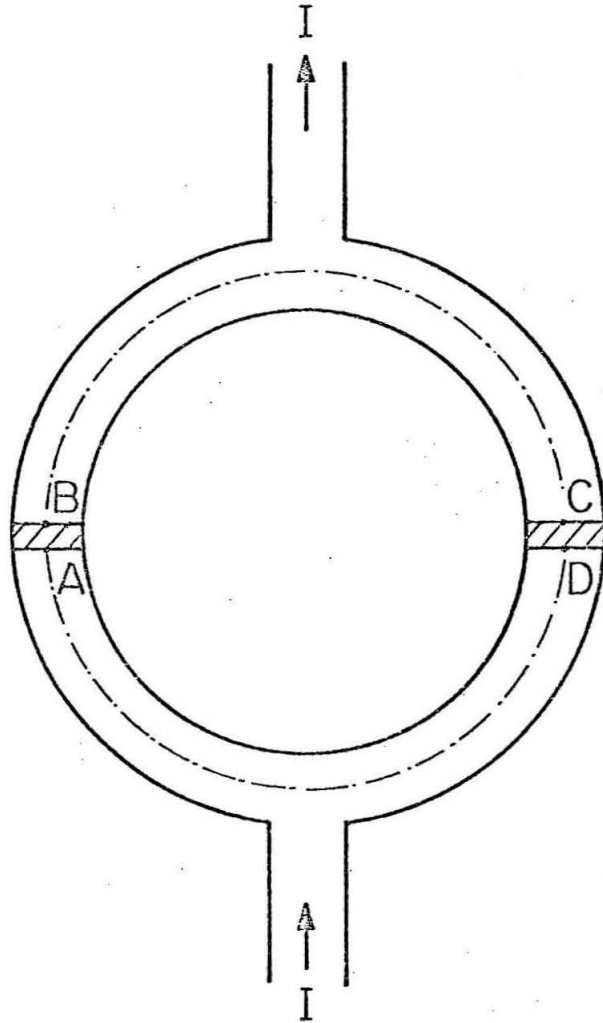


Figure 6

the path integrals. The equation can be rewritten as

$$\Delta\varphi_{\phi} = \delta_1 - \delta_2 - \frac{2e}{\hbar} \oint \vec{A} \cdot d\vec{l} - \frac{m}{2e\hbar\rho} \oint \vec{J} \cdot d\vec{l} \quad (1.53)$$

This time

$$\delta_1 = (\Delta\varphi)_{AB} + \frac{2e}{\hbar} \int_0^L \vec{A} \cdot d\vec{l}$$

$$2 \quad DC$$

is the gauge invariant phase which is the correct argument of the phase-current relations. $\Delta\varphi_{\phi}$ must be a multiple of 2π , otherwise the wavefunction would not be single-valued. So the quantization relation is gotten as

$$\delta_1 - \delta_2 = 2\pi n + \frac{2e}{\hbar} \oint \vec{A} \cdot d\vec{l} + \frac{m}{2e\hbar\rho} \oint \vec{J} \cdot d\vec{l} \quad (1.54)$$

In this equation $\oint \vec{A} \cdot d\vec{l}$ is the total magnetic flux through the path of integration consisting of contributions from external sources and from the supercurrents in the ring. Accordingly,

$$\delta_1 - \delta_2 = 2\pi \left(n + \frac{\Phi_E}{\Phi_0} + \frac{\Phi_S}{\Phi_0} + \frac{\Phi_K}{\Phi_0} \right) \quad (1.55)$$

where Φ_E , Φ_S , Φ_K are fluxes due to external magnetic fields, self-generated magnetic fields, and kinetic term respectively; and $\Phi_0 \equiv h/2e = 2 \times 10^{-15}$ Wb. At this point it is appropriate to comment on the term Φ_K . For the bridges

$$\dot{\delta} = \frac{2eV}{\hbar} \quad (1.56)$$

is the expression indicating that a voltage is needed to accelerate the pairs and thus cause a phase change. In fact the pairs in the rest of the circuit also have inertia, so that for the whole circuit one gets

$$EMF = \frac{d}{dt} \oint \vec{A} \cdot d\vec{l} = \dot{\delta}_1 - \dot{\delta}_2 - \frac{m}{2e\hbar\rho} \oint \vec{J} \cdot d\vec{l} \quad (1.57)$$

The last term simply indicates that the EMF accelerates pairs in the nonbridge parts of the ring as well. The total supercurrent through the two bridges is (neglecting small "single bridge" terms)

$$I_S = I_{c_1} f(\delta_1) + I_{c_2} f(2\pi n + \delta_1 - 2\pi \frac{\bar{\Phi}_K + \bar{\Phi}_S + \bar{\Phi}_E}{\bar{\Phi}_O}) \quad (1.58)$$

where the quantization condition (eq. 1.55) was used to replace δ_2 . In an experiment the phase δ_1 is fixed by the external current source. The maximum supercurrent I_c that can be passed through the interferometer at zero voltage is given by the condition

$$\frac{\partial I_S}{\partial \delta_1} = 0 \quad (1.59)$$

The equation is in reality quite complicated because the flux terms $\bar{\Phi}_S$ and $\bar{\Phi}_K$ depend on δ_1 through their dependence on currents passing in the ring.

To illustrate some features of the interferometer dynamics, the simple case of a symmetric interferometer is presented. Let $f(\delta) = \sin \delta$ and $I_{c_1} = I_{c_2} = I_o$. Then

$$I_S = I_c \sin \delta_1 - I_c \sin(\delta_1 + 2\pi \frac{\bar{\Phi}_E + \bar{\Phi}_K + \bar{\Phi}_S}{\bar{\Phi}_O}) \quad (1.60)$$

The diffraction terms can be included in I_o for this case so that

$$I_o = I_o(0) \left(1 - \pi^2 \frac{\bar{\Phi}_B^2}{\bar{\Phi}_O^2} \right) \quad (1.61)$$

Temporarily the terms $\bar{\Phi}_K$ $\bar{\Phi}_S$ shall be neglected. The maximum supercurrent for the interferometer shows quantum interference:

$$I_c = 2I_o \left| \cos \left(\pi \frac{\bar{\Phi}_E}{\bar{\Phi}_O} \right) \right| \quad (1.62)$$

The current is equally divided between the two bridges. The terms $\bar{\Phi}_K$, $\bar{\Phi}_S$ are in fact zero due to the symmetry of the geometry. (The asymmetric case is described in Chapter 2.)

References

1. F. London, Superfluids, vol. 1, John Wiley & Sons (1950)
2. V. L. Ginzburg and L. D. Landau, Sov. Phys. JETP 20, 1064 (1950)
3. J. Bardeen, L. N. Cooper, and J. R. Schrieffer, Phys. Rev. 108, 1175 (1957)
4. R. P. Feynman, Statistical Mechanics, pp. 298-303 W. A. Benjamin, Inc. (1972)
5. *ibid*, pp. 303-311
6. P. G. De Gennes, Superconductivity of Metals and Alloys, pp. 145-148, W. A. Benjamin, Inc. (1966)
7. *ibid*, pp. 3-7
8. B. S. Deaver and W. M. Fairbank, Phys. Rev. Letters 7, 43(1961); R. Doll and M. Nābauer, Phys. Rev. Letters, 7, 51(1961)
9. M. L. Yu and J. E. Mercereau, Phys. Rev. Letters 28, 1117 (1972)
10. T. J. Rieger, D. J. Scalapino, and J. E. Mercereau, Phys. Rev. Letters 27, 1787 (1971)
11. B. D. Josephson, Phys. Letters 1, 251 (1962)
12. I. Giaver, Phys. Rev. Letters 20, 1286 (1968); C. L. Huang and T. Van Duzer, Appl. Phys. Lett. 25, 753 (1974)
13. R. P. Feynman, Statistical Mechanics, pp. 306-311 W. A. Benjamin, Inc. (1972)
14. P. G. Gennes, Superconductivity of Metals and Alloys, pp. 217-225, W. A. Benjamin, Inc. (1966)
15. F. Auracher, P. L. Richards, and G. I. Rochlin, Phys. Rev. B 8, 4182 (1973)
16. H. A. Notarys and J. E. Mercereau, J. Appl. Phys. 44, 1821 (1973)
17. Stephen K. Decker, Ph. D. Thesis (California Institute of Technology 1975)
18. R. K. Kirschman, Ph. D. Thesis (California Institute of Technology 1972)

References (cont'd)

19. W. F. Vinen, Superconductivity (ed. by R. D. Parks), pp. 1168-1234, Marcel Dekker, Inc. (1969)
20. M. L. Yu, Ph. D. Thesis (California Institute of Technology 1974)
21. T. J. Rieger, D. J. Scalapino, and J. E. Mercereau, Phys. Rev. Letters 27, 1787 (1971)
22. H. A. Notarys, M. L. Yu and J. E. Mercereau, Phys. Rev. Letters 30, 743 (1973)
23. W. J. Skocpol, M. R. Beasley and M. Tinkham, J. of Low Temp. Phys. 16, 145 (1974)
24. A. F. Andreev, Sov. Phys. JETP 19, 1228 (1964)
25. R. K. Kirschman, H. A. Notarys, and J. E. Mercereau, Phys. Letters 34A, 209 (1971)
26. H. A. Notarys and J. E. Mercereau, Physica 55, 424 (1971)
27. P. A. Richards, F. Auracher, T. Van Duzer, Proc. IEEE 61, 36 (1973)
28. J. E. Mercereau, Superconductivity (ed. by R. D. Parks) pp. 393-421, Marcel Dekker, Inc. (1969)
29. S. K. Decker and J. E. Mercereau, Appl. Phys. Lett. 23, 347 (1973)
30. R. C. Jaklevic et al., Phys. Rev 140A, 1628 (1965)
31. H. A. Notarys and J. E. Mercereau, J. Appl. Phys. 44, 1821 (1973)

II. THE PHASE-CURRENT RELATION AT ZERO VOLTAGE IN PROXIMITY EFFECT BRIDGES

2.1 Historical Background

The phase-supercurrent relation for insulating barrier junctions was established to be sinusoidal (Ref. 1) soon after the discovery of the Josephson effect. For thin film bridges the situation remained confused for a long time, since in the naive picture a bridge can reach its critical current with an almost arbitrary phase difference across it, proportional to its length. In 1970, Baratoff et al. (Ref. 2) presented a theory (based on GL equations) according to which the phase-current relation is periodic with a period of 2π but is sinusoidal only in the limit of a very weakly superconducting link. In the same year Fulton and Dynes (Ref. 3) investigated experimentally the current-phase relation at zero voltage in Anderson-Dayem bridges. They concluded that the current-phase relation is "continuous, single valued" and "nearly sinusoidal" for critical currents smaller than $10 \mu\text{A}$. In 1972 Bardeen and Johnson (Ref. 4) using microscopic theory again proposed that the phase-current relation is sinusoidal for normal metal barrier junctions in the limit of weak coupling but is nonsinusoidal for strongly coupled junctions. In 1973, the investigation of the phase-current relation at zero voltage in proximity effect bridges was performed in our laboratory using a method similar to the Fulton-Dynes experiment. The results were presented at the American Physical Society meeting in San Francisco, December, 1973.

2.2 The Small Asymmetric Interferometer

The small asymmetric interferometer is the key element in the Fulton-Dynes method of measuring the phase-supercurrent relation. In terms of the interferometer equation (1.58) (Fig. 1)

$$I_S = I_{c_1} f(\delta_1) + I_{c_2} f\left(2\pi n + \delta_1 - 2\pi \frac{\bar{\Phi}_K + \bar{\Phi}_S + \bar{\Phi}_E}{\bar{\Phi}_O}\right) \quad (2.1)$$

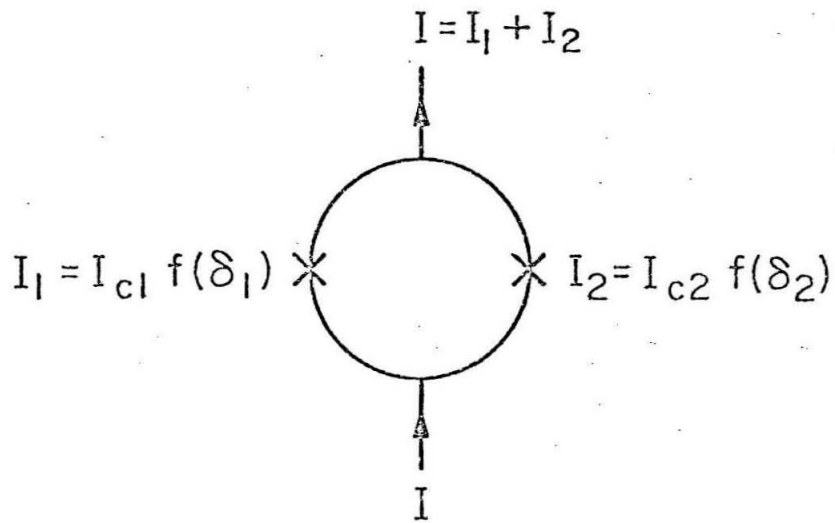
"small" means that the sum of the self-induced terms is small, i. e., $\bar{\Phi}_S + \bar{\Phi}_K < \bar{\Phi}_O$, and "asymmetric" means that $I_{c_1} \gg I_{c_2}$. As a first approximation, the critical current of the interferometer $I_c = I_{Smax}$ will be gotten by setting $\delta_1 = \delta_{1max}$ such that the first term is maximized. The second term is thereby allowed to vary as the magnetic flux from external sources is varied. The modulation of the interferometer critical current by magnetic flux is then

$$\Delta I_c = I_{c_2} f\left(2\pi n + \delta_{1max} - 2\pi \frac{\bar{\Phi}_K + \bar{\Phi}_S + \bar{\Phi}_E}{\bar{\Phi}_O}\right) \quad (2.2)$$

Neglecting $\bar{\Phi}_K$, $\bar{\Phi}_S$ (kinetic and magnetic self-induced fluxes) in the first approximation, the modulation is proportional to the phase-current relation with the argument $\left(2\pi n - \delta_{1max} - 2\pi(\bar{\Phi}_E/\bar{\Phi}_O)\right)$. Under these conditions a measurement of the modulation of the critical current of a small asymmetric interferometer by external magnetic flux is equivalent to measuring the phase-current relation. If the phase-current relation is not periodic with a period 2π , the integer n will affect the modulation curve when it changes. The experimental realization of the "smallness" condition in a strict manner, i. e., $\bar{\Phi}_S + \bar{\Phi}_K \ll \bar{\Phi}_O$ is difficult simultaneously with

Figure 1. The parameter $\bar{\phi}$ is defined as $\bar{\phi} = \bar{\phi}_K + \bar{\phi}_S + \bar{\phi}_E - n\bar{\phi}_O$.

SUPERCURRENTS IN AN INTERFEROMETER



QUANTIZATION CONDITION: $\delta_1 - \delta_2 = \frac{2\pi\phi}{\phi_0}$

Figure 1

the condition $I_{c1} \gg I_{c2}$. To show why, the fluxes will be written in the form

$$\begin{aligned}\bar{\Phi}_S &= L_S(I_1 + I_2) \\ \bar{\Phi}_K &= L_K(I_1 + I_2)\end{aligned}\tag{2.3}$$

where L_S , L_K are the self-inductance and the kinetic inductance (section 1.6) respectively, and I_1, I_2 are the currents flowing through bridges 1 and 2. Since $\bar{\Phi}_0 = 2 \times 10^{-15}$ Wb, it would be necessary to have

$$L = L_K + L_S \ll \frac{2 \times 10^{-15} \text{ Wb}}{I_1 + I_2}\tag{2.4}$$

However, the typical current noise (Ref. 5) of proximity effect bridges is $\sim 0.1 \mu\text{A}$ so that the current $I_1 \gg I_2$ would have to be $\sim 50 \mu\text{A}$, i. e.,

$$L_K + L_S \ll 4 \times 10^{-11} \text{ H}\tag{2.5}$$

The inductance $4 \times 10^{-11} \text{ H}$ corresponds to a linear dimension $\sim 4 \times 10^{-5} \text{ m} = 40 \mu\text{m}$. The dimensions of the interferometer would have to be much smaller than $40 \mu\text{m}$ to satisfy the strict smallness requirement.

A second approximation will therefore be used in which $\delta_{l\text{max}}$, $\bar{\Phi}_K$ and $\bar{\Phi}_S$ are corrected to first order using the first approximation. Since it is possible to make interferometers with a diameter of 15μ and $I_{c1} \sim 10 I_{c2}$, the second approximation can be introduced numerically after the approximate character of the phase-current relation is known from a magnetic modulation experiment.

2.3 Sample Preparation

2.3.1 General procedure

A multilayered metal film is evaporated on an insulating wafer under ultrahigh vacuum conditions. Subsequently photolithographic techniques are used to mask selectively some areas of the film. In unmasked areas the film is anodized to predetermined depth so that a layer of anodic oxide is formed. For the manufacture of proximity effect bridges (Ref. 6) the top film layer of higher intrinsic transition temperature is anodized away along a narrow ($\sim 1\mu$), rectangular area leaving the bottom film layers of lower intrinsic transition temperature as the only path of conduction. A bridge structure is thus formed where two areas of unanodized film are joined by an area where the top layer of the film is anodized away (Fig. 2). Other conduction paths (leads, rings, etc.) can be delineated by complete anodization of the film in places where conduction is not desired. In such films the unanodized regions have a higher transition temperature than the partially anodized regions while completely anodized regions are insulating.

2.3.2 The substrate and the film

A film-substrate combination for use in the preparation of proximity effect bridges and ancillary structures by anodization (Ref. 7) must meet several requirements. First, the film must show a decreasing superconducting transition temperature in the liquid helium range as a function of the depth of anodization. Second, the anodic oxide must be stable and insoluble in the

Figure 2. Diagram of a proximity effect bridge. The evaporated Nb/Ta sandwich with thickness t_s/t_n is anodized in the bridge region. The author uses bridges with $t'_s = 0$, $t'_n < t_n$ and length $\ell = 0.7 - 1.0 \mu\text{m}$.

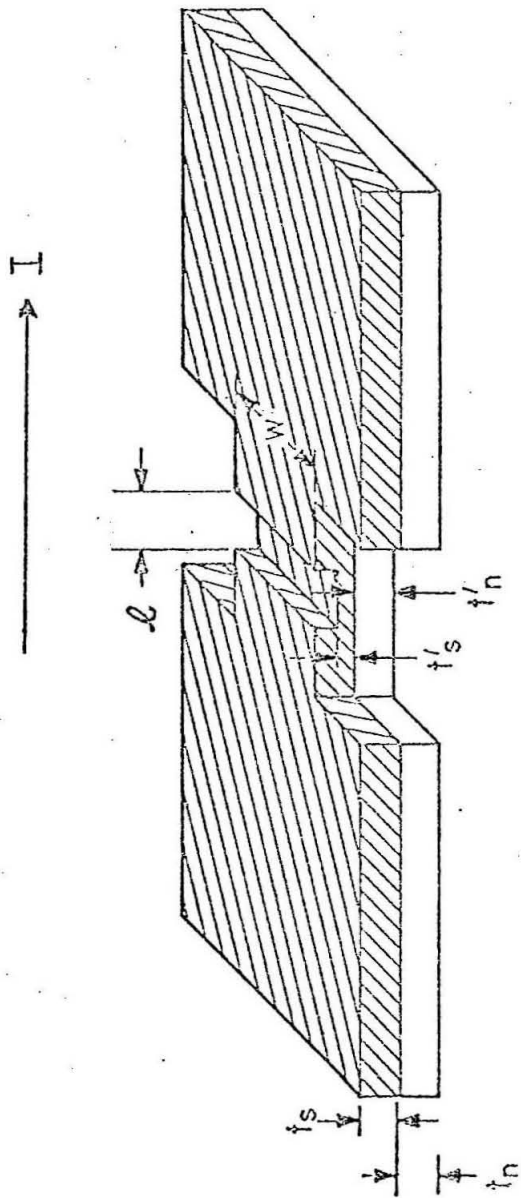


Figure 2

reagents used during the preparation of the sample. Third, the film should be tough and adhere well to the substrate. The fourth requirement, while not critical in the interferometer experiment, was nevertheless found useful in other applications: the substrate should have a high thermal conductivity at liquid helium temperatures to minimize the temperature rise due to Joule heating.

The following procedure has been used (Ref. 8) for interferometer samples. An inch by inch square, thin sapphire substrate is cleaned by washing in chromerge, distilled water and reagent quality acetone successively. The sapphire chip is then dried and placed into an ultra-high vacuum electron beam evaporator. The substrate is heated to 400°C and when pressure drops to the low 10^{-8} range, 100-200 Å of tantalum (Ta) is evaporated followed immediately by 100-200 Å of niobium (Nb). The thickness is monitored by a Sloan monitor during evaporation.

2.3.3 Photolithography and anodization (Ref. 7)

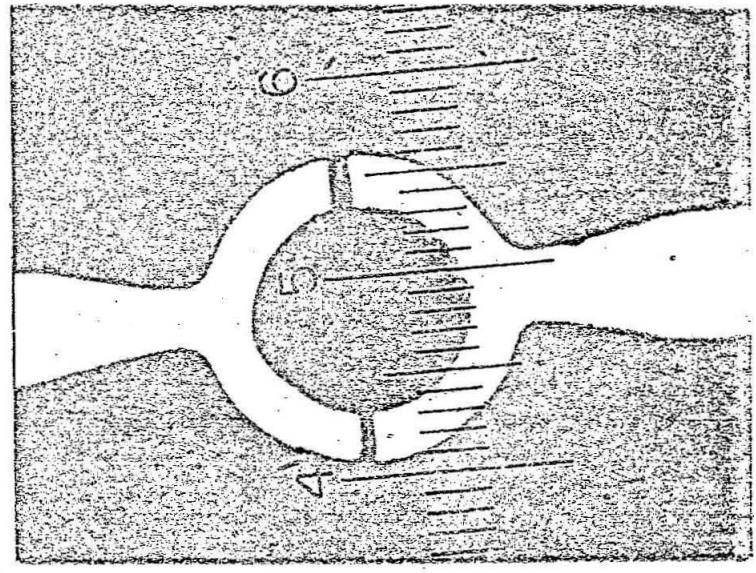
After evaporation the film is cleaned in chromerge, distilled water and acetone again. Photoresist ("PR") (Shipley AZ) is then spun on and test holes are exposed. The thickness of the Nb and Ta layers is checked by slow anodization with a voltage ramp. The empirical conversion constants between anodization voltage and film thickness anodized to oxide are: 8 Å/V for Nb, 6 Å/V for Ta, yielding 15 Å/V of oxide in both cases. After dissolving the old photoresist with acetone, a new layer is spun on and an interferometer ring mask is microprojected (in reverse) through a x100 oil immersion lens. (50x diminution

of the pattern is achieved.) The developed PR pattern covers a ring structure with two leads. Complete anodization removes all metal film not covered by PR, leaving a thin film ring with two leads. The manufacture of bridges proceeds similarly. A slit pattern is microprojected through a x100 oil immersion lens into freshly spun PR on one of the arms of the previously made ring pattern. As a result, after developing, the PR is removed over a strip $\sim 1\mu$ wide extending across one arm of the interferometer ring. Subsequent partial anodization removes the top layer of Nb and some Ta through the gap in the PR. The second bridge is made in the other arm the same way. In order to achieve asymmetry of roughly the desired magnitude the two bridges are made with somewhat different anodization voltages. A series of interferometers is made on one substrate and the suitable ones ($I_{c2}/I_{c1} \sim 1/10$) are selected through further testing. Two of the samples made by this procedure are shown in Fig. 3. These two were chosen from a total of eight complete interferometers and were used for all the experiments described in this chapter.

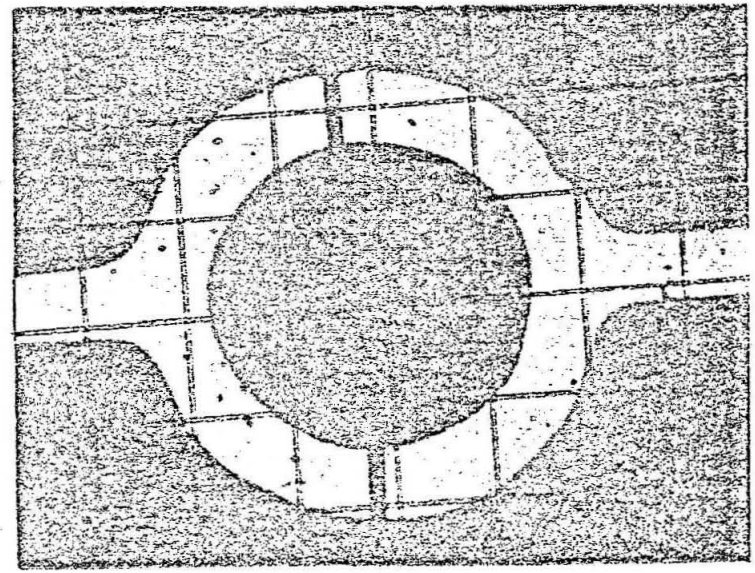
2.4 The Measurement of the Interferometer Critical Current as a Function of Applied Magnetic Field

After the manufacture of an interferometer is completed, two wires are attached to each of the two interferometer leads by pressed indium contacts so that a four-terminal measurement can be performed. The interferometer is then mounted inside of a solenoid with the plane of the interferometer ring perpendicular to the axis of the solenoid. The solenoid is positioned at the end

PHOTOMICROGRAPHS OF EXPERIMENTAL INTERFEROMETERS



10 μ



CIT 16a #6

CIT 13c #2

Figure 3

of a cryogenic probe and the probe is lowered into a cryostat. Precautions have to be taken to limit AC and RF interference as well as to minimize the effects of ambient magnetic field. These precautions include the placement of the cryostat in a shielded room, the provision of a magnetic shield around the cryostat, and the installation of a lead foil bucket inside the cryostat to create a superconducting shield around the cryogenic probe.

An electronic feedback system is used to maintain the bias current of the interferometer at its critical current even as the critical current varies with the applied magnetic field (Fig. 4). The operation of the feedback loop is described in Fig. 5. The addition of an unchopped current source consisting of the voltage source V_E and bias resistor R_2 (Fig. 4) decreases the necessary offset voltage V_F and thus lowers the operating point voltage V . The operating point voltage is chosen to lie just above the high curvature knee of the I-V characteristic so that as little distortion of the critical current waveform as possible is introduced (Fig. 6). The data are obtained in the form of an x-y plot with the horizontal axis x proportional to the solenoid current I_B and thus proportional to the magnetic flux through the interferometer due to the solenoid. The vertical axis y is driven by the output of the lock-in amplifier (including its offset voltage V_F) and is therefore proportional to the critical current I_C of the interferometer. (Fig. 4). Since the critical currents of the bridges are a function of the temperature of the bath, I_C vs. I_B plots are recorded at several temperatures.

DIAGRAM OF THE CIRCUIT FOR MEASURING I_C

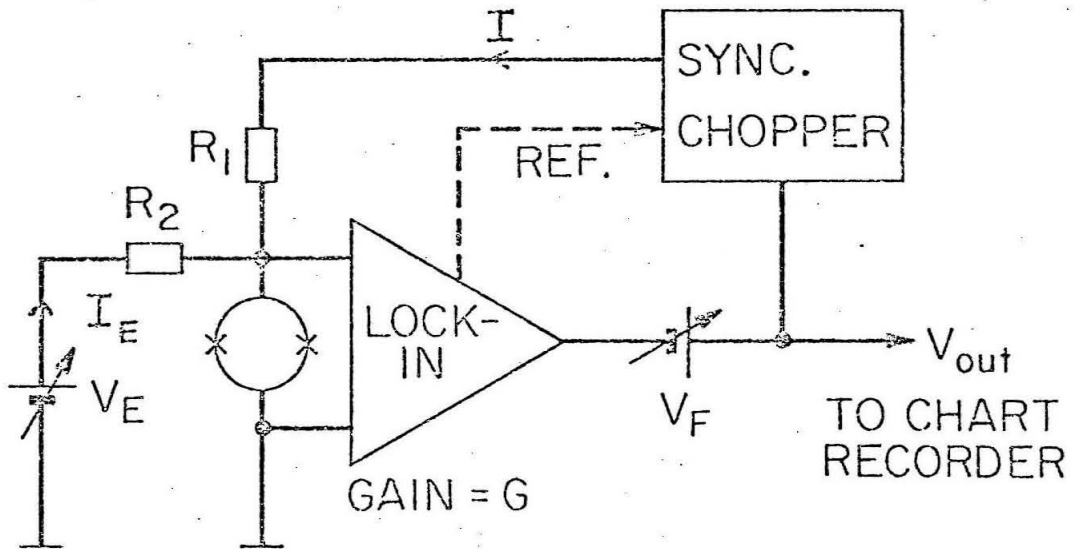


Figure 4

THE WORKING POINT OF THE CIRCUIT FOR MEASURING I_c (TYPICAL VALUES)

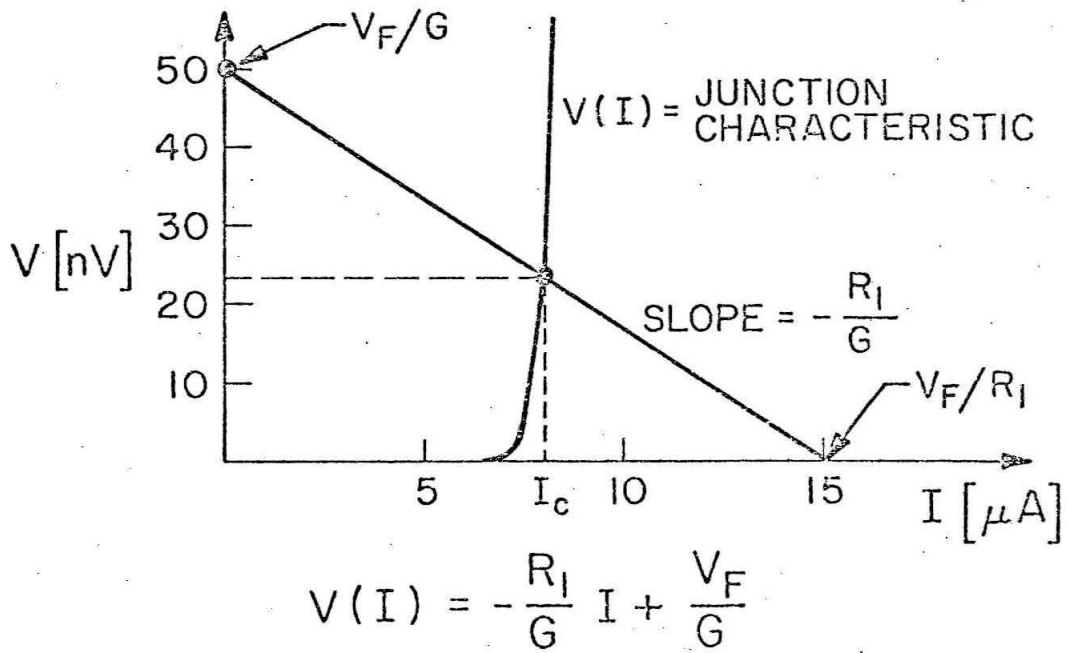


Figure 5

Figure 6. (experimental tracing) The choice of operating point of the circuit in Figures 4 and 5. The magnetic fields B_{\max} and B_{\min} produce the minima and maxima of the interference modulation of the critical current I_c .

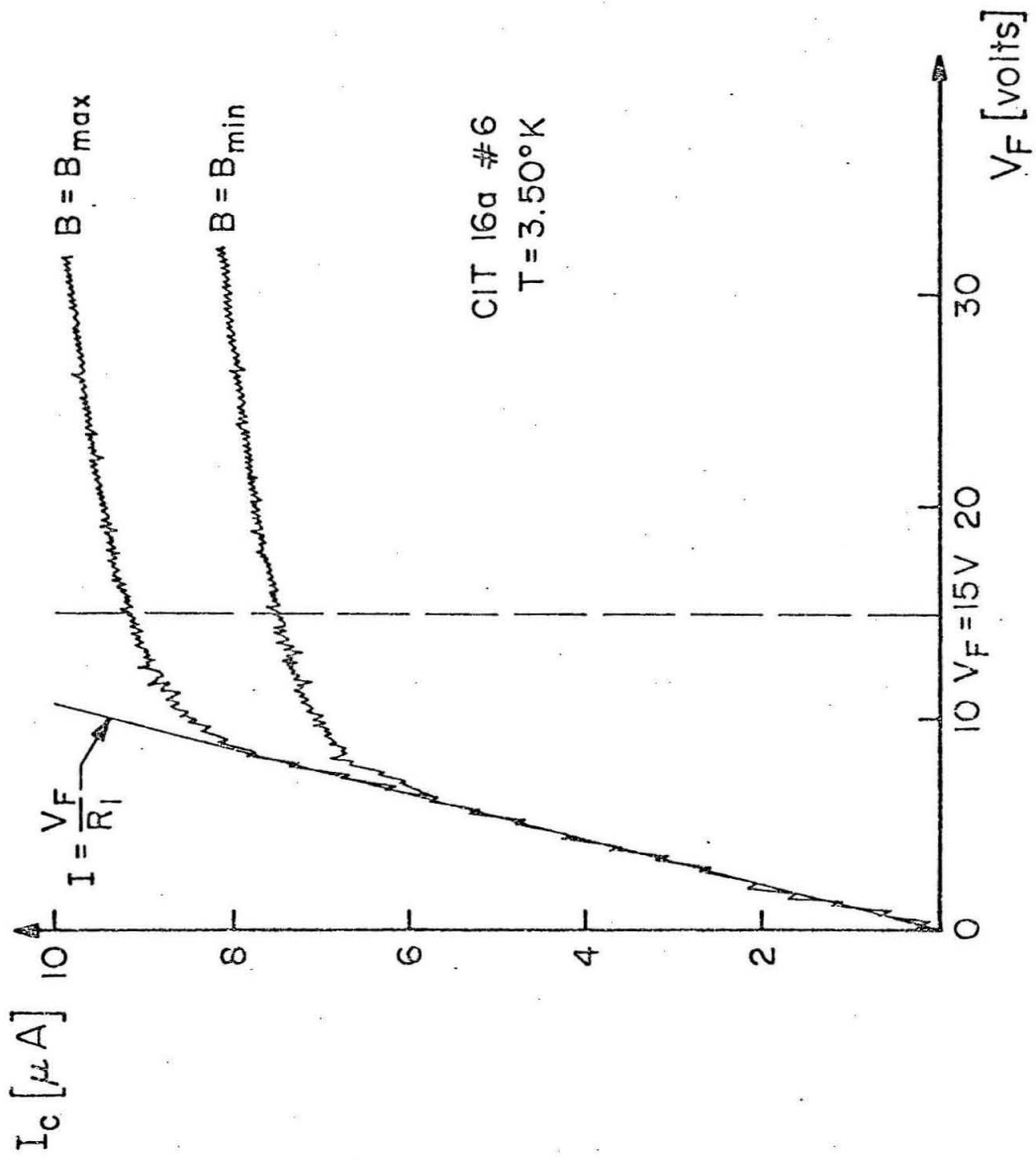


Figure 6

2.5 Data Analysis, Results and Discussion

Two interferometers (Fig. 3) were used to obtain the data to be presented. They were selected because in both cases the asymmetry I_{c_2}/I_{c_1} was roughly 1:10 in the current range $0 < I_{c_1} < 50 \mu\text{A}$ so that a compromise between the requirements of smallness and asymmetry could be achieved.

Initial measurements indicated that the modulation was roughly sinusoidal on a slowly varying background due to single bridge diffraction (Fig. 7). No effects attributable to the periodicity of the phase-current relation differing from 2π were seen (section 2.2). At this point the approach was reversed. The working hypothesis became that the phase-current relationship is sinusoidal with a period 2π , and an attempt was made to detect any deviations incompatible with this hypothesis. There are three causes of the interferometer critical current modulation deviating from the sinusoid that are compatible with a sinusoidal current-phase relation. The first of these is trivial: the single junction diffraction term causes the overall background curvature of the modulated waveform. For this reason it was decided to analyze only the few modulation periods near the peak of the background waveform where the variation is the slowest. The second effect is due to the inductance of the interferometer ring $L = L_K + L_S$, the sum of the kinetic and magnetic self-inductances (see section 2.3). As a result of kinetic and magnetic flux terms due to currents flowing in the ring, the central peak of the modulation pattern is shifted away from the point where the external magnetic

I_c vs. B IN AN INTERFEROMETER WITH $I_{c1} = 12 I_{c2}$

$I_c [\mu A]$

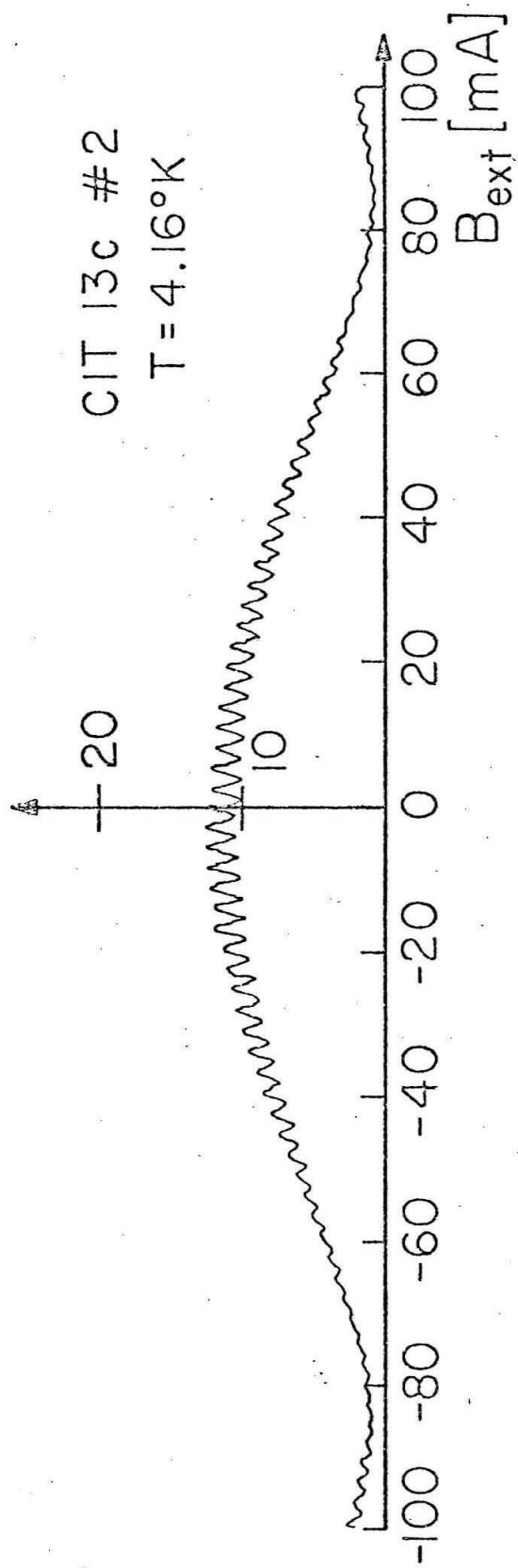


Figure 7

field is zero, and a tilt is introduced into the modulation pattern (Fig. 8). The tilt is caused by the changes in I_2 (the supercurrent through the weaker bridge) as the external magnetic field is varied. When I_2 flows in one direction it increases the total flux through the ring, in turn causing a faster rise of the current I_2 as a function of external magnetic field. When I_2 reverses it produces a flux term which diminishes the total flux causing a slower fall in I_2 as a function of external magnetic field. Both a shift and a tilt were observed in experiments with the two interferometers. The shift should vary linearly with I_{c1} , while the tilt should be proportional to I_{c2} , with approximately the same proportionality constants $L' = L$. Experimentally, this was indeed found to be the case (Table 1). Finally, the last compatible cause of the modulation deviating from the sinusoid is due to imperfect asymmetry $I_{c1} \gg I_{c2}$. With the use of trigonometric identities the interferometer equation (2.1) can be rewritten to show that the lowest order correction (for a sinusoidal phase-current relation) to equation (2.2) is

$$\Delta I_c^{(1)} = -\frac{1}{2} \frac{I_2^2}{I_{c1}} \quad (2.6)$$

This correction has a constant component and a component at the second harmonic of the sinusoidal modulation pattern. The amplitude of the second harmonic correction is $-I_{c2}^2/4I_{c1}$.

Accordingly, the data, recorded in the form of I_c vs. I_B plots as described in section 2.4, were analyzed in the following fashion. The curves were fitted with the analytical form

Figure 8. (Sketch) The effect of inductance L of the interferometer on the modulated waveform.

THE EFFECT OF INDUCTANCE ON I_c
IN INTERFEROMETERS WITH $I_{c1} \gg I_{c2}$

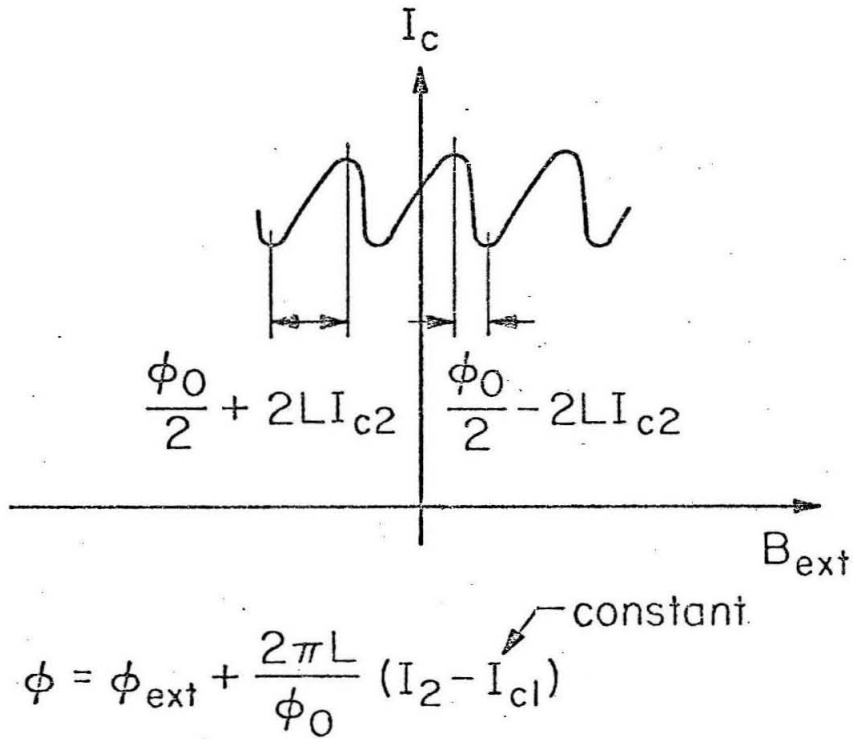


Figure 8

(cf. equation 2.1)

$$\begin{aligned}
 I_c &= I_{c_1} + I_{c_2} \sin\left(\frac{\pi}{2} - 2\pi \frac{\Phi}{\Phi_0}\right) \\
 I_B &= \frac{1}{M} \left[\Phi - LI_{c_2} \sin\left(\frac{\pi}{2} - 2\pi \frac{\Phi}{\Phi_0}\right) - \Phi' \right]
 \end{aligned}
 \tag{2.7}$$

where Φ is a free parameter corresponding to the total flux through the interferometer and where I_{c_1} , I_{c_2} are the critical currents of the two bridges, L is the inductance of the interferometer, Φ_0 is the flux quantum, MI_B is the flux through the interferometer due to the solenoid current I_B , and Φ' is the flux due to $I_1 = I_{c_1}$ and the background B field. It should be noted that all of the constants I_{c_1} , I_{c_2} , L , Φ' , M are gotten by fitting. Internal checks of the inductance L can be made by comparing data recorded at various temperatures (i.e., various critical currents I_{c_1} , I_{c_2}). In addition an independent measurement of $L' \doteq L$ can be made from the shift of the central maximum with changing I_{c_1} as the temperature is varied (i.e., $L' \equiv \partial\Phi'/\partial I_{c_1}$). A priori, it would seem that the mutual inductance M of the solenoid and interferometer in equation (2.7) can be calculated from the geometry. However, the interferometer is in close proximity to large contact pads of superconducting film. Since the superconductor is strongly diamagnetic the magnetic flux expelled from the pads is concentrated in the interferometer. The mutual inductance M therefore turns out to be much larger than M_{geom} calculated neglecting diamagnetic effects (Table 1).

Finally, the deviation of the data from the fit (equation 2.7),

if significant, was compared to that expected from imperfect asymmetry (equation 2.6).

The results are presented in Table 1 and in Figures 9 and 10. For the four curves analyzed in detail the noise amplitudes N were from 2 to 8 percent of the modulation amplitude I_{c2} and it is estimated that an incompatible periodic deviation would be detected if its amplitude exceeded 5 percent of the modulation amplitude I_{c2} . No such deviation was found in any of the data studied.

It should be noted that this study was done on bridges at zero voltage. Due to the onset of nonequilibrium behavior at finite voltages extrapolation of the zero voltage phase-current relation to finite voltages is not warranted. Additionally, the phase-current relation is thought to depend on the strength of coupling between the two superconductors separated by the normal barrier, i. e., on the geometry and material composition of the bridge. The "coupling strength" of the theoretical models is closely related to supercurrent density. In this study the supercurrent density is estimated to be about $50-100 \mu\text{A}/\mu\text{m}^2$ which is of the same order of magnitude as the supercurrent density in the typical working regime of most Nb/Ta proximity effect bridges but about ten times higher than the current density in insulating barrier junctions. It is likely that significant deviations from the sinusoidal phase-current relation at zero voltage will not be observed unless much higher supercurrent densities are reached.

TABLE 1

Interferometer	Mean Diameter [μm]	Width [μm]	M_{geom} [10^{-13}H]	M [10^{-13}H]	I_{c1} [μA]	I_{c2} [μA]	L [10^{-11}H]	L' [10^{-11}H]	$\frac{I_{c2}L}{2\pi\psi_0}$	$\frac{I_{c2}}{4I_{c1}}$	$\frac{N}{I_{c2}}$	Fit
CIT 16a #6 R = 1.6 λ	13	2	2.4	6.6	6.65	0.61	--	4	0.05*	0.02	0.08	1
				6.6	11.04	1.34	3		0.12	0.02	0.04	2
CIT 13c #2 R = 0.4 λ	18	3	3.7	10	12.32	1.04	--		0.05†	0.02	0.04	1
				10	22.13	1.82	1.5	2.6	0.08	0.02	0.02	3
					39.75	3.30	1.9	2.6	0.19			4

*Index of tilt $2\pi I_{c2} L / \psi_0$ calculated using $L = 3 \times 10^{-11}\text{H}$

†Index of tilt $2\pi I_{c2} L / \psi_0$ calculated using $L = 1.5 \times 10^{-11}\text{H}$

- Fit: 1 Fits within noise with $L = 0$ in equation 2.7
 2 Fits within noise with $L = 3 \times 10^{-11}\text{H}$
 3 $L = 1.5 \times 10^{-11}\text{H}$ used in fitting. Second harmonic deviation detected but it agrees with equation 2.6
 4 Curve used only for measurement of L and L'

Figure 9. Comparison of an experimental trace with theory
(equation 2.7)

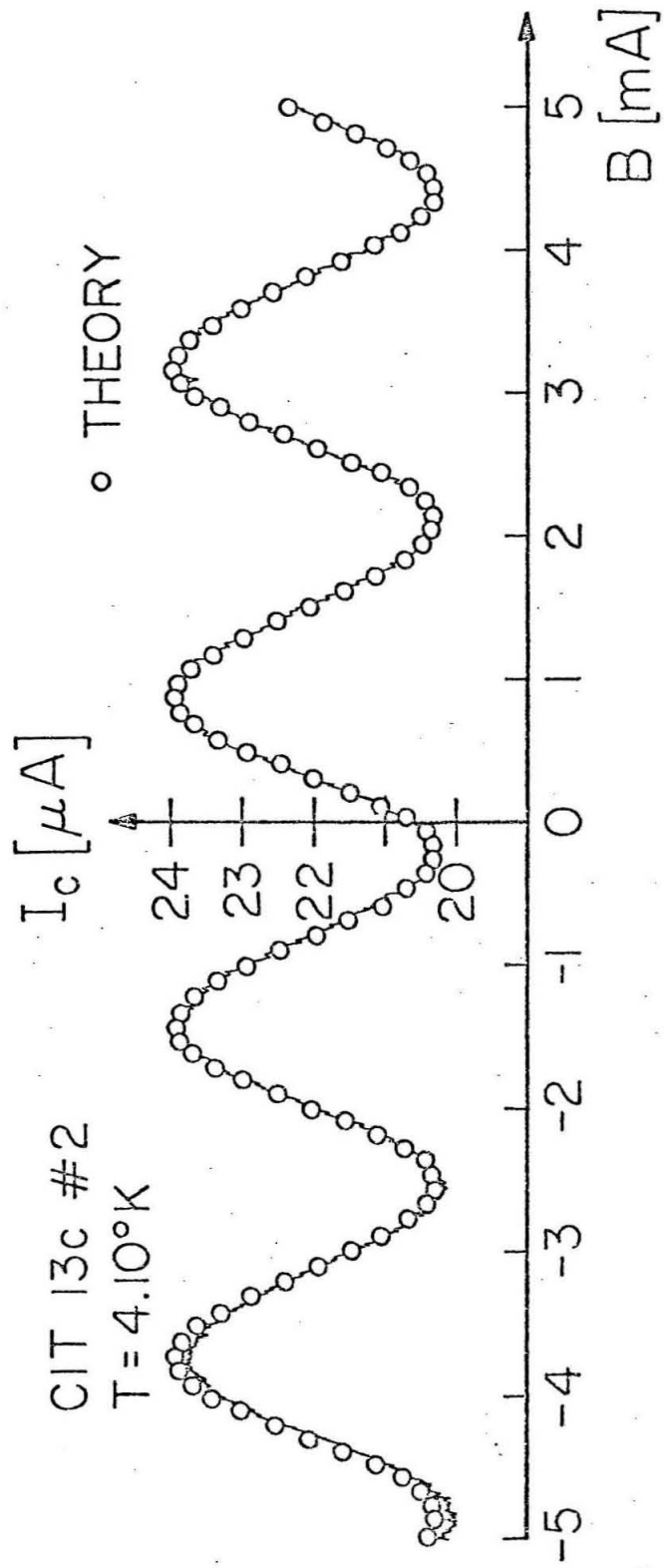


Figure 9

Figure 10. Comparison of an experimental trace with theory
(equation 2.7)

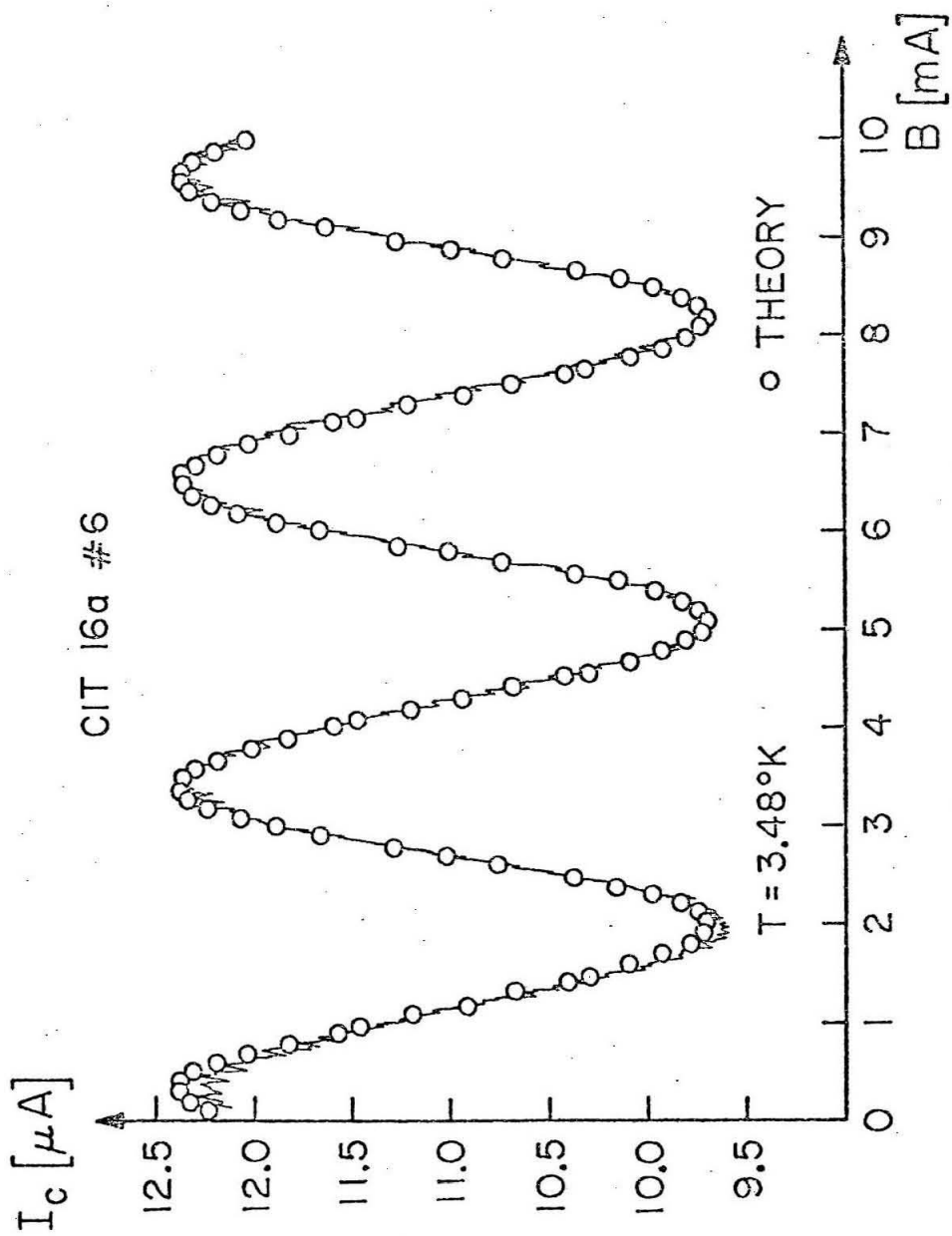


Figure 10

2.6 Conclusion

The phase-supercurrent relation in proximity effect bridges at zero voltage was experimentally determined using two asymmetric quantum interferometers. With supercurrent density in the weaker bridge estimated at $50-100 \mu\text{A}/\mu\text{m}^2$ no evidence of deviation from the Josephson phase-supercurrent relation $I_S = I_C \sin\delta$ was found. The experiment was sufficiently sensitive to detect deviations as small as $0.05 I_C$.

From theory (Refs. 2 and 4) it is expected that the deviation from the Josephson relation increases with the "strength of coupling", i. e., the supercurrent density in the bridge. The supercurrent density in this experiment is typical of proximity effect bridges in general but is about an order of magnitude larger than the maximum in insulating barrier Josephson junctions. Until any future evidence shows otherwise the simple Josephson relation can be used to describe the zero voltage regime of both proximity effect bridges and insulating barrier Josephson junctions.

References

1. R. C. Jaklevic et al., Phys. Rev. 140A, 1628 (1965)
2. A. Baratoff, J. A. Blackburn and B. B. Schwartz, Phys. Rev. Letters 25, 1096 (1970)
3. T. A. Fulton and R. C. Dynes, Phys. Rev. Letters 25, 794 (1970)
4. J. Bardeen and J. L. Johnson, Phys. Rev. 5B, 72 (1972)
5. R. K. Kirschman and J. E. Mercereau, Phys. Lett. 35A, 177 (1971)
6. H. A. Notarys and J. E. Mercereau, J. Appl. Phys. 44, 1821 (1973)
7. D. W. Palmer and S. K. Decker, Rev. Sci. Instrum. 44, 1621 (1973)
8. S. K. Decker, Ph. D. Thesis (California Institute of Technology 1975)

III. THE INTERACTION OF PROXIMITY EFFECT BRIDGES WITH SUPERCONDUCTING MICROSTRIP RESONATORS

3.1 Introduction

When Josephson devices are made to interact with RF resonators, the I-V characteristics of the devices (section 1.5) are modified. Usually, near the voltage corresponding to the resonant frequency of the cavity, a step-like structure appears in the I-V characteristic. To distinguish the structure from similar "steps" induced by external RF currents (see section 1.5) the resonator caused features are often referred to as "self-induced steps". Their study is of interest both for the characterization of Josephson devices and for device applications (Ref. 1). The first experimental observation of self-induced steps was reported by Fiske (Ref. 2) for insulating barrier Josephson junction interacting with stripline type modes within the junction itself. Subsequently self-induced steps in the I-V characteristics of point-contact devices placed in a cylindrical cavity were observed by Dayem and Grimes (Ref. 3). In 1974 Levinsen (Ref. 4) saw self-induced steps with a Dayem bridge coupled to a rectangular microwave cavity. Since thin film bridges are planar devices it was decided in this laboratory to use "planar" resonators--microstrip resonators--for the exploration of the interaction of proximity effect bridges with RF resonant systems. A preliminary report on these studies will appear in the Applied Physics Journal (Ref. 5).

Several goals have been pursued in this work. Initially,

the technology of microcircuits with microstrips and proximity effect bridges was developed. Secondly, the phenomenon of self-induced steps was studied experimentally in these microcircuits and qualitatively compared to simple models. Finally, an attempt was made to compare quantitatively the size and shape of the steps observed in the experiments to those predicted from two alternative theories of bridge dynamics and estimate the amplitude of bridge oscillation in the GHz range.

3.2 Self-induced Steps--General Considerations

According to the two-fluid model (Ref. 6), a thin film bridge can be considered as consisting of an ideal "junction element" and a shunting resistor. The junction element is a voltage controlled oscillator which allows the flow of a super-current

$$I_S = I_c f\left(\int \frac{2eV}{\hbar} dt\right) \quad (3.1)$$

where f is a periodic function with period 2π and V is the voltage across the bridge. In the current-biased mode the shunting resistor R carries the normal part of the bias current I so that the voltage across the bridge is

$$V = R(I - I_S) \quad (3.2)$$

The voltage measured in the I-V characteristic of bridges is the time average of equation (3.2), i.e.,

$$\bar{V} = R(I - \bar{I}_S) \quad (3.3)$$

In this model all the deviations from a simple resistive characteristic

$$\bar{V} = RI \quad (3.4)$$

are ascribed to the time average of the supercurrent \bar{I}_S . Two factors determine the magnitude of the average supercurrent \bar{I}_S . The first is the intrinsic dynamics of the bridge, here represented by the waveform f in equation (3.1). The second factor is self-modulation due to the oscillating behavior of the time-dependent voltage V , caused by the oscillations in the current flowing through the shunting resistor R . The voltage V oscillates about its average \bar{V} thus alternately speeding the rate of phase development when the supercurrent I_S is negative (= opposite to the bias current I) and slowing the rate down when the supercurrent I_S is positive. This effect by itself increases the average supercurrent \bar{I}_S beyond that given by the phase average of the phase-supercurrent relation $I_S = I_c f(\delta)$. When a bridge is strongly coupled to a resonator an additional shunting impedance $Z(\omega)$ is added to the bridge circuit (Fig. 1) to account for the part of the bias current flowing through the resonator. Assuming that the real part of the resonator impedance is negligible (or more accurately, that the real part of the resonator admittance is much smaller than $1/R$) the amount of self-modulation will change as the oscillation frequency of the bridge passes through the resonance of the shunting resonator.

There are two simple cases of interest. In the first case the magnitude of the impedance $Z(\omega)$ is much greater than the shunt resistance R except near resonance ω_0 where $Z(\omega_0) \ll R$. Accordingly the I-V characteristic reflects the self-modulation

Figure 1. The equivalent circuit of a proximity effect bridge of resistance R shunted by a resonator.

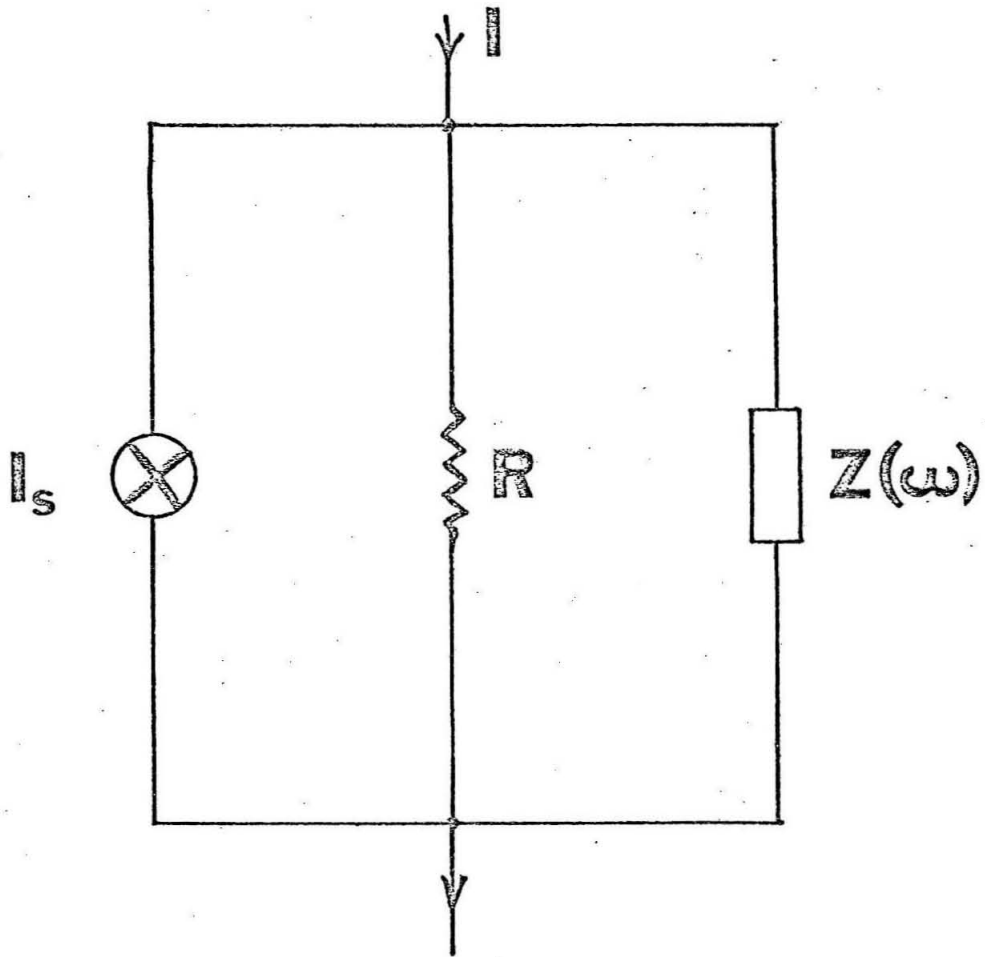


Figure 1

appropriate to the resistance R (as if the resonator were absent) except when the fundamental oscillation frequency of the bridge is near the resonant frequency ω_0 . On resonance the shunting resistor R is shorted by the resonator at the fundamental frequency of the bridge oscillation and self-modulation almost ceases. (The higher harmonics may still contribute a small amount of self-modulation.) As a result the time average supercurrent \bar{I}_S is lower at resonance than it would be in the absence of the resonator. The time average voltage \bar{V} is thus higher at resonance producing an upward (convex) step in the I-V characteristic (Fig. 2B). In the second case the resonator impedance $Z(\omega)$ is much smaller than the shunt resistor R except near the resonant frequency ω_0 . (The situation is the reverse of the first case.) The self-modulation is very small except when the bridge oscillates at the resonator frequency. As a result the time average voltage \bar{V} is higher than it would be in the absence of a resonator except on resonance where it drops roughly to what it would be in the absence of a resonator. A downward (concave) step is thus produced (Fig. 2A). In both kinds of resonator-bridge circuits the maximum size of the self-induced step ΔV is the voltage difference at a given bias current I between the characteristics of the bridge $\bar{V}(I)$ with and without the effect of self-modulation.

This introductory discussion is oversimplified in several aspects. The effects of noise have been ignored. Additional complications stem from the multiple valuedness of the time-

Figure 2. Sketch of a self-induced step in the I-V characteristic of a bridge ($I_S = I_C \sin \delta$) of resistance R coupled to a transmission line of characteristic impedance Z_0 . In A: $Z_0 \sim R/8$, while in B: $Z_0 \sim 8R$. Dotted line is the interpolated nonresonant characteristic. Dashed line is the characteristic in the absence of a resonator. (Based on computer simulation.)

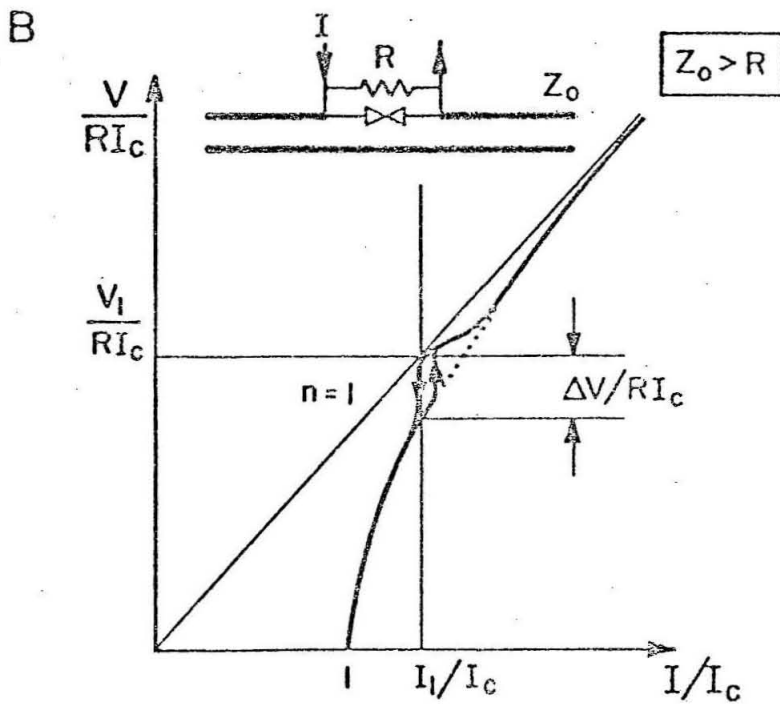
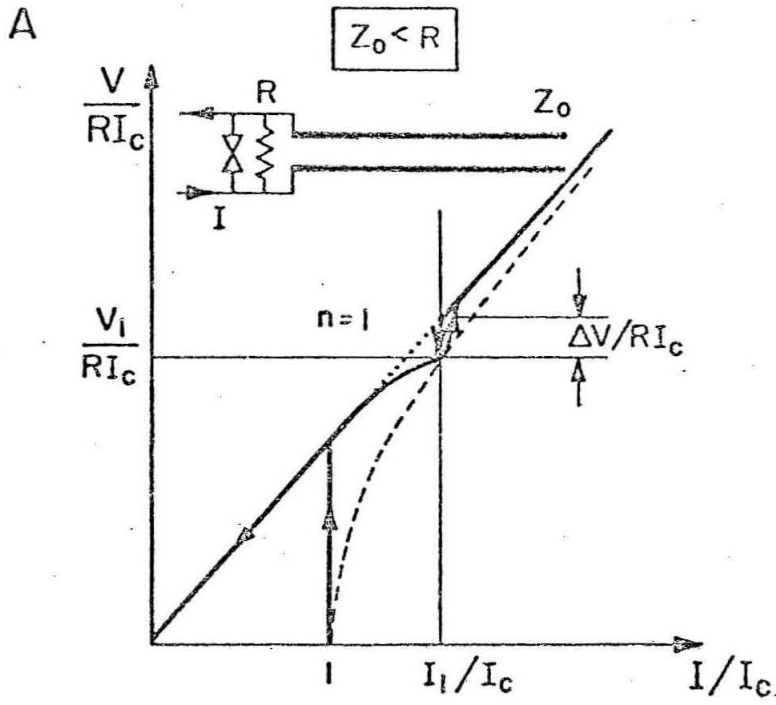


Figure 2

average voltage $\bar{V}(I)$ as a function of the bias current for a certain range of bridge and resonator parameters and from the possibly anharmonic nature of the phase-supercurrent relation $I_S = I_c f(\delta)$. These topics will be discussed in section 3.5 where a more detailed treatment will be presented.

3.3 Experimental Technique

3.3.1 The bridge-resonator circuit

The coupled bridge-resonator circuits were constructed on single silicon or sapphire chips using superconducting micro-circuitry techniques (Ref. 7). Four types of resonator circuits were made (coded 1-4). In the type 1 (Fig. 3) a two-layer niobium on tantalum ($Nb/Ta = 280 \text{ \AA}/260 \text{ \AA}$) film was deposited (see section 2.3) on a sapphire chip to form a ground plane. A dielectric strip (typ. 15mm x 2mm) was subsequently formed on the ground plane by controlled anodization of the deposited film to the depth of 30 V (equivalent to approximately 150 \AA of Nb converted into 450 \AA of Nb_2O_5) through a photoresist pattern (see section 2.3). At one end of the dielectric strip a proximity effect bridge (width 15 μ x length 1 μ) was made by further anodization to the depth of 65 V through another photoresist pattern. This was followed by the formation of a contact pad to one side of the bridge using complete anodization of the film to delineate the pad. Then a 600 μ m wide top strip of 1200 \AA of Indalloy 11 was evaporated across the bridge and onto the dielectric strip. The contact between the top strip and the ground plane is superconducting at one end of the bridge while at the other end the

Figure 3. (not to scale) The type 1 bridge-resonator circuit.
1 = sapphire substrate, 2 = Ta film (260 Å), 3 = Nb film (280 Å), 4 = anodic Nb_2O_5 (~450 Å), 5 = Indalloy 11 top strip, 6 = contact area: top strip to ground plane, 7 = proximity effect bridge.

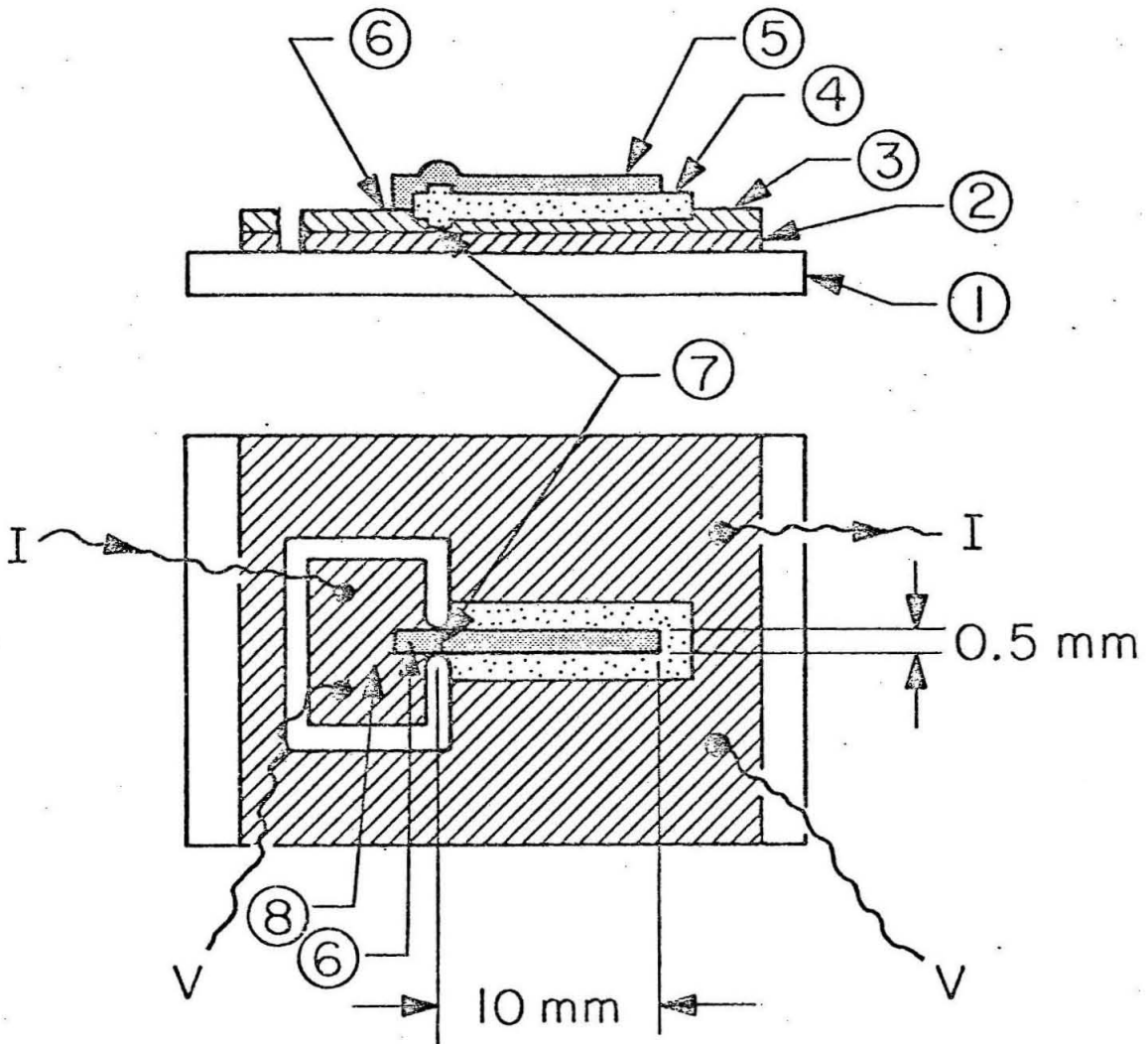


Figure 3

anodized dielectric separates the ground plane from the top Indalloy layer forming a microstrip structure open at one end terminated by a bridge at the other end. Microstrips similar to the ones employed in the type 1 circuit, with the thickness d of the dielectric comparable to the superconducting penetration depth, were studied in detail by Mason and Gould (Ref. 8) according to whom the characteristic impedance of these microstrips is given by

$$Z_0 = \sqrt{\frac{\mu_0}{\epsilon_0}} \frac{w}{d} \frac{1}{\epsilon v/c} \quad (3.5)$$

where d is the thickness of the dielectric layer, w is the width of the microstrip, v is the phase velocity and ϵ is the dielectric constant of the dielectric layer. As a result of the high dielectric constant ($\epsilon = 8-40$, Ref. 9) and the inductive loading of the microstrip by the superconductor, $v/c \ll 1$ are measured in these microstrips. Unfortunately the intrinsic Q of these superconducting microstrip resonators depends on the detailed properties of the materials used and may vary significantly from sample to sample (Ref. 8). In the circuits used in this study the effect of the intrinsic Q on self-induced steps was minimized by the strong loading of the resonators by the resistance of the bridge (typically loaded $Q \sim 10$ is aimed for). Due to technological limitations the type 1 (anodized dielectric) microstrip is best suited for characteristic impedances of $50 \text{ m}\Omega$ or less, while the typical bridge resistance is $0.1 - 0.2 \Omega$.

In the circuits of the second type (Fig. 4) the anodized

Figure 4. (not to scale) The type 2 bridge-resonator circuit. 1 = sapphire substrate, 2 = Nb/Ta film, 3 = proximity effect bridge, 4 = germanium dielectric, 5 = Indalloy 11 top strip. The several samples had microstrips of width 0.1-1 mm, length 10-15 mm and dielectric thickness 0.5-1 μm .

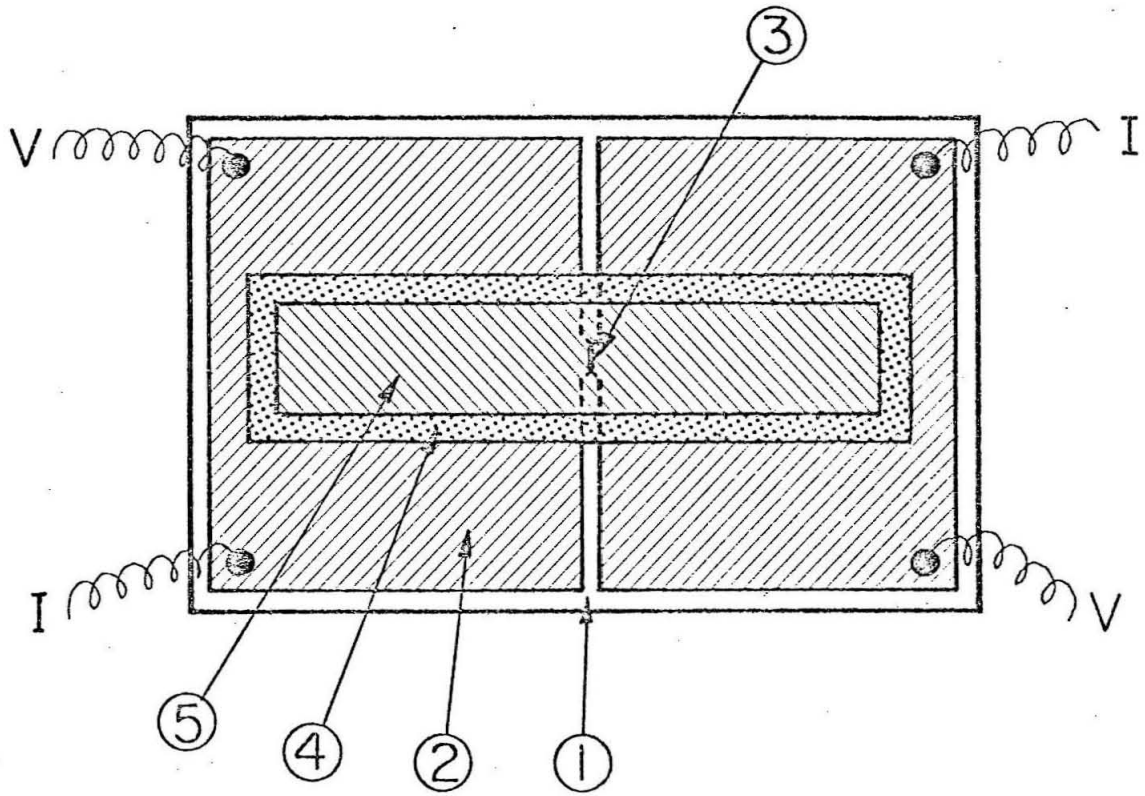


Figure 4

dielectric was replaced by an evaporated high resistivity germanium layer (typically $\approx 1 \mu\text{m}$ thick). First a bridge was made by the usual procedure (Ref. 10) in a Nb/Ta film. Next the germanium strip was evaporated across the bridge. Finally a strip of Indalloy 11 (width $100 \mu\text{m}$ to 1mm) was evaporated onto the germanium strip. The length of the top strip was set by the removal of unwanted Indalloy by a combination of photolithography and chemical etching. It should be noted that no contact is desired between the top Indalloy strip and the ground plane containing the bridge. The resulting structure is a microstrip open at both ends containing a proximity effect bridge in the ground plane at the center of the microstrip segment. The type 2 circuits are most suitable for characteristic impedance Z_0 in the $0.1 \Omega - 1 \Omega$ range. The top Indalloy strip can be selectively chemically removed and reevaporated making it possible to vary the characteristic impedance of the microstrip while retaining the same bridge.

The third type of circuit (Fig. 5) used a high resistivity silicon chip 0.4mm thick as the dielectric. On one side of the chip the top strip containing the bridge at the center was made by a combination of photolithography, anodization and plasma etching techniques (Ref. 11) in a Nb/Ta film (typ. $120 \text{ \AA}/250 \text{ \AA}$). At the same time the bridge leads were also made. The lead geometry was chosen to minimize the loading of the circuit by the leads at resonance. A ground plane film of several thousand \AA of Indalloy 11 was evaporated on the other face of the chip. This technique

Figure 5. The type 3 bridge-resonator circuit. 1 = silicon or sapphire substrate, 2 = Nb/Ta film, 3 = proximity effect bridge, 4 = contact pads for bias (I) and monitor (V) leads. The reverse side of the substrate is covered by an Indalloy 11 film forming the ground plane.

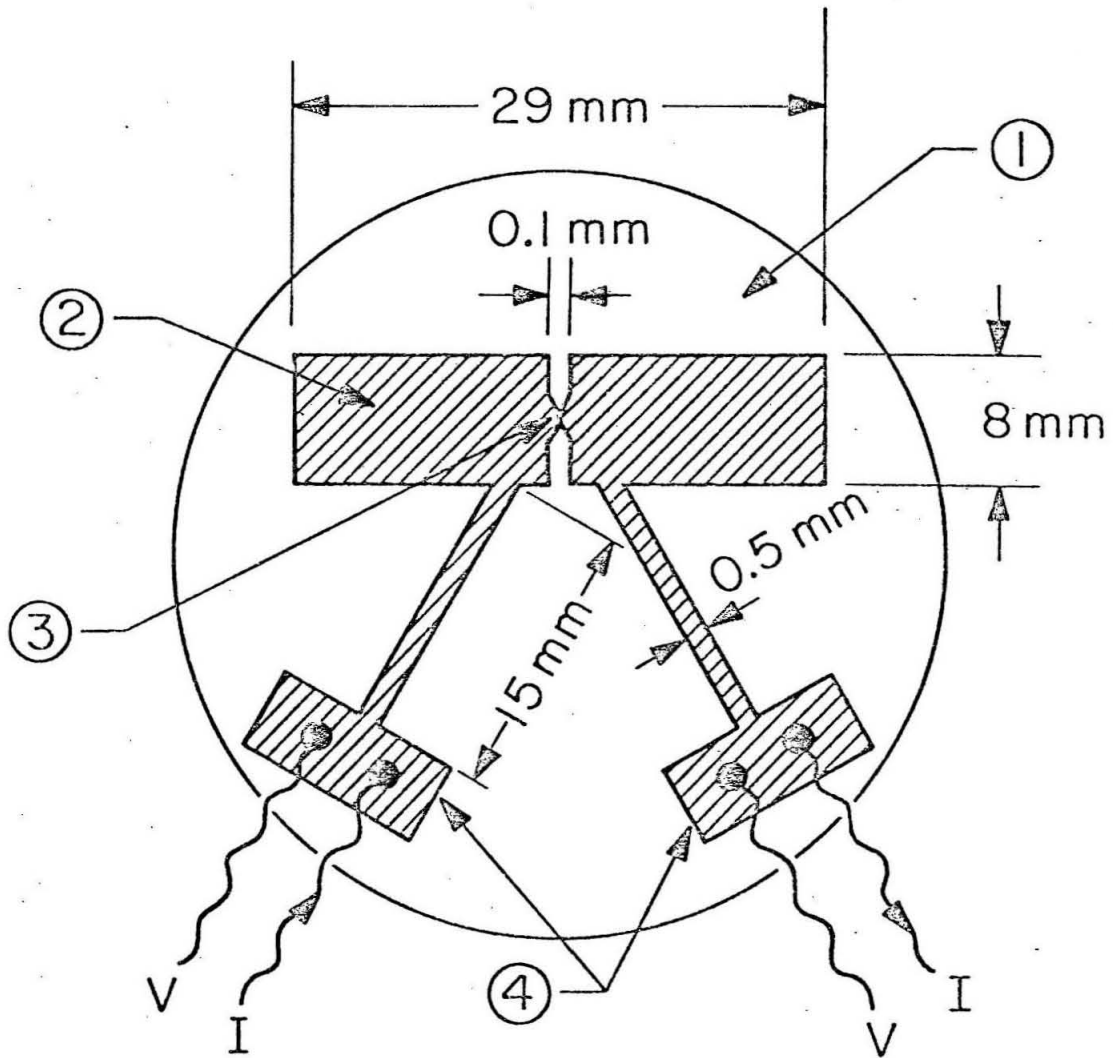


Figure 5

is most suitable for microstrips of characteristic impedance Z_0 greater than 5λ .

Finally the type 4 circuit (Fig. 6) was constructed to study the resonant interaction of two proximity effect bridges in a microstrip resonator. The circuit was made on a sapphire chip 0.25 mm thick in a Nb/Ta film ($72 \text{ \AA}/256 \text{ \AA}$) by the technique used for type 3 circuits. The two bridges were separated by 3 mm, and three superconducting bridge leads were employed for independent biasing and monitoring of the two bridges. As before, the ground plane on the reverse side of the chip was an evaporated film of Indalloy 11 (1000 \AA).

3.3.2 The measurement of $d\bar{V}/dI$ vs. I and \bar{V} vs. I characteristics

In theoretical studies it is customary to work with the V vs. I characteristic of bridges due to the convenience of calculation. The $d\bar{V}/dI$ vs. I characteristic was preferred experimentally since it was easier to measure and gave better resolution of small features. It was obtained by adding a small AC component ($i = 0.1 \mu\text{A RMS}$) to the DC bias current I of the bridge and synchronously measuring the voltage across the bridge with a lock-in amplifier (HR-8, Princeton Applied Research) as a function of the bias current I . In those cases where a \bar{V} vs. I characteristic was desired, the whole bias current I was chopped by a synchronous chopper and the voltage \bar{V} was measured by the lock-in amplifier across the bridge. In all cases a four-terminal measurement was employed.

Figure 6. The type 4 bridge-resonator circuit. There are two bridges in the microstrip. They can be biased and monitored independently. The construction of the circuit is otherwise similar to that of type 3 circuits.

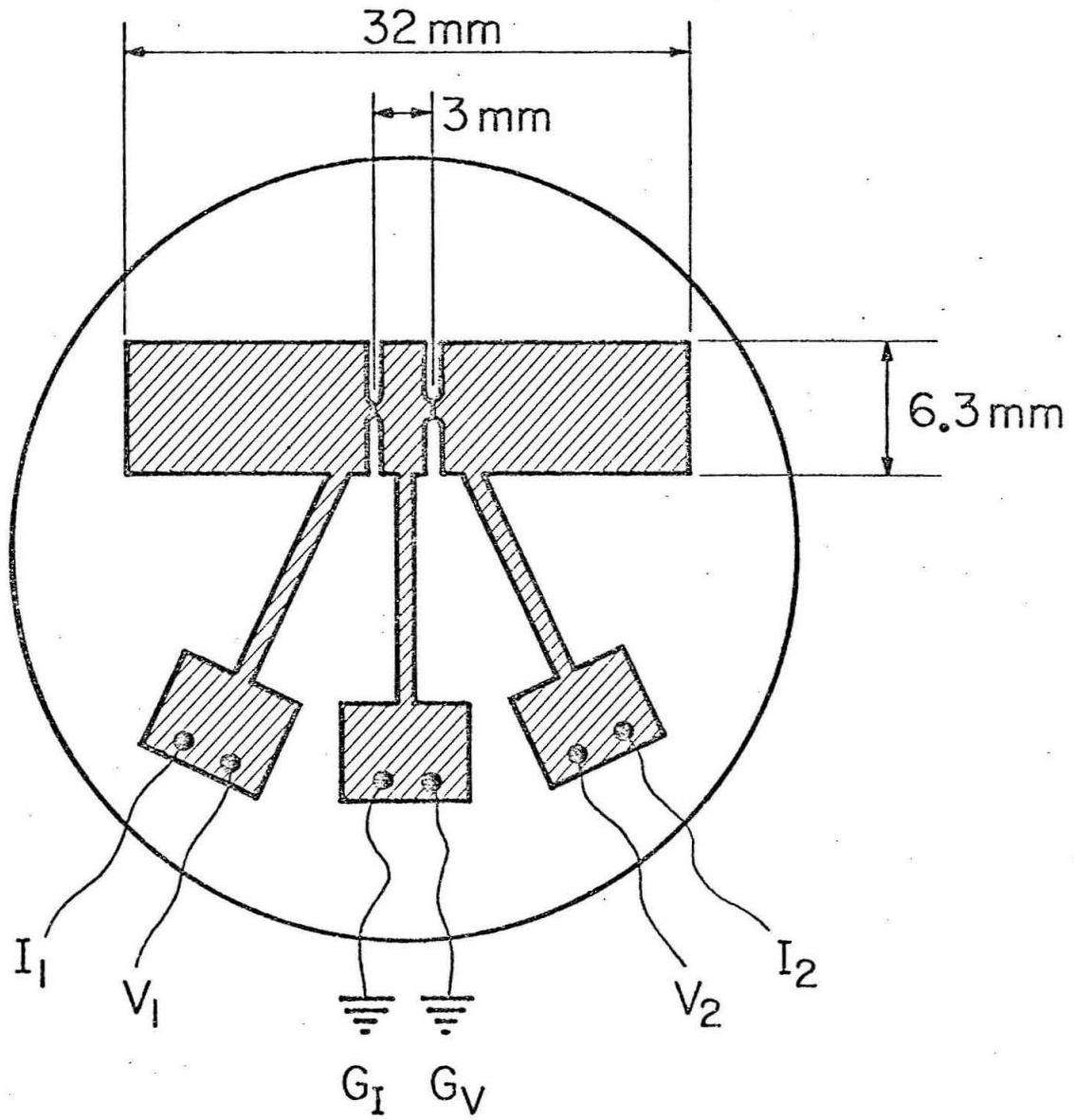


Figure 6

For all proximity effect bridges $d\bar{V}/dI$ vs. I traces were obtained both before and after their inclusion in a resonant circuit. Increasing and decreasing bias current sweeps were used to detect possible hysteresis. Both bias current directions were tested in several samples to guard against possible offset in the bias current.

To minimize RF interference and stray magnetic fields all the measurements were performed in a shielded room in a cryostat jacketed by a magnetic shield. The tip of the cryogenic probe, where the bridge-resonator sample was located, was shielded by a superconducting lead shield. To reduce the noise input through the bias (I) and monitor ($d\bar{V}/dI$) leads to the bridge, coaxial cables were used in the cryogenic probe. In addition a $1K\Omega$ resistor was placed into one bridge bias lead in the cryogenic space. A transformer input (type B) preamplifier was used in all experiments.

3.4 Observations

3.4.1 Self-induced steps

Experimentally, "self-induced steps" in the V vs. I characteristic of a bridge coupled to a resonant system are step-like features satisfying three criteria:

- a) the steps occur in the absence of external RF signal only when the bridge is coupled to the resonant system,
- b) the steps are at voltages (frequencies) corresponding to the modes of the resonant system, and
- c) no steps are seen above the transition temperature of the bridge (i. e., above the temperature where the bridge

begins to carry a detectable supercurrent).

Self-induced steps satisfying these criteria were seen in the I-V characteristics of bridge-resonator circuits of all four types. Usually the first derivative of such steps was recorded in the $d\bar{V}/dI$ vs. I characteristic of these circuits where a convex step showed up as a crest followed by a trough whereas a concave step appeared as a trough followed by a crest.

The circuits of the first type contained a microstrip resonator which acted as an RF short off resonance but had a high impedance on resonance (relative to the bridge resistance R). These circuits yielded concave steps (Figs. 7 and 8). On the other hand the circuits of types 2-4 contained resonators with relatively high impedance off resonance but their impedance on resonance acted as an RF short for the bridge. These circuits gave convex steps (Figs. 9 and 10). In all cases the knee of the step was at a voltage (frequency) corresponding to a mode of the resonator as well as could be determined by a priori calculations. Commonly several steps could be observed corresponding to the sequential modes of the resonator. The fundamental resonances were in the 0.6 GHz - 4 GHz range depending on the length and composition of the microstrip. The size of the steps was a function of the critical current of the bridge (i.e., of the temperature of the bath) with steps becoming more prominent at higher critical currents (Fig. 10). When several steps were present their amplitude would decrease with increasing mode frequency until they became unobservable (usually above 10 GHz).

Figure 7. The characteristics of a type 1 bridge-resonator circuit (AF-1). The resonant frequencies are sequential multiples of the lowest resonant frequency $f_1 = 0.7$ GHz. Voltages V corresponding to the resonant frequencies are indicated by arrows. The characteristic impedance of the microstrip is estimated as $Z_0 = (30 \pm 20) \text{ m}\Omega$ (depending on the assumed microstrip dielectric constant ϵ), while the bridge resistance is $R \doteq 135 \text{ m}\Omega$.

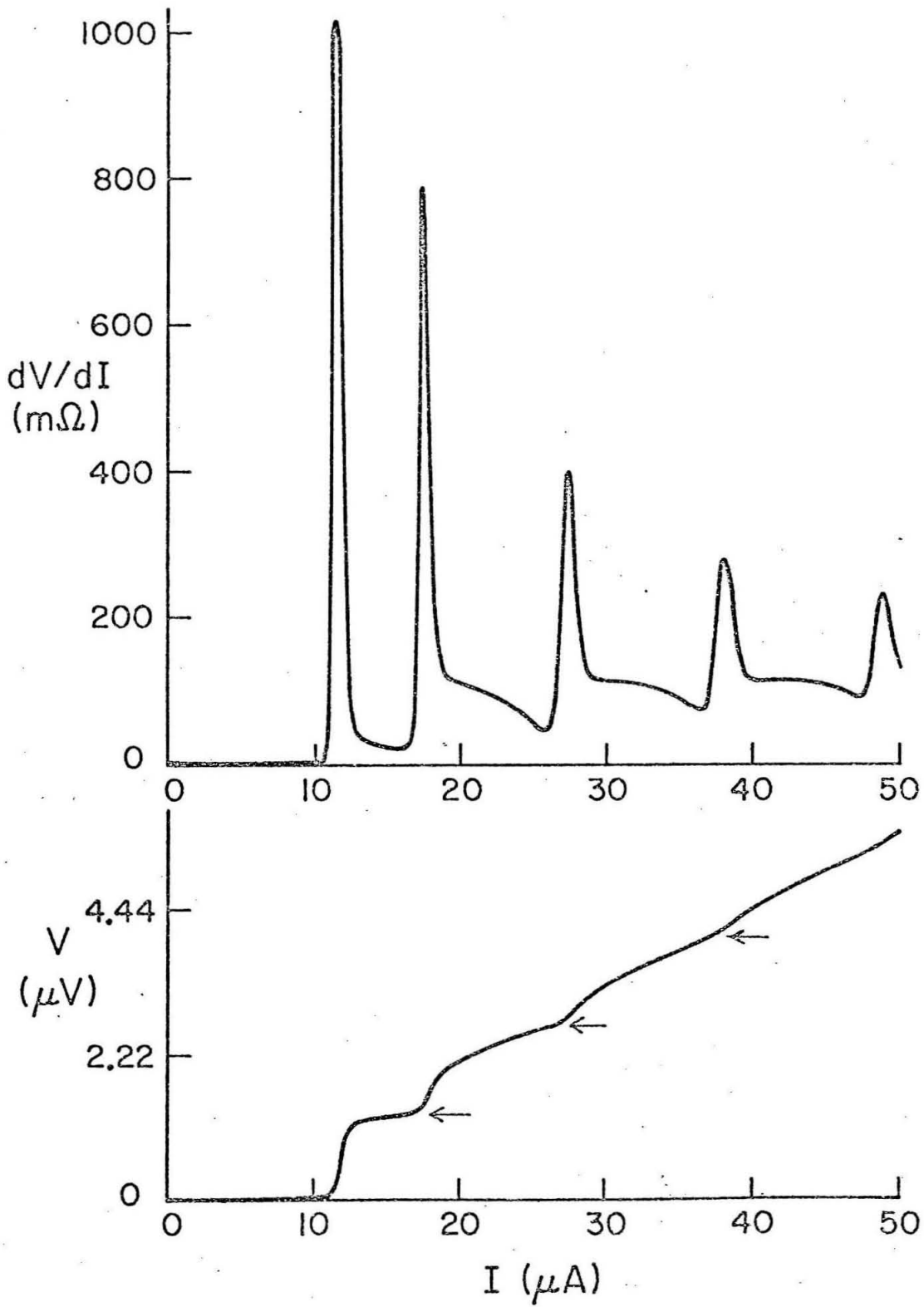


Figure 7

Figure 8. The dV/dI vs. I characteristic of a bridge (AF-2) before (top graph) and after (bottom graph) its inclusion in a type 1 bridge-resonator circuit ($Z_0 = 30 \pm 20 \text{ m}\Omega$, $R = 130 \text{ m}\Omega$). Both traces were recorded at the same temperature of the bath.

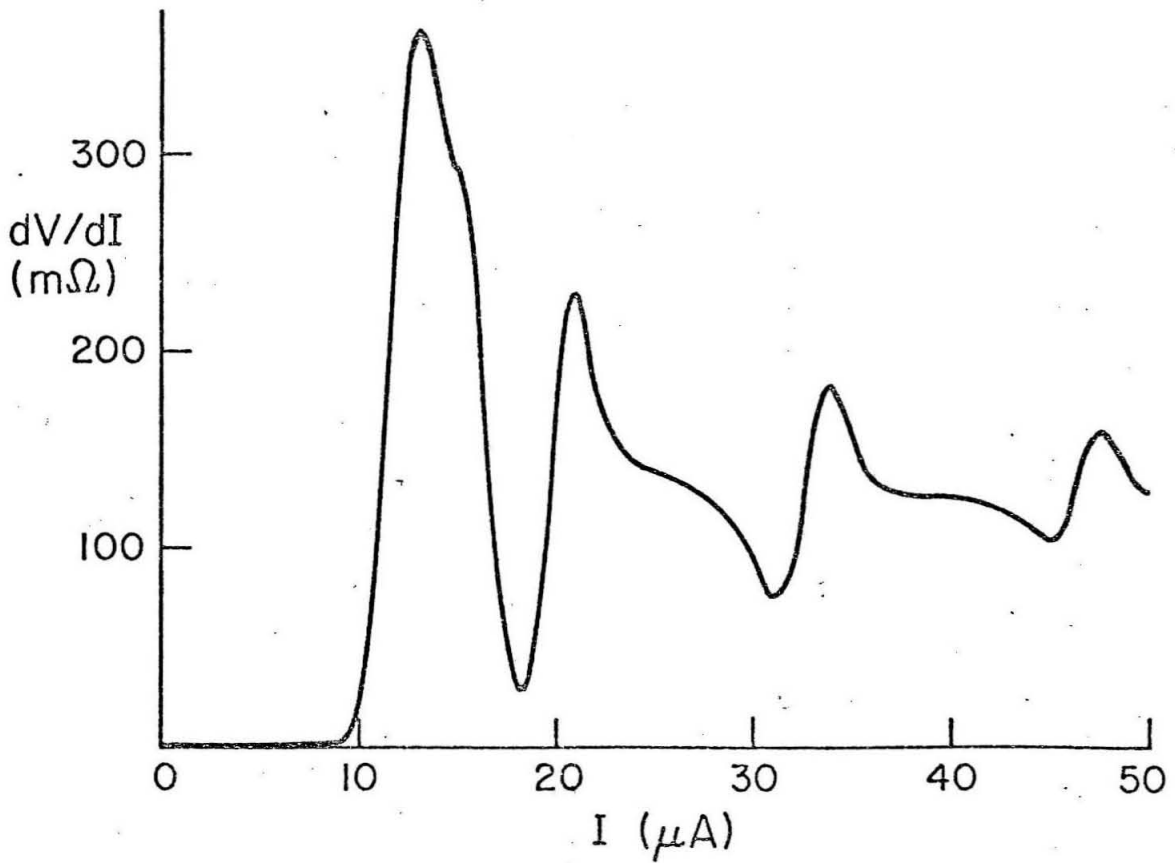
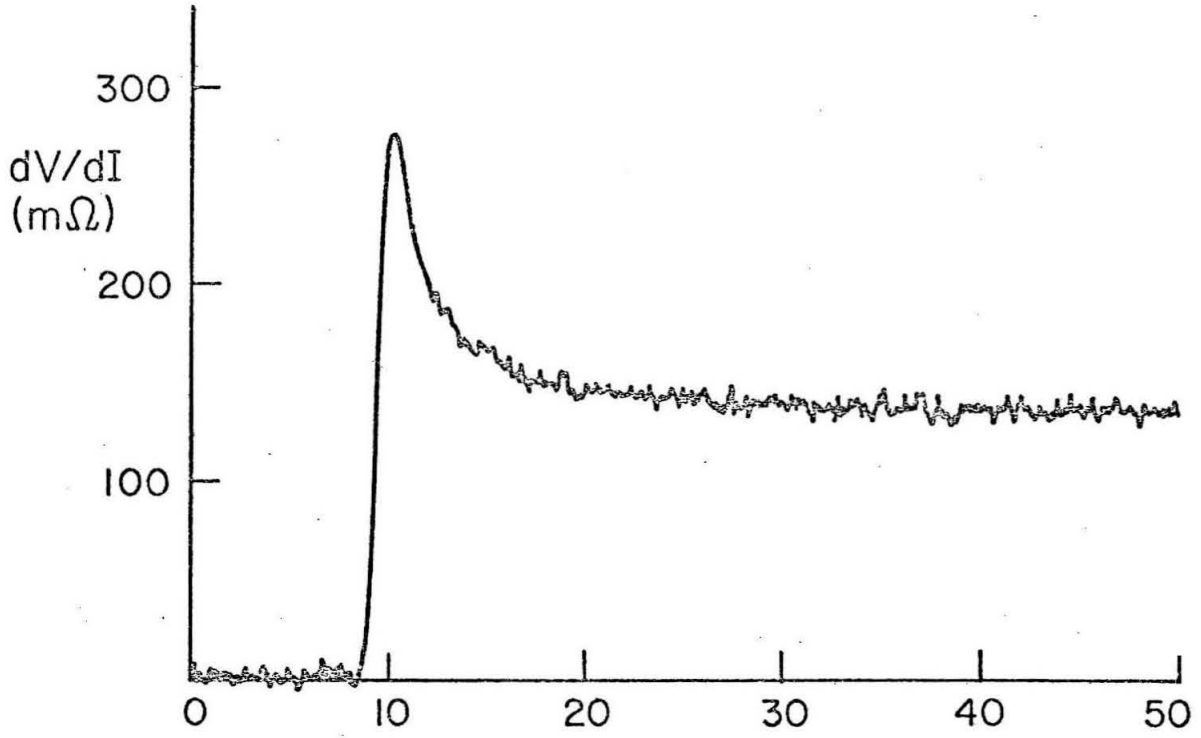


Figure 8

Figure 9. The dV/dI vs. I characteristics of a type 2 circuit (CIT 16 BC) at two different bath temperatures. The most prominent step occurring at a bias current 40-55 μA is due to the interaction of the Josephson oscillation with the lowest resonant frequency $f_1 \doteq 1.9$ GHz. The smaller steps are due to the second harmonic of the Josephson oscillation.

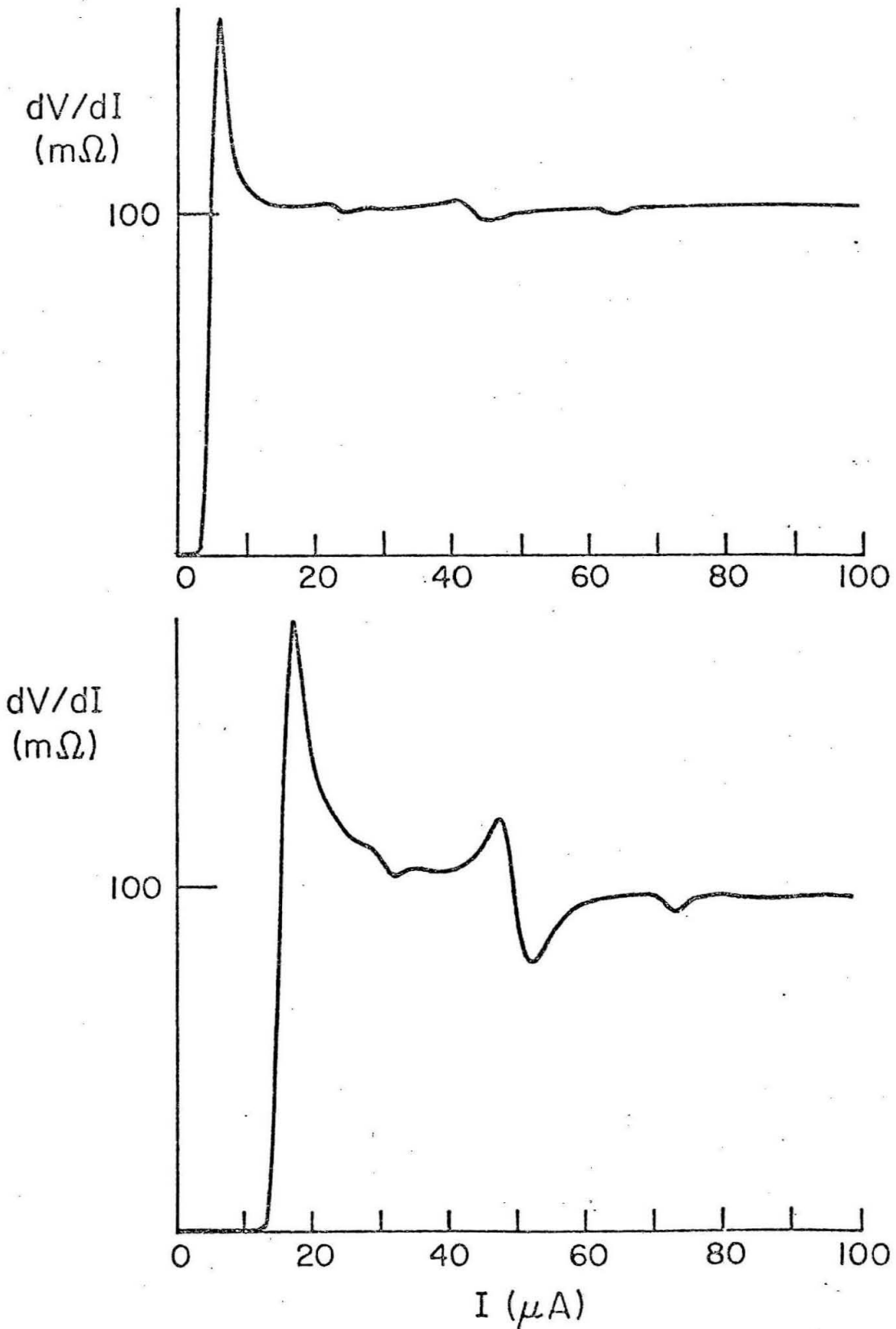


Figure 9

Figure 10. The dV/dI vs. I characteristics of a bridge (0-1) before (top graph) and after (bottom graph) its inclusion in a type 3 resonant circuit ($Z_0 = 5.5\Omega$, $R = 170\text{ m}\Omega$). Both graphs were recorded at the same temperature.

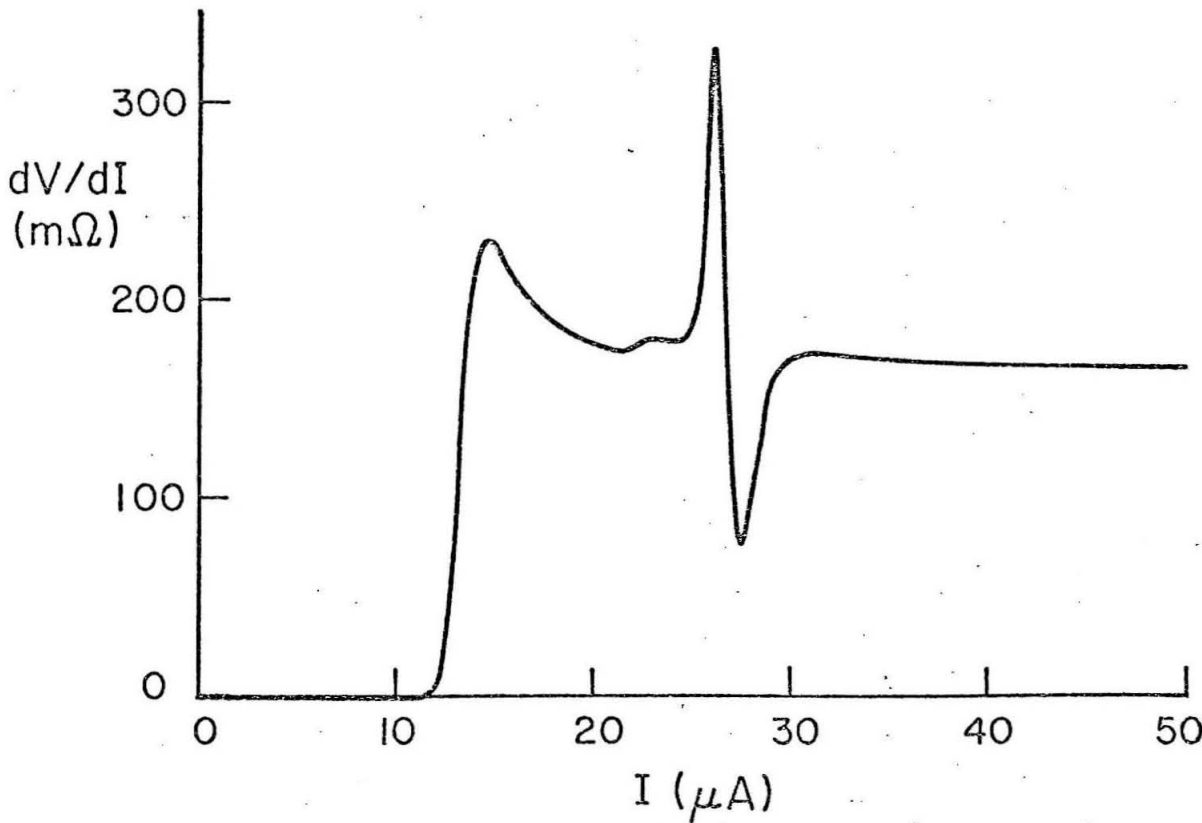
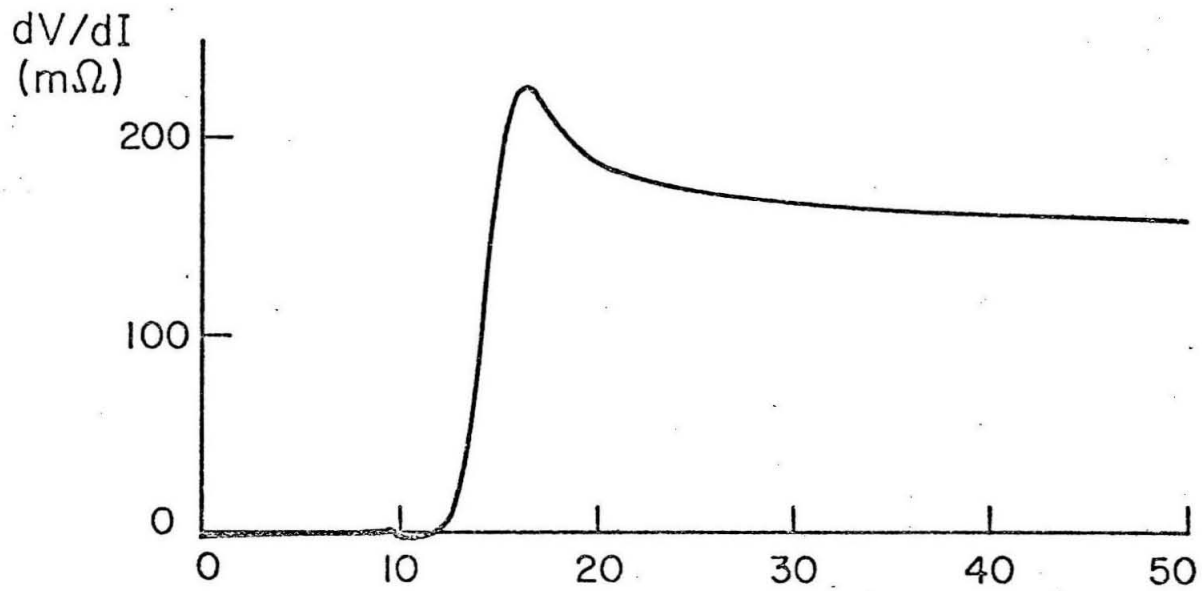


Figure 10

In circuits 2-4, steps corresponding to the interaction of the second harmonic of the bridge oscillation with the resonant modes were also seen but their amplitude was relatively small (Fig. 10). It was noted that the resonators with a lower loaded Q yielded relatively broader steps in the bias current domain than those with a higher loaded Q (cf. Figs. 9 and 10).

The type 3 circuits with the highest Q ($Q = 40$ at 1.56 GHz) were seen to be very sensitive to ambient RF interference. When the door of the screen room was opened the step size would decrease and the steps would broaden. No such effect was seen with circuits of lower Q . To account for these observations a more detailed model of the interaction of proximity effect bridges with microstrip resonators was developed (section 3.5).

3.4.2 Resonant interaction between two bridges coupled by a microstrip resonator

Preliminary observations were made in one circuit of type 4. The circuit contained two bridges approximately 3 mm apart at the center of the top strip of a microstrip segment (Fig. 6). The two bridges were biased and monitored independently of each other. The $d\bar{V}/dI$ vs. I characteristics of both bridges showed a self-induced step corresponding to the lowest resonant mode of the microstrip resonator. The size and shape of the self-induced step of one bridge changed markedly depending on the bias point of the other bridge (Fig. 11). Qualitatively, the behavior of the system can be understood in terms of two effects: first, the contribution of the impedance of the second

Figure 11. The characteristics of two coupled bridges in the type 4 circuit. Bridge 1 characteristics (graphs A, B, C) are given as a function of bridge 2 bias current (graph D). Bias points A, B, C correspond to graphs A, B, C respectively. For bias below the critical current of bridge 2 (A) maximum Q is obtained. For step bias (B) the deepening of the step in graph B is evidence of phase-locking between the bridges. For bias (C) above the step the Q of the step of bridge 1 is lower than in (A).

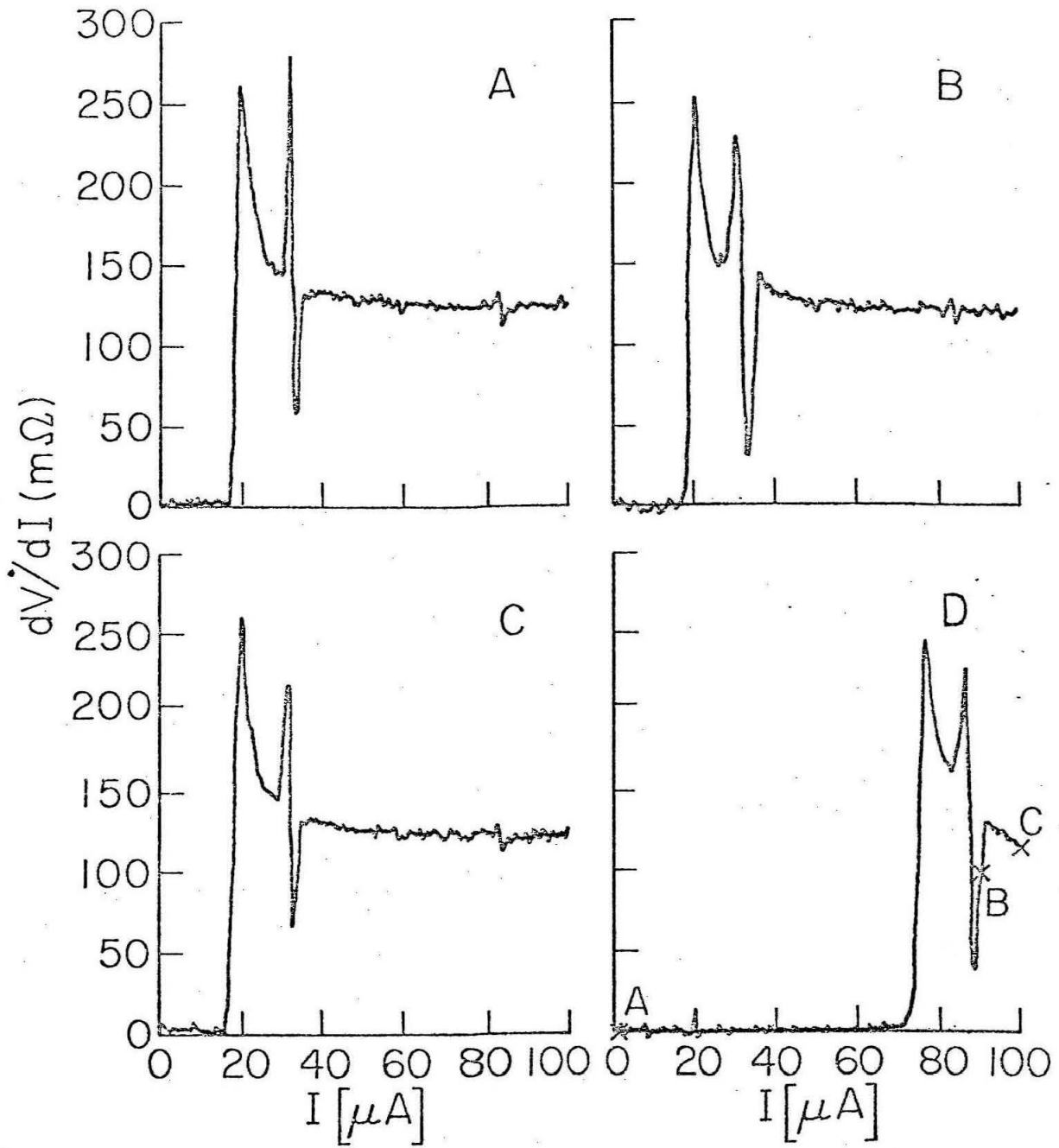


Figure 11

bridge to the total impedance at the terminals of the first bridge; and second, the phase locking between the two bridges when both oscillate at the resonant frequency of the resonator. Accordingly the characteristic of one bridge displays a self-induced step corresponding to a resonant mode whose Q (and possibly frequency?) depends on the bias point of the other bridge. When both bridges are on resonance both display a characteristic which is a superposition of a self-induced step with an externally induced step.

The system consisting of two bridges coupled by a resonator is a rich (Ref. 11) and mathematically complex system. Its detailed exploration, however, is outside the scope of this work.

3.5 Self-induced Steps for a Simple Harmonic Phase-Supercurrent Relation -- Theory

3.5.1 The model equations

Two kinds of phase-supercurrent relations are currently used to describe Josephson devices (see Chapter 1). For devices in which the supercurrent flow at finite voltages involves tunneling through a barrier or an equivalent process the phase-supercurrent relation is (Ref. 12)

$$I_S = I_C \sin \delta \quad (3.6)$$

whereas for devices in which a phase-slip process occurs the phase-supercurrent relation is believed to be (Ref. 13)

$$I_S = \frac{I_C}{2} (1 + \cos \delta) \quad (3.7)$$

At finite voltages an additional so-called "quasiparticle

interference" term is thought to play a role in tunneling devices (Ref. 12). In proximity effect bridges quasiparticle interference effects have not been observed to date (Ref. 14) and will not be further considered here. It should be noted that regardless of the phase-supercurrent relation the phase develops according to the relation (Chapter 1)

$$\dot{\delta} = \frac{2e}{\hbar} V \quad (3.8)$$

The two phase-supercurrent relations equations (3.6) and (3.7) can for simplicity of writing be condensed for finite voltages as:

$$I_S = I_C (1 - q + q \sin \int \frac{2e}{\hbar} V dt) \quad (3.9)$$

where $q = 1$ is equivalent to equations (3.6) and (3.8) while $q = \frac{1}{2}$ is equivalent to equation (3.7) and (3.8).

Assuming the two fluid model for a bridge of resistance R biased by a current source I , one obtains the integral equation

$$V = R \left[I - I_C (1 - q + q \sin \int \frac{2e}{\hbar} V dt) \right] \quad (3.10)$$

which can be solved to give

$$V(t) = R \left[I - (1 - q) I_C \right] \frac{1 - a^2}{1 + a \sin \delta_0 t} \quad (3.11)$$

where

$$a \equiv \frac{q I_C}{I - (1 - q) I_C} \quad \text{and} \quad \omega_0 \equiv \frac{2e \overline{V}(t)}{\hbar} .$$

The bridge voltage $V(t)$ can be expanded in a Fourier series

$$V(t) = V_0 - V_1 \sin \omega_0 t - V_2 \cos 2\omega_0 t + \dots$$

where

$$V_0 \equiv \overline{V}(t) = R \left[I - (1 - q) I_C \right] \sqrt{1 - a^2}$$

$$V_1 = qRI_c \frac{2(1-a^2)}{a^2} \left(1 - \frac{1}{\sqrt{1-a^2}} \right) \quad (3.12)$$

$$V_2 = qRI_c \frac{2(1-a^2)}{a} \left[\frac{1}{\sqrt{1-a^2}} - \frac{2}{1+\sqrt{1-a^2}} \right]$$

Terms V_3 and higher become negligible very rapidly as the parameter a increases so that apart from a small region where $a \doteq 1$ the voltage oscillation can be well described by the DC term, the fundamental and the second harmonic.

If the bridge is in addition shunted by a lossless resonator with reactance $iX(\omega)$ the integral equation becomes

$$\begin{aligned} V_o + \sum_{n=1}^{\infty} V_n \sin(n\omega_o t + \delta_n) = \\ -qRI_c \sin[\omega_o t - \sum_{n=1}^{\infty} \frac{V_n}{nV_o} \cos(n\omega_o t + \delta_n)] \\ + \sum_{n=1}^{\infty} \frac{RV_n}{X(n\omega_o)} \cos(n\omega_o t + \delta_n) + R[I - I_c(1-q)] \end{aligned} \quad (3.13)$$

The Fourier expansion will be cut off at $n = 2$ as before so that the equation can be transformed into a set of coupled equations involving Bessel functions. Retaining only Bessel functions up to order 2 one can write:

$$\begin{aligned} \frac{V_o}{qRI_c} &= \frac{1}{a} + J_1\left(\frac{V_1}{V_o}\right) J_o\left(\frac{V_2}{2V_o}\right) \cos \delta_1 + J_1\left(\frac{V_1}{V_o}\right) J_1\left(\frac{V_2}{2V_o}\right) \sin(\delta_2 - \delta_1) \\ -\frac{V_1}{qRI_c} &= \left[J_o\left(\frac{V_1}{V_o}\right) - J_2\left(\frac{V_1}{V_o}\right) \right] J_o\left(\frac{V_2}{2V_o}\right) \cos \delta_1 \\ &+ \left[J_o\left(\frac{V_1}{V_o}\right) + J_2\left(\frac{V_1}{V_o}\right) \right] J_1\left(\frac{V_2}{2V_o}\right) \sin(\delta_2 - \delta_1) + \end{aligned}$$

$$\begin{aligned}
 & - J_2\left(\frac{V_1}{V_0}\right) J_2\left(\frac{V_2}{2V_0}\right) \cos(2\delta_2 - 3\delta_1) \\
 - \frac{V_1}{qX(\omega_0)I_c} & = \left[J_0\left(\frac{V_1}{V_0}\right) + J_2\left(\frac{V_1}{V_0}\right) \right] J_0\left(\frac{V_2}{2V_0}\right) \sin\delta_1 \\
 & - \left[J_0\left(\frac{V_1}{V_0}\right) - J_2\left(\frac{V_1}{V_0}\right) \right] J_1\left(\frac{V_2}{2V_0}\right) \cos(\delta_2 - \delta_1) \\
 & - J_2\left(\frac{V_1}{V_0}\right) J_2\left(\frac{V_2}{2V_0}\right) \cos(2\delta_2 - 3\delta_1) \\
 - \frac{V_2}{qRI_c} & = J_1\left(\frac{V_1}{V_0}\right) \left[J_0\left(\frac{V_2}{2V_0}\right) - J_2\left(\frac{V_2}{2V_0}\right) \right] \sin(\delta_2 - \delta_1) \\
 & - J_1\left(\frac{V_1}{V_0}\right) J_1\left(\frac{V_2}{2V_0}\right) \cos\delta_1 \\
 \frac{V_2}{qX(2\omega_0)I_c} & = -J_1\left(\frac{V_1}{V_0}\right) \left[J_0\left(\frac{V_2}{2V_0}\right) + J_2\left(\frac{V_2}{2V_0}\right) \right] \cos(\delta_2 - \delta_1) \\
 & + J_1\left(\frac{V_1}{V_0}\right) J_1\left(\frac{V_2}{2V_0}\right) \sin\delta_1
 \end{aligned} \tag{3.14}$$

3.5.2 Step size

Equations (3.12) and (3.14) can be used to calculate the size of the self-induced steps in the harmonic model by determining the voltage difference $\Delta\bar{V}_{\max}$ at a given bias current I between the voltage $V_0 \equiv \bar{V}$ with the resonator on resonance and the voltage V_0 with the resonator off resonance. (In experiments the size of the steps $\Delta\bar{V}_{\max}$ is defined as the maximum voltage difference between the experimental I-V characteristic in the step region and the curve interpolated from outside the step region.)

As a first approximation the size of the self-induced step is obtained by calculating the voltage difference at a given current between the situation where the resonator reactance X is zero and infinite respectively. The simplest case occurs when all the harmonics can resonate simultaneously (e. g., in certain types of microstrip resonators). The size of the self-induced step is then

$$\begin{aligned} \Delta \bar{V}_{\max} &= V_o(I, X(\omega_o) = X(2\omega_o) = \dots = 0) \\ &- V_o(I, X(\omega_o) = X(2\omega_o) = \dots = \infty) \end{aligned} \quad (3.15)$$

The first and second terms are the time averaged voltages in the absence and in the presence of self-modulation, respectively.

Using equations (3.10) and (3.12) one obtains for this case

$$\frac{\Delta \bar{V}_{\max}}{qRI_c} = \frac{1}{a} \cdot (1 - \sqrt{1-a^2}) \quad (3.16)$$

In the second case of interest only the fundamental frequency resonates but the second harmonic interacts with a nonresonant large reactance. The size of the step is calculated as

$$\begin{aligned} \Delta \bar{V}_{\max} &= V_o(I, X(\omega_o) = 0, X(2\omega_o) = \infty) \\ &- V_o(I, X(\omega_o) = \infty, X(2\omega_o) = \infty) \end{aligned} \quad (3.17)$$

and the effect of higher harmonics is neglected. The set of equations (3.14) can be solved by successive approximation to show that

$$\frac{\Delta V_{\max}}{qRI_c} = \frac{1}{2} a + \frac{1}{8} a^3 + O(a^5) \quad (3.18)$$

i. e., to the order a^4 the result is the same as for all the harmonics resonating. If $X(\omega) \ll R$ for ω near $2\omega_o$ one obtains

$$\begin{aligned} \Delta \bar{V}_{\max} &\equiv V_o(I, X(\omega_o) = X(2\omega_o) = 0) \\ &- V_o(I, X(\omega_o) = \infty, X(2\omega_o) = 0) \end{aligned} \quad (3.19)$$

i. e.,

$$\frac{\Delta \bar{V}_{\max}}{qRI_c} = \frac{1}{2} a + O(a^5) \quad (3.20)$$

The last case of interest occurs when only the second harmonic resonates

$$\begin{aligned} \Delta \bar{V}_{\max} &\equiv V_o(I, X(\omega_o) = \infty, X(2\omega_o) = 0) \\ &- V_o(I, X(\omega_o) = \infty, X(2\omega_o) = \infty) \end{aligned} \quad (3.21)$$

which gives

$$\frac{\Delta \bar{V}_{\max}}{qRI_c} = \frac{1}{8} a^3 + O(a^5) \quad (3.22)$$

It can be seen that the second harmonic will resonate when the Josephson frequency $\omega_o = 2eV/(\hbar)$ is one half of the resonator mode frequency and the size of the second harmonic self-induced step is smaller by a factor of $\sim \frac{1}{4} a^2$ than the corresponding fundamental step would be.

3.5.3 Step shape

The shape of the self-induced step in the harmonic model is considered next. Due to the complexity of the equation (3.14) only the lowest order terms exhibiting a self-induced step are calculated. Accordingly equations (3.14) are approximated as

$$\begin{aligned} \frac{V_o}{qRI_c} &= \frac{1}{a} + \frac{1}{2} \frac{V_1}{V_o} \cos \delta_1 \\ - \frac{V_1}{qRI_c} &= \cos \delta_1 \end{aligned}$$

$$\begin{aligned}
 -\frac{V_1}{qX(\omega_o)I_c} &= \sin \delta_1 \\
 V_2 &= 0
 \end{aligned}
 \tag{3.23}$$

In this approximation the time average voltage V_o is given by

$$\frac{V_o}{qRI_c} = \frac{1}{a} - \frac{1}{2} a \frac{1}{1+R^2/X^2(\omega_o)}
 \tag{3.24}$$

If the functional form of $X(\omega_o) \equiv X(2eV_o/\hbar)$ is known the shape of the self-induced step can be readily calculated.

The model circuits used in this work will be discussed in more detail. The first circuit consists of a bridge of resistance R shunting one end of a lossless microstrip of characteristic impedance $Z_o < R$ which is open at the other end. The reactance of the microstrip resonator at the bridge terminals is

$$X(\omega_o) = -Z_o \cot \left(\pi \frac{\omega_o}{\Omega} \right)
 \tag{3.25}$$

where Ω is the lowest resonant frequency. If ω_o is near the n -th mode frequency $n\Omega$, the equation (3.25) can be approximated as

$$X(\omega_o) \approx \frac{Z_o}{\pi \left(\frac{\omega_o}{\Omega} - n \right)}
 \tag{3.26}$$

where

$$\frac{\omega_o}{\Omega} - n \ll 1.$$

The shape of the I-V characteristic in the neighborhood of resonance is gotten by using the form (3.26) in equation (3.24), i. e.,

$$\frac{\bar{V}}{qRI_c} = \frac{1}{a} - \frac{1}{2} a \frac{1}{1 + 4Q_n^2 \left(\frac{2e\bar{V}}{\hbar\Omega} - 1 \right)^2} \quad (3.27)$$

where $Q \equiv \pi R / 2Z_o$ and $\Omega_n = n\Omega$ is the n -th resonant frequency. The equation is a cubic equation for \bar{V} (the time average voltage) in terms of $1/a$ (the dimensionless bias current) so that in general more than one time average voltage may correspond to a given bias current in the vicinity of resonance and the characteristic contains a negative resistance region. Single valued I-V characteristics $\bar{V}(a)$ or $\bar{V}(I)$ result if

$$aQ < 1.5 \frac{\hbar\Omega}{2eqRI_c} \quad (3.28)$$

The voltage deviation $\Delta_n \bar{V}$ due to the n -th resonance can be identified from equation (3.27) as

$$\frac{\Delta_n \bar{V}}{qRI_c} = -\frac{1}{2} a \cdot \frac{1}{1 + 4n^2 Q^2 \left(\frac{\Delta_n \bar{V}}{\bar{V}_n} + \frac{qRI_c}{a\bar{V}_n} - 1 \right)^2} \quad (3.29)$$

where

$$\bar{V}_n = \frac{\hbar\Omega_n}{2e} \quad \text{and} \quad \Delta_n \bar{V} = \bar{V} - \frac{qRI_c}{a}$$

and, as expected, for

$$\frac{\Delta_n \bar{V}}{\bar{V}_n} \ll 1$$

the width of the step in the domain of the dimensionless current variable $1/a$ is proportional to the parameter Q .

The second model circuit has a bridge of resistance R connected in series at the center of a lossless microstrip segment of characteristic impedance $Z_o > R$ open at both ends.

The reactance of the microstrip segment at the bridge terminals is

$$X(\omega_0) = -2Z_0 \cot\left(\frac{\pi}{2} \frac{\omega_0}{\Omega}\right) \quad (3.30)$$

where, as before, Ω is the lowest resonant frequency. Following the procedure employed in the previous case a single valued I-V characteristic results if

$$aQ < 1.5 \frac{\hbar\Omega}{2eqRI_c} \quad (3.31)$$

where $Q \equiv \pi Z_0/2R$. The voltage deviation of the I- \bar{V} characteristic due to the n-th resonance is given by

$$\frac{\Delta_n \bar{V}}{qRI_c} = +\frac{1}{2} a \frac{1}{1 + 4(2n+1)^2 Q^2 \left[\frac{\Delta_n \bar{V}}{V_n} + \frac{qRI_c}{V_n} \left(\frac{1}{a} - \frac{1}{2} a \right) - 1 \right]^2} \quad (3.32)$$

where only the lowest order term (in the dimensionless current $1/a$) contributing to the self-induced step is shown. The sign of the deviation $\Delta_n \bar{V}$ at resonance is the reverse of (3.29).

3.5.4 Noise

In the above discussion the effects of noise on the shape and magnitude of self-induced steps have been neglected. However, as shown by Kirschman (Ref. 15), the bandwidth of Josephson oscillation in proximity effect bridges is determined by the amplitude of noise voltage across the bridge. When environmental sources of noise voltage are kept to a minimum the bandwidth of the bridge oscillation is due to Johnson noise in the normal current through the bridge. According to Kirschman the oscillation bandwidth for a proximity effect bridge is given by the equation

$$\Delta f = \sqrt{\frac{k_B T I_c R^2}{\Phi_0^3}} \quad (3.33)$$

where k_B , T , I_c , Φ_0 are the Boltzmann constant, the temperature of the bridge, the critical current of the bridge and the flux quantum, respectively. If the oscillation bandwidth Δf is much smaller than the resonator bandwidth f_0/Q , the noise will not modify the self-induced step magnitude and shape appreciably, provided that the theoretical I-V curve is single valued. If, however, the bridge oscillation bandwidth exceeds the bandwidth of the resonator, part of the power spectrum of the oscillation will not couple to the resonator and the size $\Delta \bar{V}_{\max}$ of the self-induced step will be reduced. At the same time the sharp features of the self-induced steps will be washed out or broadened. If the theoretical I-V curve is multivalued in the absence of noise, the effect of noise may be to induce transitions between the several points on the I-V characteristic at a given bias current I . Experimentally, a single averaged voltage may be measured in such a situation. This would also reduce the step size from the maximum value predicted from the noiseless model.

3.6 Results and Discussion

Both the size and the shape of self-induced steps observed in the I-V characteristics of bridge-resonator systems lend themselves to comparison with the theory presented in section 3.5. To avoid the complications due to the possible complex effects of noise (equation 3.33) and negative resistance (equations 3.28, 3.31) on the shape of the steps only the low loaded Q

resonators were employed for the comparison. Two type 1 circuits and one type 2 circuit were thus chosen to obtain the step size and shape data.

3.6.1 Step size

The type 1 circuits yielded multiple steps (at sequential mode frequencies) enabling measurements of step size over the range 0.7 - 2.7 GHz. Additional data on frequency dependence were gotten by modification of one circuit of each type extending the data to 3.2 GHz. The range of resonant frequencies and bridge critical currents over which analyzable data could be collected was limited by the small step size (relative to noise) at low critical currents I_c and high voltages \bar{V} ($\bar{V} \gg RI_c$), and by the extension of the lowest step into the critical current region ($\hbar\Omega/2e \sim RI_c$) at high critical currents I_c or low first resonant frequency Ω . Between these limits the step size (defined as the maximum voltage deviation $\Delta\bar{V}_{\max}$ from the I-V curve interpolated from the nonresonant portions of the I-V characteristic) was measured by planimetry from the $d\bar{V}/dI$ vs. I characteristic.

The step size ΔV_{\max} thus measured was normalized to $\Delta V_{\max}/RI_c$ and plotted against the normalized inverse bias current I_c/I . Figures 12-14 show the normalized data in comparison with the theoretical values (equations 3.15 - 3.20) based on the two alternative phase-supercurrent relations.

It is readily apparent that the data points fall between the values predicted from the two alternative theories. The data points at the lower voltages (frequencies) and lower critical

currents are generally fitted better by the $q = 1$ curve ($I_S = I_C \sin \delta$) whereas the data at the highest frequencies and the highest critical currents deviate significantly towards the $q = 1/2$ curve ($I = \frac{I_C}{2}(1 + \cos \delta)$).

This trend is interpreted as resulting from a true change in the amplitude of Josephson oscillation in the proximity effect bridges used in these experiments. At low critical currents ($\lesssim 10 \mu\text{A}$) and low voltages ($\lesssim 3 \mu\text{V}$) the amplitude of the Josephson oscillation is probably equal to the DC critical current of the bridge. At higher voltages and/or higher critical currents the amplitude of supercurrent oscillation relative to the critical current I_C is progressively reduced. These are indications both from the present study and from the work of Franson (Ref. 14) that at still higher voltages ($> 6 \mu\text{V}$) the reduction of the amplitude of Josephson oscillation with voltage continues. Franson deduced the amplitude of the oscillating supercurrent from microwave impedance measurements in a Ta/W proximity effect bridge of dimensions similar to the bridges used in this work except for the length (ℓ (Franson) = $0.5 \mu\text{m}$, ℓ (Ganz) = $0.8 - 1 \mu\text{m}$). At the frequency of 10 GHz, critical current $I_C = 40 \mu\text{A}$, bias current $I = 150 \mu\text{A}$ and resistance $R = 0.17 \Omega$ he found that the amplitude of the Josephson oscillation was $(0.62 \pm 0.05) I_C$. At still higher frequencies ($2e\bar{V}/\hbar \gg 10 \text{ GHz}$) the behavior of proximity effect bridges is a strong function of their geometry (Ref. 16). In this region the relaxation time associated with the length of the bridge, and heating due to dissipation become the important parameters

(Ref. 16).

The possible dependence of the phase-supercurrent relation on the supercurrent density in the bridge was predicted by Notarys et al. (Ref. 17) on the basis of a modified phase-slip model. The dependence of the phase-supercurrent relation on the voltage \bar{V} across the bridge can be made plausible by the following argument. Evidence was presented in Chapter 2 that the phase-supercurrent relation at $\bar{V} = 0$ is $I_S = I_c \sin \delta$. The phase-slip model predicts that at finite voltages $I_S = \frac{I_c}{2}(1 + \cos \delta)$ holds. It is likely that a transition region exists at intermediate voltages \bar{V} where the amplitude of the supercurrent oscillation is intermediate between I_c and $I_c/2$.

3.6.2 Step shape

An important and sensitive check on the validity of the theoretical description of the origin of self-induced steps (section 3.5) is the comparison of the shape of experimentally observed self-induced steps with the theoretical shape (equations 3.26 and 3.31). The sensitivity of the test is increased by using the first derivative $d\bar{V}/dI$ rather than the voltage \bar{V} as the basis for comparison. The theoretical points were obtained by the numerical solution of the equation for the deviation $\Delta_n \bar{V}(I)$

$$\frac{\Delta_n \bar{V}(I)}{RI_c} = \pm \frac{1}{2} \frac{I_c}{I} \frac{1}{1 + 4Q_n^2 \left[\frac{RI - \Delta_n \bar{V}}{R(I_n^2 - I_c^2/2I)} - 1 \right]^2} \quad (3.34)$$

where the upper signs were used for type 2 circuits while the lower signs were used for type 1 circuits. The equation (3.34)

is an equivalent form of equations (3.29) and (3.32) for $q = 1$ (i. e., $I_S = I_C \sin \delta$). The parameter I_n is the bias current at the center of the step and Q_n is the loaded Q of the n-th step. The first derivative was also obtained numerically using the approximate form

$$\frac{d\bar{V}}{dI} = \frac{d(\Delta_n \bar{V})}{dI} + R \quad (3.35)$$

For type 2 circuits, where the characteristic impedance Z_o of the resonator can be accurately determined from the known dimensions only the current I_n at the center of the step was gotten by direct fitting. The parameters I_C and R were measured from the portions of the $d\bar{V}/dI$ vs. I curve outside the resonant regions while $Q_1 = \frac{\pi}{2} Z_o/R$.

For type 1 circuits where the characteristic impedance Z_o was known only approximately, the parameter Q_1 was obtained by fitting as was the current I_n , while Q_n was calculated from the equation

$$Q_n = nQ_1 \quad (3.36)$$

Figure 15 shows the typical data for relatively low critical currents and voltages. At higher voltages ($\bar{V} > 5\mu V$) and higher critical currents ($I_C > 10\mu A$) the agreement between the data and the theory deteriorates, presumably due to the progressive decrease of the amplitude of the oscillating supercurrent compared to the critical current I_C .

3.7 Conclusion

Self-induced steps have been observed in the I-V and $\frac{d\bar{V}}{dI}$

vs. I characteristics of proximity effect bridges strongly coupled to superconducting microstrip resonators. The characteristic impedance of the various resonators ranged from $10\text{ m}\Omega$ to $6\ \Omega$ with bridge resistances $0.1\text{-}0.2\ \Omega$. Steps corresponding to resonant modes from $0.7\ \text{GHz}$ to $10\ \text{GHz}$ have been seen. Small steps generated by the second harmonic of Josephson oscillation have also been observed in several samples.

For low critical currents ($I_c < 10\ \mu\text{A}$) and low voltages ($\bar{V} < 3\ \mu\text{V}$) the size and shape of self-induced steps agree with a simple two fluid model assuming the phase-supercurrent relation $I_S = I_c \sin\delta$. The deviation at higher voltages and/or critical currents towards the model which assumes the alternative phase-supercurrent relation $I_S = \frac{I_c}{2} (1 + \cos\delta)$ is interpreted to indicate a progressive reduction (relative to the critical current I_c) of the amplitude of Josephson oscillation with increasing voltage \bar{V} and critical current I_c .

Figure 12. The normalized step size as a function of inverse normalized bias current for a type 1 bridge-resonator circuit (AF-1). The theoretical curves were calculated from equation (3.16). The frequencies f_1 , f_2 and f_3 are the frequencies of the first three step resonances. Experimental points are labeled by the critical current I_c in μA . The bridge resistance varied from $R = 140 \text{ m}\Omega$ at $I_c = 3.2 \mu\text{A}$ to $R = 130 \text{ m}\Omega$ at $I_c = 8.2 \mu\text{A}$. The characteristic impedance of the microstrip is estimated to be $Z_0 = (30 \pm 20) \text{ m}\Omega$.

Figure 13. The normalized step size as a function of inverse normalized bias current for a type 1 bridge-resonator circuit (AF-2). The theoretical curves were calculated from equation (3.16). The second set f_1, f_2 resulted from modification of the microstrip¹ after the first set of data was obtained. The bridge resistance varied from $R = 135 \text{ m}\Omega$ at $I_c = 4.5 \mu\text{A}$ to $R = 125 \text{ m}\Omega$ at $I_c = 12.2 \mu\text{A}$. The characteristic impedance $Z_0 = (30 \pm 20) \text{ m}\Omega$ as in Fig. 12.

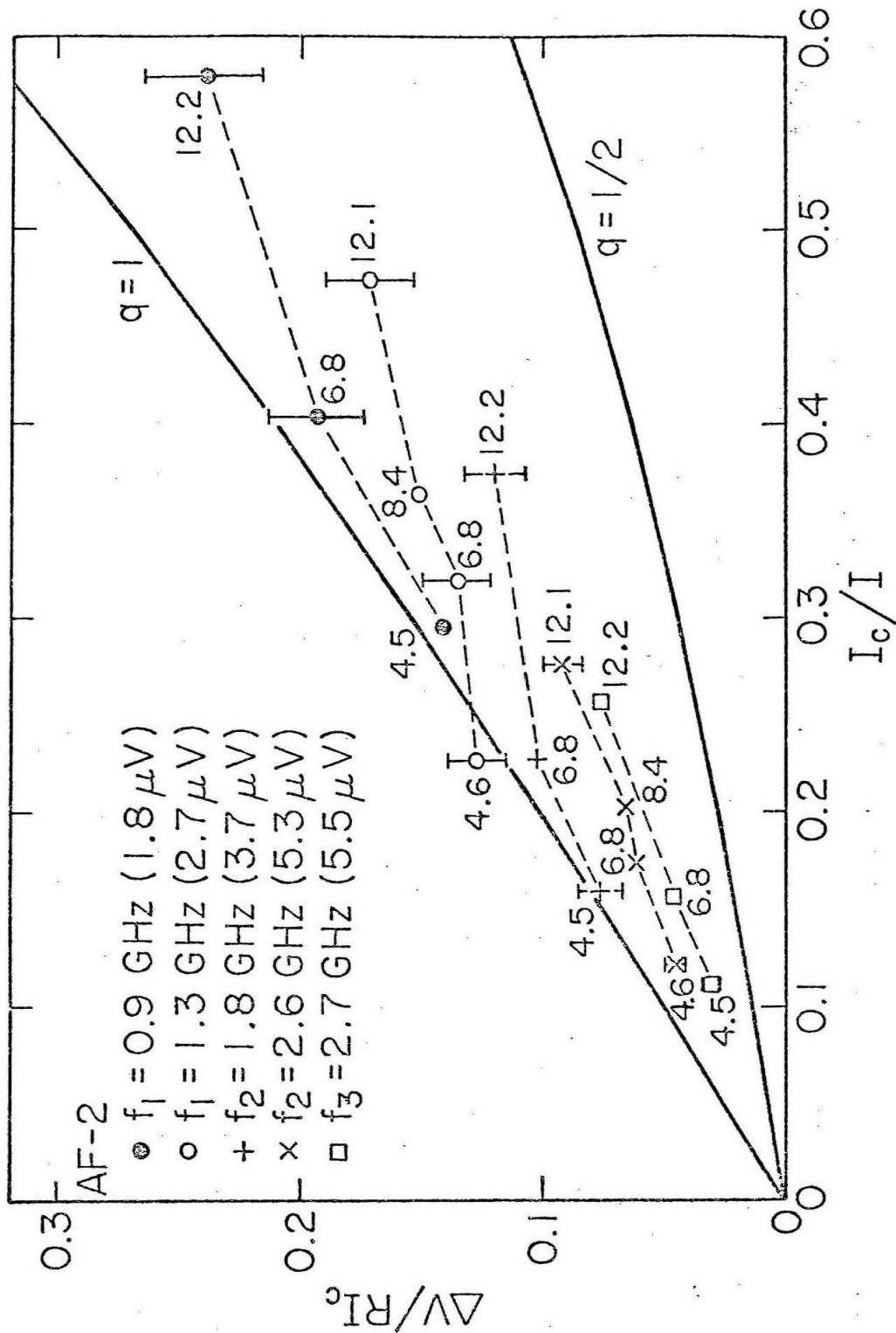


Figure 13

Figure 14. The normalized step size as a function of inverse normalized bias current for a type 2 bridge-resonator circuit (CIT-16BC). The theoretical curves were calculated from equation (3.20). The higher frequency data were obtained after microstrip modification. The bridge resistance varied from $R = 100 \text{ m}\Omega$ at $I_c = 3.5 \mu\text{A}$ to $R = 90 \text{ m}\Omega$ at $I_c = 14.5 \mu\text{A}$. The characteristic impedance could be determined accurately in this case to be $Z_o = (240 \pm 20) \text{ m}\Omega$.

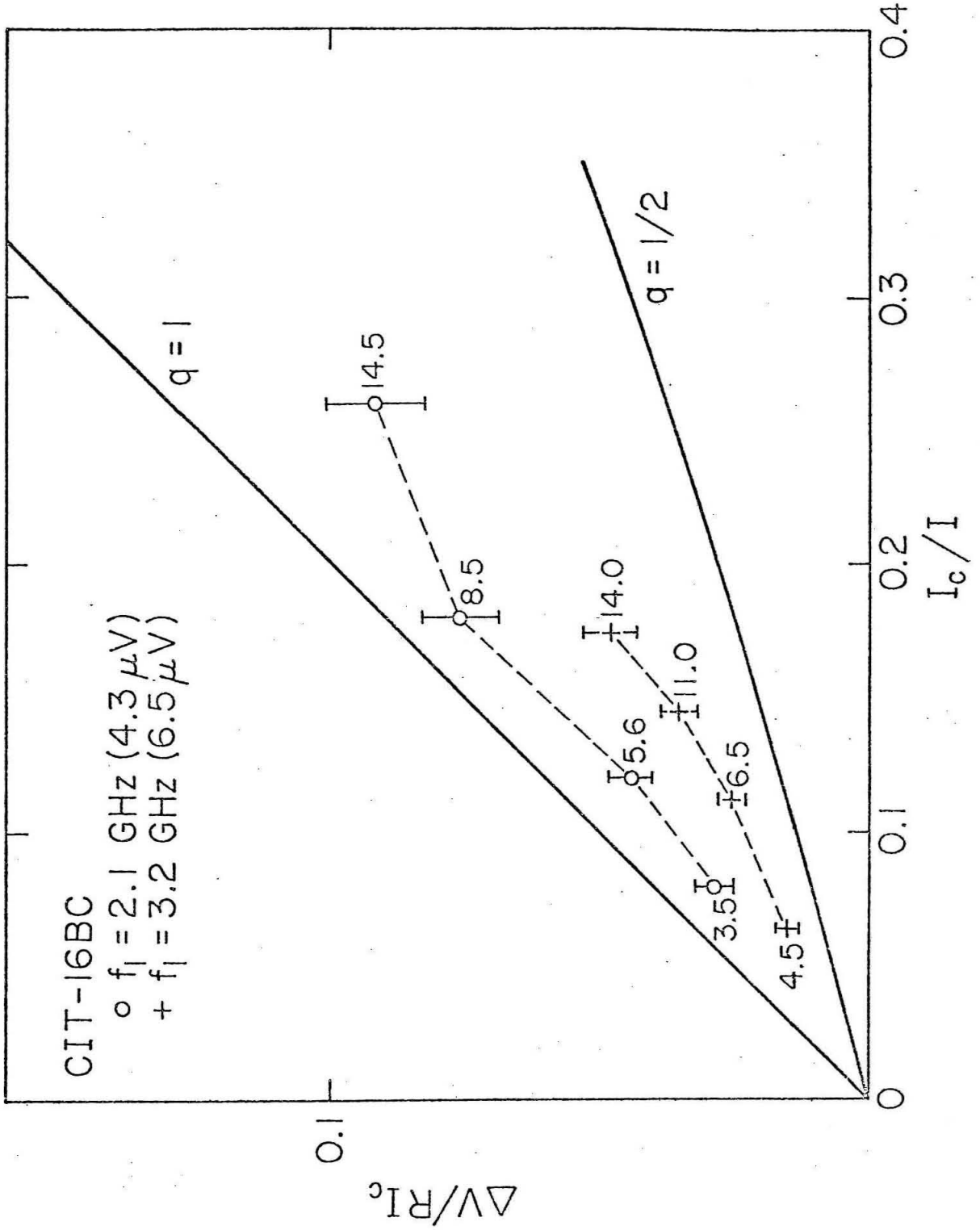


Figure 14

Figure 15. The comparison of theory (equations 3.34-3.36) with experimental dV/dI vs. I traces. In graph A the theory (dots) corresponds to $Q_1 = 4$ as determined from best fit (expected $Q_1 = \pi R/2Z_0 = 12 \pm 8$). The Q_1 in graph B was calculated a priori to be $Q_1 = \pi Z_0/2R = 4 \pm 0.4$. The theory (dots) corresponds to $Q_1 = 4$.

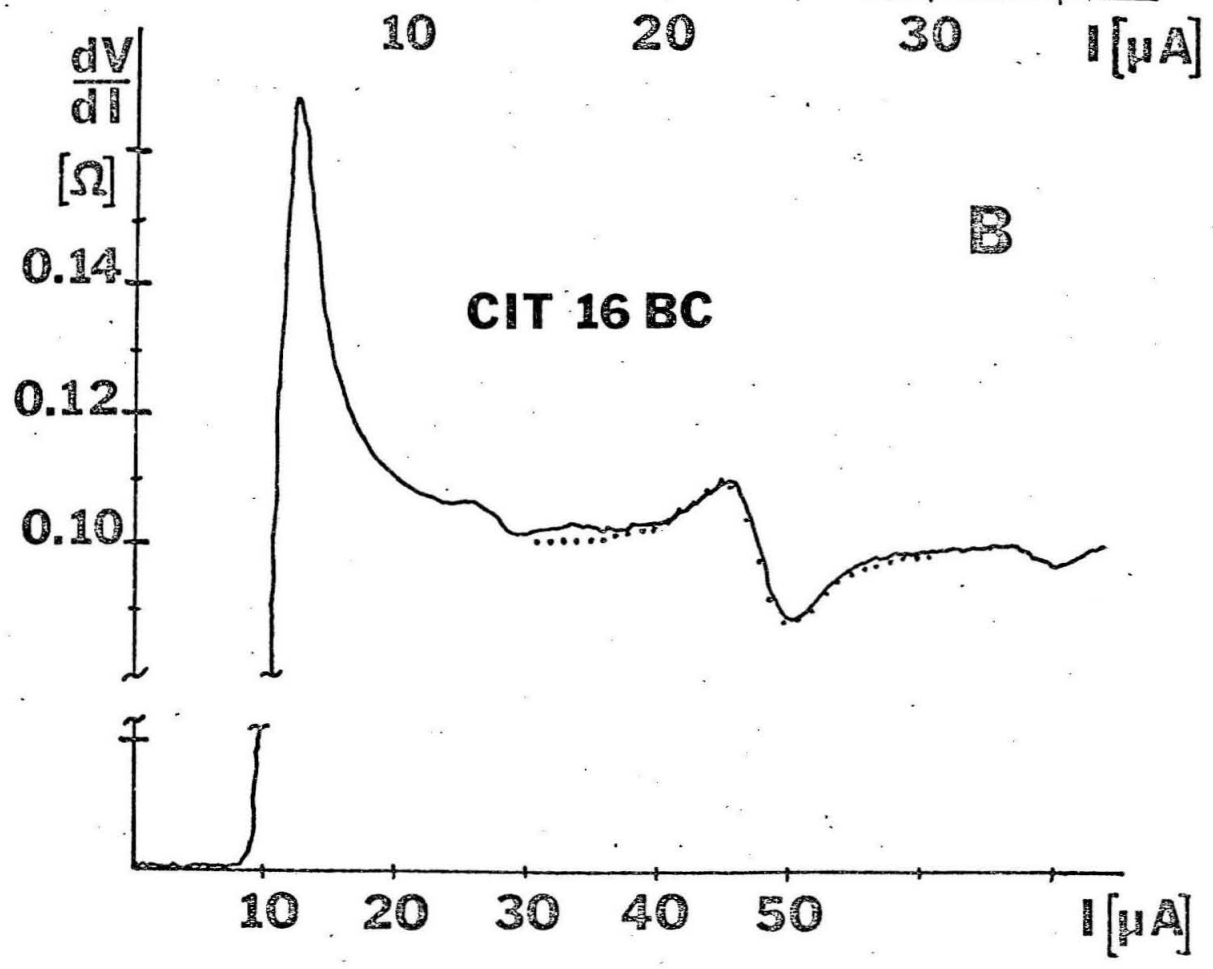
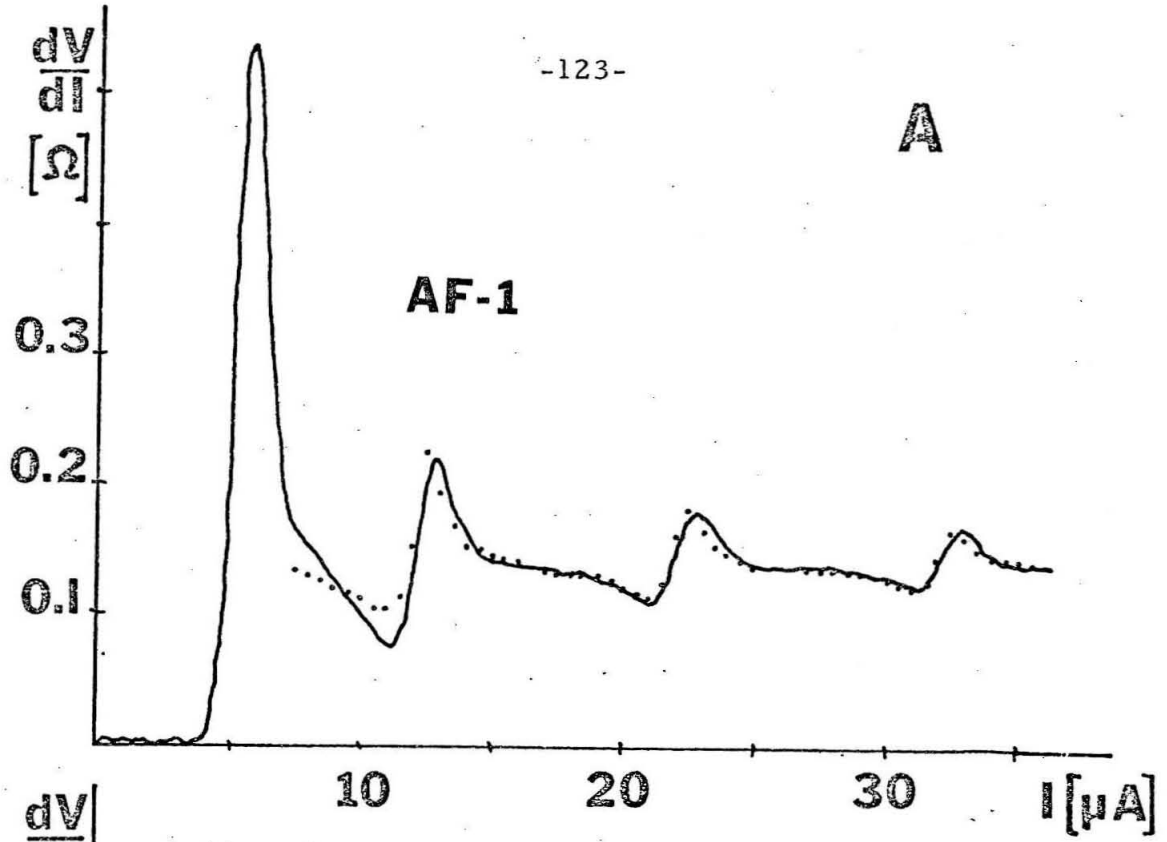


Figure 15

References

1. P. L. Richards, F. Auracher, and T. Van Duzer, Proc. IEEE 61, 36 (1973); A. Longacre, Proc. of the Applied Superconductivity Conference, Annapolis, Maryland, 1972 (IEEE, New York 1972) pp. 712-715; T. F. Finnegan, J. Wilson, and J. Toots, Rev. de Phys. Appl. 9, 199 (1974)
2. M. D. Fiske, Rev. Mod. Phys. 36, 221 (1964)
3. A. H. Dayem and C. C. Grimes, Appl. Phys. Lett. 9, 47 (1966)
4. M. T. Levinsen, Appl. Phys. Lett. 24, 247 (1974)
5. T. Ganz and J. E. Mercereau, J. Appl. Phys. 46, 4986 (1975)
6. D. E. McCumber, J. Appl. Phys. 39, 3113 (1968)
7. D. W. Palmer, Ph. D. Thesis (California Institute of Technology 1975); H. A. Notarys and J. E. Mercereau, J. Appl. Phys. 44, 1821 (1973)
8. P. V. Mason and R. W. Gould, J. of Appl. Phys. 40, 2039 (1969); J. of Appl. Phys. 42, 97 (1971)
9. L. Young, Anodic Oxide Films, p. 188 (Academic Press, London (1961)); E. L. Garwin and M. Rabinowitz, Lettere al Nuovo Cimento 2, 450 (1971)
10. D. W. Palmer, and S. K. Decker, Rev. Sci. Instrum. 44, 1621 (1973)
11. T. F. Finnegan, J. Wilson, and J. Toots, Rev. de Phys. Appl. 9, 199 (1974)
12. B. D. Josephson, Phys. Letters 1, 251 (1962)
13. R. K. Kirschman, H. A. Notarys, and J. E. Mercereau, Phys. Letters 34A, 209 (1971)
14. J. D. Franson (to be published)
15. R. K. Kirschman and J. E. Mercereau, Phys. Letters 35A, 177 (1971)
16. D. W. Palmer, Ph. D. Thesis (California Institute of Technology 1975)

References (cont'd)

17. H. A. Notarys, M. L. Yu and J. E. Mercereau, Phys. Rev. Letters 30, 743 (1973)